UNIVERSITY OF OKLAHOMA GRADUATE COLLEGE

EXPLORATION OF CHAOTIC ORBITS IN THE NEPTUNE-TRITON SYSTEM FOR ENHANCED SPACECRAFT CAPTURE

A THESIS

SUBMITTED TO THE GRADUATE FACULTY

in partial fulfillment of the requirements for the

Degree of

Master of Science

by Matthew Hancock Dobbs

Norman, Oklahoma

2025

EXPLORATION OF CHAOTIC ORBITS IN THE NEPTUNE-TRITON SYSTEM FOR ENHANCED SPACECRAFT CAPTURE

A THESIS APPROVED FOR THE

School of Aerospace and Mechanical Engineering

BY THE COMMITTEE CONSISTING OF:

Dr. Diogo Merguizo Sanchez, Chair

Dr. Prakash Vedula

Dr. Wei Sun

List of Figures

List of Tables

ABSTRACT

This work examines chaotic regions of orbits in the Neptune/Triton system to affect Δv savings during spacecraft capture around Triton. The Neptune/Triton system is represented with an n-body model in a Neptunian Equatorial reference frame. The model includes the Sun, Neptune, Triton, and the J2 perturbation of Neptune and Triton. A matrix of Initial Conditions is analyzed to discover regions of chaotic motion using Perturbation Maps and orbital deviation methods. Once chaotic regions are located, a technique of evaluating the orbits of spacecraft by integrating time backward to an escape, then using the end state vector of the reverse time integration as initial conditions of forward integration of time to capture are run. This study shows where chaotic regions can be used to affect the capture of a satellite around Triton with less than zero two-body energy with respect to Triton, and hence less Δv than a traditional capture technique. Examples of the potential chaotic regions and the reverse and forward time integration capture trajectories are shown.

Chapter 1. Introduction

Description of the problem

Exploration of the farthest reaches of the solar system requires time and energy. Time, due to the vast distances that separate the planets of the solar system and energy to put the spacecraft on the correct trajectory. While the distances are finite and relatively fixed, the energy required to move the spacecraft can come from a variety of sources. The most common source of energy for spacecraft is mass carried as propellant. The mass is accelerated by various means, expelled from the spacecraft and Newton's 2nd Law imparts velocity on the spacecraft proportionate to the speed and mass of the propellent expelled. In this case the propellant mass is carried by the spacecraft, and it is necessary to accelerate the unused propellant as well as the spacecraft along the desired trajectory. The second method of adding energy to a spacecraft is through a 'gravity assisted flyby' of a planet or moon. In the flyby the spacecraft 'steals' some angular momentum from the planet or moon and is accelerated by the exchange. The planet or moon also loses energy, but the mass differential between the planet and the spacecraft ensures that the planet only loses a miniscule amount of energy[1]. While this energy change is effectively 'free' to the spacecraft, the utility of the flyby maneuver depends on the geometry of the solar system for the duration of the mission. A third way to change the energy of a spacecraft is through 'aero assisted' trajectories. The aero-assist primarily decreases energy and occurs when a spacecraft is flown through a sensible atmosphere and utilizes the drag force imparted onto the spacecraft to change the energy and trajectory of the spacecraft. This is specifically useful in the outer planets as they are all gas giants, but does entail a significant risk. A technique of changing energy must be used when a spacecraft changes its orbit to depart, arrive, or modify its current trajectory. The challenge this thesis undertakes is to utilize chaotic orbital regions where a very small change in orbital initial conditions creates a large change in trajectory. Identifying these chaotic regions and further finding specific useful trajectories will enable "chaotic" capture of a spacecraft around a planet or moon or orbital element changes with reduced change in energy compared to using propellent or traditional gravity/aero -assisted maneuvers. The energy savings can be directly translated into reduced propellant carried onboard a spacecraft.

The Neptune, Triton System

Due to the large distance and long enroute time required for missions to Neptune, the majority of information on Neptune and its moons has derived from observations from Earth and Voyager 2. Voyager 2 has been the only mission to Neptune to date and revealed a significant amount of information on the planet and its moons.[2]

Neptune Characteristics-

Neptune is a large ice giant and the last official planet in the Solar System. It is made up of primarily hydrogen, helium, and methane. The planet consists of a cloud layer over a slushy core comprised of ice, ammonia, and some rock. The rocky core, if present, would constitute a small, less than two, percentage of the total mass of the planet. The majority of the planet's mass is concentrated in the slushy intermediate region. The temperature in Neptunes atmosphere ranges from 120 – 50 Kelvin with variations in latitude as would be expected in a planet with an axis inclined with respect to the sun. Due to the extreme distance Neptune is from the sun the amount of energy reaching the plant is 1.51 W/m^2. Compared to Earth's value of incident solar flux of 1400 W/m^2. Orbital elements used in the work are enumerated in Table 1.

Like the other gas giants, Neptune has a ring system. Unlike the rest of the gas giants the rings were difficult to detect from ground based observations and the confirmation of rings did not occur until the Voyager 2 mission. There are 5 rings ranging from 42,000 km to 63,000 km radial distance from Neptune's center of mass. The outermost ring also has distinct variations in density along several arcs of the ring. As the rings have very low density, they will not gravitationally affect the satellite in the study. There is also little danger of ring material colliding with the satellite in orbit around Triton.

TABLE 1. Neptune Orbital Characteristics w.r.t. Sun, 1 Jan 2000

a (km)	E	I (°)	ω (°)	Ω (°)	Θ (°)
$4.5x10^9$	0.01115	1.77	266.8	131.8	265.3
Mass (kg)	μ (km^3/s^2)	J_2	Period (years)	Rotation (hrs)	
$102x10^{24}$	6835099.9	$3411x10^{-6}$	165	16.11	

Triton Characteristics-

Triton is an icy moon and is the seventh largest moon in the known solar system. Triton's surface has a high reflectivity at 0.85 and is composed of nitrogen, methane, carbon dioxide, and water ice. The surface morphology of the moon is varied and relatively young. The surface temperature is only 38 K and is possibly the coldest body in the solar system. Despite the cold temperatures there is enough subsurface heating to generate hydrogen and dust plumes erupting from the surface with some regularity at the poles. The dust plumes are supported by an extremely tenuous atmosphere composed of 99% Nitrogen. The rest of the atmosphere is composed of small amounts of the same materials that make up the surface ice. Triton's orbital elements are unusual as well as the moon orbits retrograde in an orbit with no eccentricity. The specifics of the orbital elements used in the work are enumerated in Table 2. The obliquity of Triton has been determined to be very small. There are two values for Triton's obliquity, the value with the most adverse effect on the trajectory of artificial satellites is used in this study and is given in Table 5[3].

TABLE 2. Triton Orbital Characteristics w.r.t. Neptune, 1 Jan 2000

a (km)	E	I (°)	ω (°)	Ω (°)	Θ (°)
3.5476673×10^5	0.00	130.25	8.45	215.85	35.55
Mass (kg)	μ (km^3/s^2)	J_2	Period (days)	Rotation	
2.13×10^{22}	1428.5	2.07×10^{-4}	5.87	Tidal Locked	

<u>Neptune's other moons</u>

In the early 2000s there were only eight known satellites of Neptune[4], six of which were discovered by the Voyager 2 flyby. At the time only 2 other moons were named, Proteus and Nereid. 4 small moons were discovered orbiting just outside Neptune's ring system. Nereid travels in a highly elliptical and inclined orbit to Neptune that takes nearly a year to complete an orbit. The rest of the 8 initially discovered moons are in fairly circular orbits with fast periods. There are now 16 known moons of Neptune many more being discovered as observational and analytical techniques have improved[5].

Literature Review

<u>Challenges on missions to Neptune/Triton</u>

Due to its remote nature, low solar energy available, and large gravitational field, traditional trajectories are energy intensive and require significant time and Δv for arrival and capture. Over the last two decades, several missions have been proposed to explore Neptune, its moons and its rings. The missions range from a relatively "simple" fly-by of the system to orbital insertion around Neptune for an extended scientific mission.

NExTEP: - In a 2006 study, Solar Electric Powered (SEP) trajectory was used for a continuous thrust ellipse that adds significant Δv along with Earth gravity assist. The SEP section is discarded once the space craft is on a hyperbolic departure from Earth. It has a relatively quick 6.7-year transit time with an aerocapture in Neptunes atmosphere. V_∞ at arrival is approximately 19.2 km/s which is relatively high closure to Neptune's orbit. The aerobraking capture used to establish an orbit around Neptune has a Δv of 7 km/s. A traditional chemical rocket is planned on being used for orbit tuning once the initial orbit is established. The final science orbit around Neptune is elliptical[6]. Aerocapture is a difficult maneuver to execute and increases the mission risk significantly despite the great savings in onboard propellant when the technique is used. In 2020 a paper studied new controllers for using legacy blunt body aeroshells for aerocapture at Neptune and have indicated that successful use of the technique is more likely, even with older aeroshell technology[7]. This improvement in control algorithms can save propellant and reduce the risks involved when executing an aerocapture.

Outer Solar System - This 2011 study planned a 2020 launch of a joint ESA/NASA mission to make a fly-by of the Neptune-Triton system on the way to Kuiper Belt object fly-by. Two trajectories were proposed utilizing gravity assist to add Δv to the spacecraft without using propellant. One that would pass Venus and then two passes past Earth (VEE). The other involving two Earth passes with a third pass around Saturn (EES). Both have a travel time of approximately thirteen years. The Venus/Earth trajectory arrives in the Neptune-Triton region with a V_∞ of 13.79 km/s and the Earth/Saturn Trajectory arrives with a V_∞ of 11.04 km/s. In general, a slower flyby would give a longer observation period for science missions[8].

Trident - In 2021 Trident was proposed for NASA's Discovery Program. The mission was a single Triton 13-day encounter. Using similar a gravity assist from around Jupiter the mission had a proposed 2025 launch date with a 13 year transit time[9].

Neptune Odyssey - This 2019 study for NASA submitted in 2020. The Flagship Mission, similar in size and scope to the Cassini probe, proposed a 2030 launch with a 12-year enroute with Jupiter Gravity assist. If the launch was delayed past 2031, a 16-year direct trajectory would still be available. The mission plan calls for an orbit insertion burn and then utilizes perturbations from

Triton and Neptune to shape the science orbits for the next 4 years. The study report does not give details on the velocities involved at capture. It does give a propellant mass of 1910 kg with a 2 kg contingency[10].

Efforts in Trajectory Planning

In a study on gravity assist trajectories to Neptune, Sloarzano, Sukahnov, and Prado, analyzed different configurations of gravity assists given the solar system configuration in 2008-2020. From a variety of launch dates and gravity assist trajectories a general trend of the longer the transfer less Δv is required and a lower V_∞ is generated on arrival to the Neptune system. The study also shows that for a given transfer time, the chosen trajectory can vary the Δv required by as much two km/s and the V_∞ by as much as eight km/s[11]. This study helps illustrate the importance of trajectory selection and the effectiveness of proper selection and orbital analysis. While the previous work was not specifically a Neptune-Triton study similar principles will apply to this study. More recent studies endeavor to build a library of motion primitives or “building blocks” to create a trajectory between two bodies[12]. The system is based on running a large number of simulations and using machine learning to group the trajectories generated into families of ‘primitives.’ These families are then used like links in a chain to create a trajectory. The system is still being developed and is currently used between two natural bodies with a negligible mass spacecraft in a Circular Restricted 3 Body Problem. The primarily focus is on periodic orbital transfers.[3] A follow on study applies the technique of the motion primitives to the Neptune-Triton system in the CR3BP frame.[13] These studies are being developed to speed the process of trajectory design and ‘initial guess’ guidance. The motion primitive approach aggregates trajectories and searches broad sets of trajectories for similarities. The current work enhances the trajectory selection process by actively looking for chaotic trajectories in narrow regions of space in a full n-body model. In 1990 the MUSES-B spacecraft, a Japanese mission, malfunctioned on its way to the moon. The MUSES-A ‘parent’ spacecraft was to stay in Earth orbit and act as a communications relay for the MUSES-B. However, MUSES-A used a low delta-v ballistic trajectory to fly to and be captured by the moon’s gravity. The calculated Δv was 30 m/s as compared to the Hohman Δv of approximately 200 m/s. The trajectory was planned and modeled in a pseudo circular restricted four-body problem in three dimensions (PR4BP-3D) and was the first time an actual mission utilized gravitational transfer and capture. The planning process used similar techniques used in this thesis, but did not specifically utilize chaotic regions for transfers and captures. Further, it was modeled as two PR3BP-3D solutions and not a continuous n-body integration as this thesis proposes.[14] Sanchez, Prado, and Yokoyama conducted a study of natural gravitational capture of a satellite around Pluto and Charon. An n-body system was used with perturbations added for J_2 and J_{22} of Pluto and Charon. They worked to identify areas of initial conditions around Pluto and Charon that a satellite would be captured and remain in orbit around Pluto for 10 years or more. The work they undertook identified minimum energy captures and time of flight. They also identified orbits with little perturbation and would require very little propellant for station keeping and orbit maintenance[15]. The work of this thesis extends the ideas in the Pluto-Charon paper in that it seeks to identify natural gravity captures but focuses on the chaotic areas of the system.

Goals and Organization of Thesis

The work presented here is a new application of chaotic orbit determination techniques to identify and utilize low-energy chaotic transfers and captures in the Neptune-Triton system using full n-body perturbed model. It highlights the feasibility of moving to an orbit around Triton from a Neptune centered orbit. It adds to the previous work by specifically finding chaotic areas to implement low energy 'natural' capture and enhances mission trajectory design by lowering the overall Δv required to orbit Triton from a Neptune centered orbit. Specific orbits exhibiting this behavior are found and quantified. The explorations undertaken in the work presented will enable Δv savings to further refine mission efficiencies that are critical to exploring the farthest reaches of the solar system. The following thesis will begin with a description of the two body and *n*-body dynamics, J2 gravitational perturbations, reference frames, and reference frame harmonization. The general concepts will be augmented with a description of their application in the thesis. The method used to generate the orbits and plots is then outlined followed by the analysis techniques used on the data. The results of the orbital simulations and analysis are given and the plots and trajectories explained in detail. Future work is recommended at the conclusion of the thesis body.

Chapter 2. Background, Theory, and Model

In this section theories of motion are developed following the principles and process outlined in Curtis,[1]

2-body dynamics

The two body dynamics are based in an 'inertial frame' that is fixed in space. The following development derives the accelerations due to gravitational forces between the 2 bodies in the 2-body system both in a 'fixed' inertial frame. The axes are an X, Y, Z orthogonal irrotational frame. The positions of two masses are given as

$$\boldsymbol{R}_1 = X_1\hat{\mathbf{I}} + Y_1\hat{\mathbf{J}} + Z_1\hat{\mathbf{K}}$$
$$\boldsymbol{R}_2 = X_2\hat{\mathbf{I}} + Y_2\hat{\mathbf{J}} + Z_2\hat{\mathbf{K}} \tag{1}$$

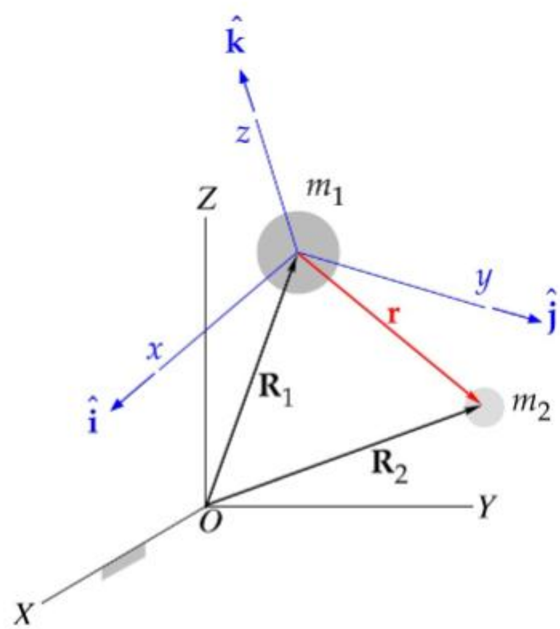

Figure 1-Inertial Reference Frame and Position Vectors (adapted from Curtis[1])

The only forces acting on the bodies are the gravitational forces of the bodies acting on each other. So that $\mathbf{F}_{12}$ is the force on m_1 by m_2 and $\mathbf{F}_{21}$ is the force on m_2 from m_1. For the purposes of the brief development here the position vector between the two bodies, **r** is given as m_2 relative to m_1 so that

$$\mathbf{r} = \boldsymbol{R}_2 - \boldsymbol{R}_1 \tag{2}$$

then the force of m_2 on m_1 is given by

$$\boldsymbol{F}_{12} = \frac{Gm_1m_2}{r^2}\hat{\boldsymbol{u}}_r \tag{3}$$

A form of Newton's law of gravitation where G is the universal gravitational constant
When expanded into component form the terms are given as

$$\mathbf{r} = (X_2 - X_1)\hat{\mathbf{I}} + (Y_2 - Y_1)\hat{\mathbf{J}} + (Z_2 - Z_1)\hat{\mathbf{K}} \tag{4}$$

And the unit vector along the vector **r** is

$$\hat{\boldsymbol{u}}_{\boldsymbol{r}} = \frac{\mathbf{r}}{r} \tag{5}$$

and

$$\mathrm{r} = \sqrt{(X_2 - X_1)^2 + (Y_2 - Y_1)^2 + (Z_2 - Z_1)^2} \tag{6}$$

Given that the force on the second body is equal and opposite that of the force on the first from Newton's 3rd law

$$\boldsymbol{F}_{21} = -\frac{Gm_1m_2}{r^2}\hat{\boldsymbol{u}}_r \tag{7}$$

this is an expected result. Utilizing Newton's 2nd law and framing the forces on m_1 and m_2 as the absolute acceleration of the bodies due to the force gravity

$$\begin{aligned} \boldsymbol{F}_{12} &= m_1\ddot{\boldsymbol{R}}_1 \\ \boldsymbol{F}_{21} &= m_2\ddot{\boldsymbol{R}}_2 \end{aligned} \tag{8}$$

gives nearly the last step in the development. Taking equations (3) and (7) and setting equal to their respective counterpart in (8) and dividing out the common terms yields

$$\ddot{\boldsymbol{R}}_1 = \frac{Gm_2}{r^2}\hat{\boldsymbol{u}}_r \tag{9}$$

$$\ddot{\boldsymbol{R}}_2 = -\frac{Gm_1}{r^2}\hat{\boldsymbol{u}}_r$$

Simplifying the vector terms show the expression for the acceleration of the two masses in relation to the inertial reference frame.

$$\ddot{\boldsymbol{R}}_1 = Gm_2\frac{\mathbf{r}}{r^3}$$

$$\ddot{\boldsymbol{R}}_2 = Gm_1\frac{\mathbf{r}}{r^3} \tag{10}$$

While the equations of acceleration in (10) are a good analytical result, most problems in astrodynamics are focused on a body moving in relation to another body.

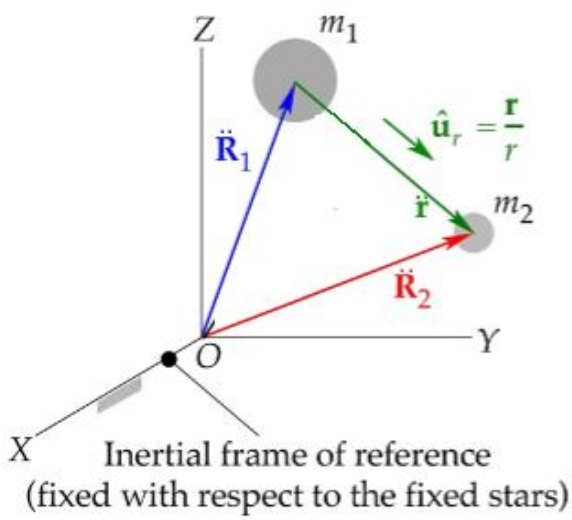

Figure 2- Relative Acceleration Vectors (adapted from Curtis[1])

The expression for this motion is taken by differentiating (2) twice to obtain

$$\ddot{\mathbf{r}} = \ddot{\boldsymbol{R}}_2 - \ddot{\boldsymbol{R}}_1 \tag{11}$$

and then substituting (9) into the equation above which yields

$$\ddot{\mathbf{r}} = -\frac{G(m_1+m_2)}{r^2}\hat{\boldsymbol{u}}_r \tag{12}$$

Finally, utilizing the simplification of the gravitational parameter μ as $\mu = G(m_1 + m_2)$ the classic expression for the acceleration of a body gravitationally attracted to another body is found to be

$$\ddot{\mathbf{r}} = -\frac{\mu}{r^3}\mathbf{r} \tag{13}$$

In the following work there are essentially three two-body systems. The Sun-Neptune, Neptune-Triton, and Triton-Spacecraft two-body systems each have their own gravitational parameter used when under analysis. Shown in Table 3 are the values of μ used in the simulation and other calculations between the bodies. In the case of Triton-Satellite or Neptune-Satellite, the value used is simply that of the central body as the mass of the satellite is so small relative to the central body.[16]

Table 3. μ-values of primary systems

2-body System	μ-value $\left({km^3}/{s^2}\right)$
Sun-Neptune	132,719,275,117.97
Neptune-Triton (system)	6,836,528.47
Triton-Satellite	1428.5

N-Body Dynamics

In an n-body system, there are more than just a primary body and a satellite. Any number of additional gravitational sources may be present and affect the accelerations in the system under consideration. The perturbations caused by additional bodies can be combined with the gravitational force of a primary body to determine the total acceleration due to gravity on a body in an n-body system. With a third mass added to a two-body system, the acceleration on the two 'primary bodies' becomes

$$\begin{gathered}\boldsymbol{a}_1 = \frac{Gm_2(\boldsymbol{R}_2 - \boldsymbol{R}_1)}{\|\boldsymbol{R}_2 - \boldsymbol{R}_1\|^3} + \frac{Gm_3(\boldsymbol{R}_3 - \boldsymbol{R}_1)}{\|\boldsymbol{R}_3 - \boldsymbol{R}_1\|^3} \\ \boldsymbol{a}_2 = \frac{Gm_1(\boldsymbol{R}_1 - \boldsymbol{R}_2)}{\|\boldsymbol{R}_1 - \boldsymbol{R}_2\|^3} + \frac{Gm_3(\boldsymbol{R}_3 - \boldsymbol{R}_2)}{\|\boldsymbol{R}_3 - \boldsymbol{R}_2\|^3}\end{gathered} \tag{14}$$

when finding the acceleration of body two relative to body one while under the influence of the third body is given by $\mathbf{a}_{12/3} = \mathbf{a}_2 - \mathbf{a}_1$ and expanded is

$$\mathbf{a}_{12/3} = \frac{Gm_1(\boldsymbol{R}_1 - \boldsymbol{R}_2)}{\|\boldsymbol{R}_1 - \boldsymbol{R}_2\|^3} + \frac{Gm_3(\boldsymbol{R}_3 - \boldsymbol{R}_2)}{\|\boldsymbol{R}_3 - \boldsymbol{R}_2\|^3} - \frac{Gm_2(\boldsymbol{R}_2 - \boldsymbol{R}_1)}{\|\boldsymbol{R}_2 - \boldsymbol{R}_1\|^3} + \frac{Gm_3(\boldsymbol{R}_3 - \boldsymbol{R}_1)}{\|\boldsymbol{R}_3 - \boldsymbol{R}_1\|^3} \tag{15}$$

rearranged is becomes

$$\mathbf{a}_{12/3} = -\mu \frac{(\boldsymbol{R}_2 - \boldsymbol{R}_1)}{\|\boldsymbol{R}_2 - \boldsymbol{R}_1\|^3} + \mu_3 \left(\frac{(\boldsymbol{R}_3 - \boldsymbol{R}_2)}{\|\boldsymbol{R}_3 - \boldsymbol{R}_2\|^3} - \frac{(\boldsymbol{R}_3 - \boldsymbol{R}_1)}{\|\boldsymbol{R}_3 - \boldsymbol{R}_1\|^3} \right) \tag{16}$$

In the thesis work to follow the perturbations of the satellite under study are from Triton and the Sun with Neptune as the central body in the n-body system.

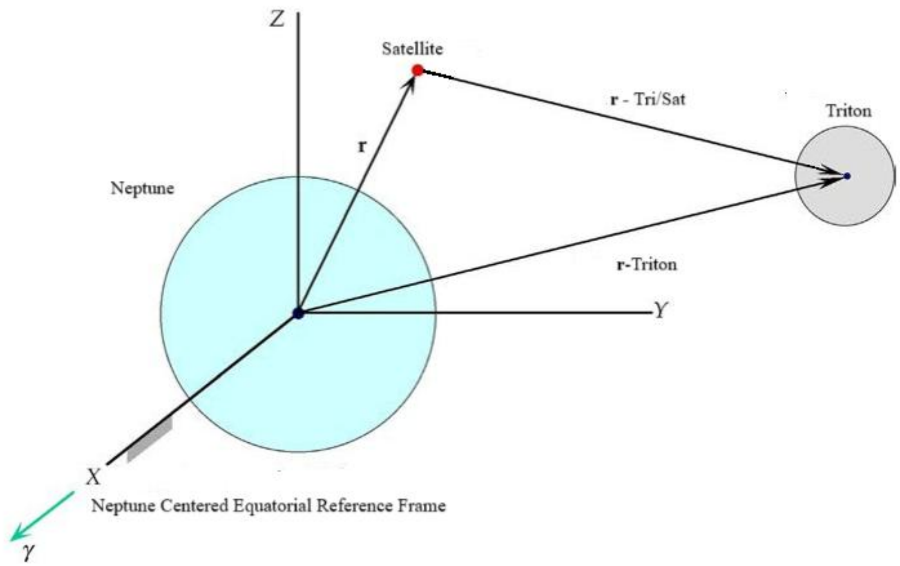

Figure 3-Neptune, Triton, Satellite Vectors (adapted from Curtis[1])

For the case of taking the 3rd body to be Triton the terms in (16) become

$$\mathbf{r} = \boldsymbol{R}_2 - \boldsymbol{R}_1$$
$$\ddot{\mathbf{r}} = \mathbf{a}_{12/3}$$
$$\mathbf{r}_{triton} = \boldsymbol{R}_3 - \boldsymbol{R}_1$$
$$\mathbf{r}_{t/s} = \boldsymbol{R}_3 - \boldsymbol{R}_2 = \mathbf{r}_{triton} - \mathbf{r}$$
$$\mathbf{p}_{triton/satellite} = \mu_{triton} \left(\frac{\mathbf{r}_{s/t}}{r_{s/t}^3} - \frac{\mathbf{r}_{triton}}{\mathbf{r}_{triton}{}^3} \right) \tag{17}$$

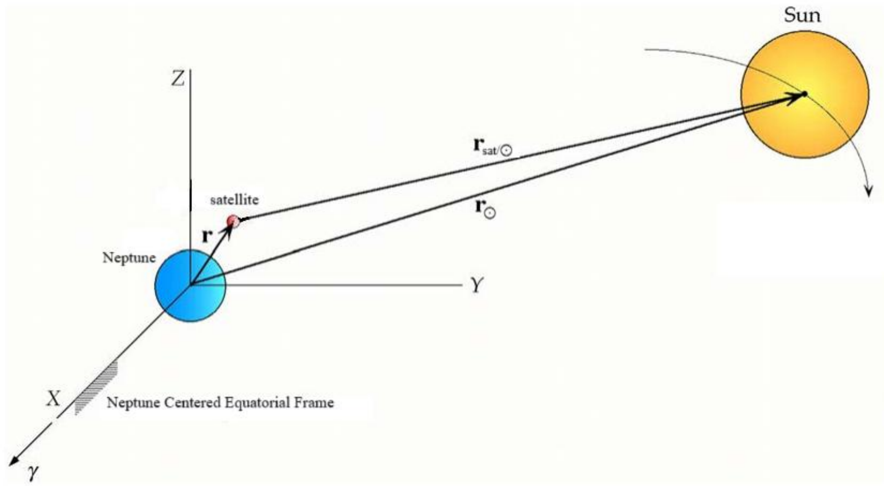

Figure 4-Sun, Neptune, Satellite Position Vectors (adapted from Curtis[1])

A similar method of constructing the vectors will yield the perturbation from the Sun on the satellite and yields the expression

$$\mathbf{p}_{sun/sat} = \mu_{sun}\left(\frac{\mathbf{r}_{sat/sun}}{r^3_{sat/sun}} - \frac{\mathbf{r}_{sun}}{\mathbf{r}_{sun}{}^3}\right) \tag{18}$$

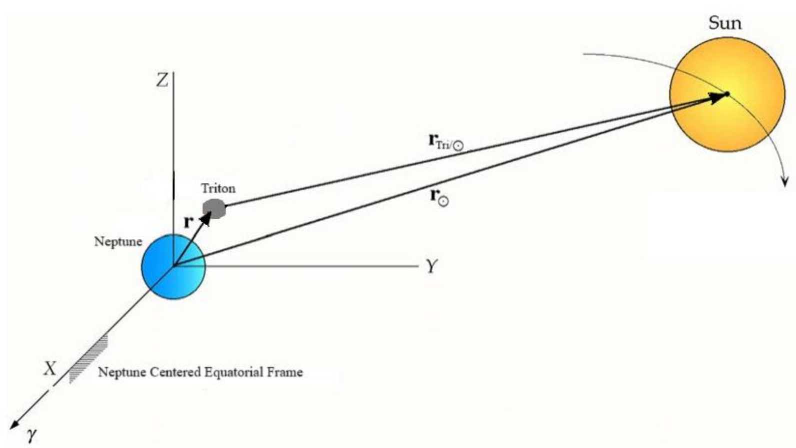

Figure 5- Sun, Neptune, Triton Position Vectors (adapted from Curtis[#####])

Additionally, the solar perturbation on Triton will be

$$\mathbf{p}_{sun/triton} = \mu_{sun}\left(\frac{\mathbf{r}_{triton/sun}}{r^3_{triton/sun}} - \frac{\mathbf{r}_{sun}}{\mathbf{r}_{sun}{}^3}\right) \tag{19}$$

J2 and J2 Perturbations

In celestial bodies, especially ones with great mass like Neptune, Earth, and Triton, the mass of the body is not uniformly spherical. Most rotating bodies will bulge near the equator. The equatorial bulge or unequal distribution of mass creates a perturbing force on satellites and other objects that orbit the central oblate body. The mass at the equator creates an additional direction of the force of gravity and certain alignments of the equatorial bulge will cause a greater or lesser force deriving from the geometry of an orbit or a bodies location relative to the additional mass around the middle. Figure 6 conveys the vectors and angles used in the following exposition.

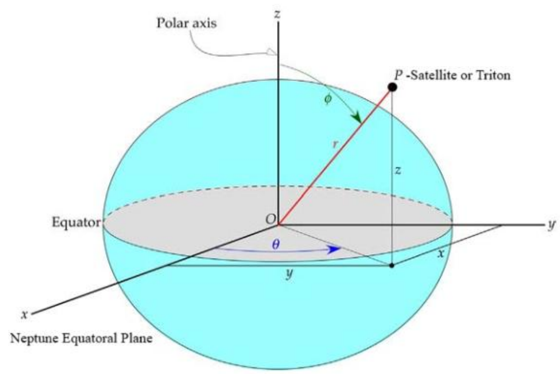

Figure 6-Oblate Body and Equatorial Frame for J_2 Perturbation Calculation (adapted from Curtis[1])

Mathematically a perfectly spherical body would have a perfect spherical gravitational potential. When the gravitational potential energy is given as V = -μ/r and the usual del operator of

$$\nabla = \left(\frac{\partial}{\partial x}\hat{\mathbf{i}} + \frac{\partial}{\partial y}\hat{\mathbf{j}} + \frac{\partial}{\partial z}\hat{\mathbf{k}}\right) \tag{20}$$

Are combined and simplified the classic acceleration expression results

$$\mathbf{a} = -\mu\frac{\mathbf{r}}{r^3} \tag{21}$$

To develop the gravitational potential of an the oblate body further it is more convenient to switch to polar coordinates for the first steps. The assumption is made that the oblate body is symmetrical around its polar axis so that the perturbation does not depend on the azimuth (θ) angle of the polar conversion. The change to polar coordinates of the gravitational potential given

$$\phi = \ tan^{-1}\frac{\sqrt{x^2+y^2}}{z} \tag{22}$$

is given as potential V(r,ϕ)

$$V(r,\phi) = -\frac{\mu}{r} + \Phi(r,\phi) \tag{23}$$

with

$$\Phi(r,\phi) = \ \frac{\mu}{r}\sum_{k=2}^{\infty} J_k\left(\frac{R}{r}\right)^k P_k(cos\phi) \tag{24}$$

P_k is the Legendre polynomial for J_x. The J_2 term in the infinite series is the largest term by a great amount. For Neptune and Triton, the J_2 zonal harmonic is also the best known term determined from observations. In this work, the J_2 term is the one that will be used to determine and implement the perturbative forces in the model.[17] The J_2 terms of Neptune and Triton are given in Table 4.

Table 4. J_2 terms for Neptune and Triton

Body	J_2
Neptune	3411e-6
Triton	2.07e-4

Higher terms are estimated from interior studies of the planet and moon and would not add significant perturbation. In addition, sectoral and tesseral harmonics are not used as they are not well known for Neptune and Triton. Using just the J_2 term the Legendre polynomial and Φ function reduce to

$$P_2(x) = \frac{1}{2}(3x^2 - 1)$$
$$\Phi(r,\phi) = \frac{J_2\mu}{2r}\left(\frac{R}{r}\right)^2 (3cos^2\phi - 1) \tag{25}$$

The perturbative force from the J_2 in cartesian coordinates can be expressed as

$$\mathbf{p} = -\nabla\Phi = -\frac{\partial\Phi}{\partial x}\hat{\mathbf{i}} - \frac{\partial\Phi}{\partial y}\hat{\mathbf{j}} - \frac{\partial\Phi}{\partial z}\hat{\mathbf{k}} \tag{26}$$

using the chain rule on the partial derivatives on (26) gives the following three partial derivatives

$$\frac{\partial\Phi}{\partial x} = \frac{\partial\Phi\partial r}{\partial r\partial x} + \frac{\partial\Phi\partial\phi}{\partial\phi\partial x}$$
$$\frac{\partial\Phi}{\partial y} = \frac{\partial\Phi\partial r}{\partial r\partial y} + \frac{\partial\Phi\partial\phi}{\partial\phi\partial y}$$
$$\frac{\partial\Phi}{\partial z} = \frac{\partial\Phi\partial r}{\partial r\partial z} + \frac{\partial\Phi\partial\phi}{\partial\phi\partial z} \tag{27}$$

Multiplying, reducing, and collecting like terms of the derivatives in (27) results in the three partial differentials results in the J_2 perturbation force in cartesian reference frame

$$\mathbf{p} = \frac{3J_2R^2}{2r^4}\left[\frac{x}{r}\left(5\frac{z^2}{r^2} - 1\right)\hat{\mathbf{i}} + \frac{y}{r}\left(5\frac{z^2}{r^2} - 1\right)\hat{\mathbf{j}} + \frac{z}{r}\left(5\frac{z^2}{r^2} - 3\right)\hat{\mathbf{k}}\right] \tag{28}$$

This perturbation force is in the equatorial frame of the central body in cartesian coordinates.

Reference Frames, Rotations and Translations.

In the work following the integrations in the model are done in a 3-axis orthogonal cartesian coordinate system. The center of the coordinate system is located at the center of mass of Neptune with the x and y axes in plane with the equatorial plane of the planet. Two other coordinate systems are used in the model to set up initial conditions and to analyze the orbital motion of the artificial satellite. One system is the sun-centered system Neptune orbiting the Sun with the plane along ecliptic matching the x-y plane. The other system used in the model is the Triton-centered reference frame. The center of the frame is the center of mass of Triton and the x-y plane lies along the equatorial plane of Triton. The Triton-centered reference frame is used to set up the initial conditions of the satellite around Triton. All reference frames are oriented with the x-axis aligned in the same direction as the axis around which the obliquity of the respective orbits are measured. Obliquity is the angle between the equator of a body and orbital plane of the body with respect to the ecliptic.

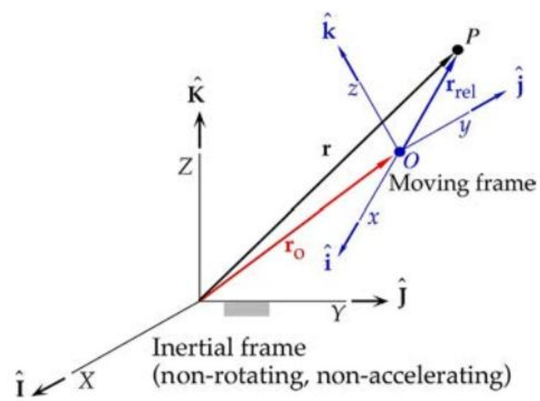

Figure 7-Multiple Reference Frame Example (from Curtis[1])

Perifocal Reference Frames-

The satellite and Triton's initial conditions are set in the perifocal reference frame. The perifocal frame is defined by the orbital plane of the satellite with the origin of the frame at the focus of the orbit nearest the central body. The orthogonal reference vectors are aligned with the periapsis in the plane of the orbit, along the Semilatus rectum and the third is aligned with the angular velocity vector. To be usable in the integration the initial conditions need to be converted from the perifocal to body centric equatorial using the relationships below

$$\mathbf{r}_p = \frac{h^2}{\mu(1+e\,cos\theta)}(cos\theta\hat{\mathbf{p}} + sin\theta\hat{\mathbf{q}}) \tag{29}$$

$$\mathbf{v}_p = \frac{\mu}{h}[-sin\theta\hat{\mathbf{p}} + (e + cos\theta)\hat{\mathbf{q}}] \tag{30}$$

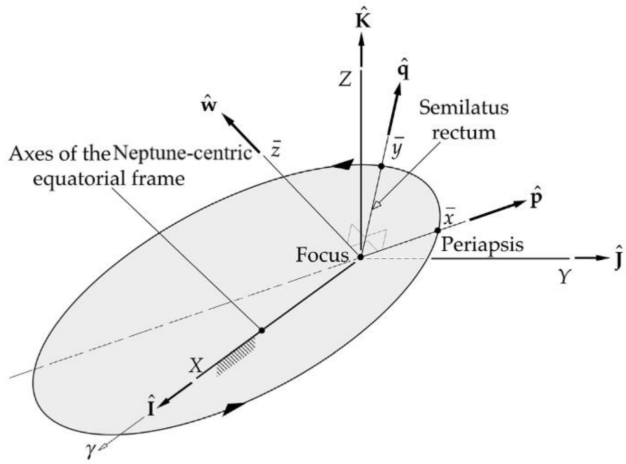

Figure 8- Perifocal and Inertial Frames (Adapted from Curtis[1])

h is the angular momentum of the satellite, μ the gravitational parameter of the system, e is the eccentricity and θ is the true anomaly. This transforms the orbital elements into an initial state vector consisting of position and velocity in the perifocal frame which is then rotated into the central body equatorial frame by the Direction Cosine Matrix (DCM) based on the Euler 313 rotation sequence or

$$[\boldsymbol{Q}]_{pX} = [\mathbf{R}_3(\Omega)][\mathbf{R}_1(\mathrm{I})][\mathbf{R}_3(\omega)] \tag{31}$$

$$[\boldsymbol{Q}]_{pX} = \begin{bmatrix} -sin\Omega\cos\mathrm{I}sin\omega + cos\Omega cos\omega & -sin\Omega\cos\mathrm{I}cos\omega - cos\Omega sin\omega & sin\Omega sin\mathrm{I} \\ sin\Omega\cos\mathrm{I}sin\omega + sin\Omega cos\omega & cos\Omega\cos\mathrm{I}cos\omega - sin\Omega sin\omega & -cos\Omega sin\mathrm{I} \\ sin\mathrm{I}sin\omega & sin\mathrm{I}cos\omega & cos\mathrm{I} \end{bmatrix} \tag{32}$$

Using the transformations above the position and velocity vectors in the body-centered equatorial frame are

$$\mathbf{r}_X = [\boldsymbol{Q}]_{pX}(\mathbf{r}_p) \tag{33}$$

$$\mathbf{v}_X = [\boldsymbol{Q}]_{pX}(\mathbf{v}_p) \tag{34}$$

The following procedure was used in the order shown to ensure that the elements are recovered effectively, it follows Algorithm 4.2 in Curtis using the body-centered equatorial position and velocity vectors as the initial conditions to find the orbital elements. First the magnitude of the distance, (r) and velocity (v) are calculated. The radial velocity is then determined by

$$v_r = \frac{\mathbf{r}\cdot\mathbf{v}}{r} \tag{35}$$

Specific angular momentum (h) is found by taking the magnitude of

$$\mathbf{h} = \mathbf{r} \times \mathbf{v},\ h = \sqrt{\mathbf{h}\cdot\mathbf{h}} \tag{36}$$

Inclination is found with

$$i = cos^{-1}\left({}^{h_z}\!/_{h}\right) \tag{37}$$

To find the Longitude of the Ascending Node (Ω), the line of node is found with the unit vector $\hat{\mathbf{k}}$ of the body-centered equatorial frame and the specific angular momentum vector

$$\mathbf{N} = \hat{\mathbf{k}} \times \mathbf{h},\ N = \sqrt{\mathbf{N}\cdot\mathbf{N}} \tag{38}$$

The Longitude of the Ascending Node must be placed in the correct quadrant, the value of N_y is checked to place Ω

$$\Omega = \begin{cases} cos^{-1}\left(\frac{N_x}{N}\right) & if\ N_y \geq 0 \\ 360 - cos^{-1}\left(\frac{N_x}{N}\right) & if\ N_y < 0 \end{cases} \tag{39}$$

Eccentricity is found using vectors or only scalars as shown below

$$\mathbf{e} = \frac{1}{\mu}\left[\left(v^2 - \frac{\mu}{r}\right)\mathbf{r} - r v_r \mathbf{v}\right] \qquad e = \sqrt{1 + \frac{h^2}{\mu^2}\left(v^2 - \frac{2\mu}{r}\right)} \tag{40}$$

The argument of perigee also has a quadrant dependency based on the z-axis component of eccentricity.

$$\omega = \begin{cases} cos^{-1}\left(\frac{\mathbf{N}\cdot\mathbf{e}}{N}\right) & if\ e_z \geq 0 \\ 360 - cos^{-1}\left(\frac{\mathbf{N}\cdot\mathbf{e}}{N}\right) & if\ e_z < 0 \end{cases} \tag{41}$$

Finally, true anomaly can be found with quadrant depending on the radial velocity

$$\theta = \begin{cases} cos^{-1}\left(\frac{\mathbf{e}}{e}\cdot\frac{\mathbf{r}}{r}\right) & if\ v_r \geq 0 \\ 360 - cos^{-1}\left(\frac{\mathbf{e}}{e}\cdot\frac{\mathbf{r}}{r}\right) & if\ v_r < 0 \end{cases} \tag{42}$$

Rotation-

As all the bodies modeled and under study in this work have a measure of obliquity and are rotated to match the Neptune Equatorial reference frame. The position and velocity vectors are rotated using the rotation matrix

$$\boldsymbol{R}_x(\varepsilon) = \begin{bmatrix} 1 & 0 & 0 \\ 0 & \cos(\varepsilon) & \sin(\varepsilon) \\ 0 & -\sin(\varepsilon) & \cos(\varepsilon) \end{bmatrix} \tag{42}$$

where ε is the obliquity of the reference frame. The obliquity of the reference frames are given in Table 5.

Table 5. Obliquity (ε) terms for Neptune and Triton

Body	Obliquity, ε (degrees)
Triton	.7
Neptune	29.56

Once the reference frames have been rotated into alignment, they can be translated into a single frame.

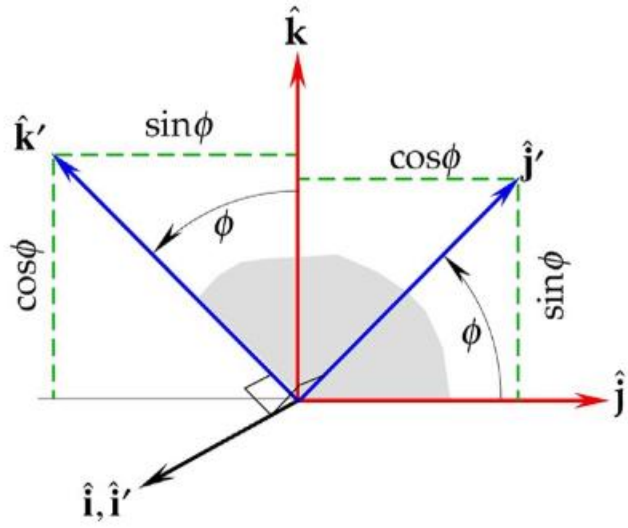

Figure 9- X-axis Obliquity Rotations where ϕ is obliquity from Table 5. (adapted from Curtis[1])

Translation-

Moving a reference frame from one center to another is done by adding the position vector from the center of the original frame to the center of the new frame. In the model used for integration the reference frames centered on the Sun and Triton are used to define the initial conditions of the satellite around Triton and Neptune around the Sun. The Sun's position around Neptune is the opposite vector of Neptune's position around the Suan. Since both reference frames are at the center of mass of the bodies (28) is simply the opposite vector of $\mathbf{r}_{sun/nep}$. Where $\mathbf{r}_{sun/nep}$is the vector from the Sun to Neptune.

$$\mathbf{r}_{nep/sun} = -\mathbf{r}_{sun/nep} \tag{44}$$

For the satellite, the initial conditions are set up in the Triton centered reference frame where $\mathbf{r}_{tri/sat}$ is the vector from Triton to the satellite and $\mathbf{r}_{nep/tri}$ is the vector from Neptune to Triton. This results in

$$\mathbf{r}_{nep/sat} = \mathbf{r}_{nep/tri} + \mathbf{r}_{tri/sat} \tag{45}$$

State vectors and Energy

Once the position vectors of all the bodies are shifted to a Neptune centered equatorial frame, the initial state vectors of all the bodies can be framed as

$$\mathbf{state}_i = [r_x, r_y, r_z, v_x, v_y, v_z] \tag{46}$$

Utilizing the norm of the r-vector and v-vector the state of any body, but in particular the satellite can be converted into a two-body energy statement where the energy E of the satellite is a constant. The expression

$$E = \frac{v^2}{2} - \frac{\mu}{r} \tag{47}$$

consists of a kinetic and potential term. The kinetic being $v^2/2$ and the potential term is $-\mu/r$. The two body energy is useful in this study as a satellite with positive energy is usually in a hyperbolic orbit and a satellite with negative energy has been captured or is in a closed orbit around the primary body. The 'vis viva' equation, as it is called, is a measure of the specific mechanical energy of the satellite or body and describes how energy is conserved in the two-body problem. The energy equation is utilized at the end of the orbit discovery process to estimate the Δv between the escape trajectory and the stable orbit trajectory of the initial reverse time integration. The satellite's energy is measured from the initial conditions of the reverse time integration that resulted in a reverse time escape until the satellite no longer escapes. As the energy is slowly reduced, the orbital radius is held constant at the initial conditions. The new orbital velocity is determined form the new energy state and the vis-viva equation (47). The velocity difference between the escape trajectory and the final 'stable' orbit found by the energy reduction technique is the Δv savings gained through the capture of the satellite using natural perturbations.

Measures of Stability and Chaos

The primary techniques used to identify instability and chaotic behaviors were analysis of end states, r-bar, and two Perturbation Indices. The analysis of end states was accomplished by plotting the end state of a satellite on a matrix of initial conditions varying in semi-major axis and eccentricity. Three end states were considered, collision with Triton, escape from Triton, and still in orbit around Triton at the end of the integration period. Escape was considered to have occurred when the eccentricity of the satellite's orbit reached or exceeded 0.99. Collision was considered to have occurred when the orbital radius of the satellite fell below the average radius of the surface of Triton. When plotted, the plot was inspected and areas where the end state changed quickly or several times in the space of a small change in eccentricity or semi-major axis initial conditions were found and considered as initial indicators of potential chaotic behavior.

r-bar-

The r-bar technique measures the average radial distance from the primary body to the satellite over the total integration time. The expression

$$\bar{r} = \left(\frac{r_{max} - r_{min}}{r_{initial}}\right) \tag{48}$$

shows the average radial distance with respect to the initial orbital radius. Values of zero or near to zero indicate very little change in the orbital radius over the integration time. This is a generally potentially stable orbit from the initial conditions. If the value is very high or changes in a short period of time, depending on how it is plotted, it is an indication that chaotic behavior may be present in that orbital region. While r-bar is not a direct measure of chaotic behavior it is useful to approximate the behavior of eccentricity changes when eccentricity cannot be directly calculated.

Perturbation Indices-

Perturbation indices and their associated plots are generated by using the integral of the disturbing accelerations of a satellite in an n-body calculation. In the literature there are four types of Perturbation Indices[18]. For the work in the thesis indexes two and four are the most relevant to finding potential chaotic motion. All the indices are divided by the total integration time to enable comparisons between different initial conditions and integration times.

PI_{ii} is the integral of the disturbing accelerations with respect to the direction of the velocity of the satellite. It is specifically the integral of the dot product between the sum of the disturbing accelerations, $\boldsymbol{a}$ and the unit vector of the velocity of the satellite, $\hat{\boldsymbol{v}} = \boldsymbol{v}/|v|$ over the total integration time, T.

$$PI_{ii} = \frac{1}{T}\int_0^T (\boldsymbol{a} \cdot \hat{\boldsymbol{v}})\, dt \tag{49}$$

When PI_{ii} is calculated and plotted it will show the average energy change experienced by the satellite over the integration time. A positive number indicates that the satellite experiences a net energy gain and thus moves to a higher orbit towards escape. A negative number indicates a net energy loss and a movement of the satellite to a lower orbit and a possible collision if the energy loss persists.

PI_{iv} is calculated using the integral of the vector $\boldsymbol{A} = \ddot{\boldsymbol{r}} - \ddot{\boldsymbol{r}}_{ref}$ over the three axes x, y, and z the normalizing them into the magnitude PI_{iv}. $\ddot{\boldsymbol{r}}_{ref}$ is the acceleration of the satellite along a reference orbit between the primary body and the satellite in a two-body approximation. $\ddot{\boldsymbol{r}}$ is the total acceleration of the satellite in the full model. In the integration below T is the total integration time over which p_j is calculated and where $j = x, y, z$.

$$PI_{iv} = \left(p_x^2 + p_y^2 + p_z^2\right)^{1/2}$$

$$p_j = \frac{1}{T}\int_0^T A_j \, dt \tag{50}$$

The PI_{iv} results give the total acceleration from the perturbative forces over the integration time. High values indicate a greatly perturbed orbit where low values indicate an orbit that is not under the influence of very many additional forces. In the work of this thesis the Perturbation Indices are calculated for the satellite around Triton and used to help determine the areas where chaotic motion is most likely among the sets of initial conditions.

Chapter 3. Methods and Simulation Details

The simulation of the Neptune-Triton-Sun-Satellite system was built up in the Python [*] programming language. The standard numpy[†], scipy[‡], and matplotlib[§] packages were utilized to create the orbit simulator and iterators.

<u>Orbit Simulator</u>-

The orbit simulation portion of the program sets the initial conditions of the iteration of the acceleration of the satellite and other bodies in a Neptune centered equatorial cartesian coordinate system. The Orbit Simulator calculates the path and behavior of a single satellite around Triton.

[*] https://www.python.org
[†] https://numpy.org/
[‡] https://scipy.org/
[§] https://matplotlib.org/

The initial conditions for the natural bodies are set from the JPL Horizons ephemeris system[**] locations for the natural bodies at 1 January 2000. The natural bodies initial conditions are not changed throughout the rest of the iterations/work done in the thesis. The satellite initial conditions are set using perifocal orbital elements. The initial conditions of the satellite and all the bodies are converted to a 1 x 18 state vector for the Initial State to be input to the iterator.

$$Intial\ State = \begin{bmatrix} r_{sat,x} \\ r_{sat,y} \\ r_{sat,z} \\ v_{sat,x} \\ v_{sat,y} \\ v_{sat,z} \\ r_{tri,x} \\ r_{tri,y} \\ r_{tri,z} \\ v_{tri,x} \\ v_{tri,y} \\ v_{tri,z} \\ r_{sun.x} \\ r_{sun,y} \\ r_{sun,z} \\ v_{sun,x} \\ v_{sun,y} \\ v_{sun,z} \end{bmatrix}^T \tag{51}$$

The iterator used is the 'solve_ivp'[††] function that is a standard part of the scipy package for Python. The 'sovlve_ivp' function takes in a statement of the derivatives in question (usually a function itself), the time span of integration in seconds, and an initial state vector at minimum. Additionally, any events that need to be tracked or cause the integration to terminate, the method of integration, integration step size, and relative and/or absolute tolerances for solutions can be set as well. Events tracked in the simulation were 'Escape' and 'Collision.' Escape was set as the eccentricity of the orbit of the satellite around Triton exceeding 0.99. Collision was set as occurring when the norm of the r_{sat} vector became lower than the radius of Triton. Both were 'terminal' events and would end the simulation and plot the results up to the last integration time step. In the implementation of this thesis the method of integration used was the 'LSODA' method. The LSODA method is a wrapper for the ODEPACK solver for Fortran. Integration size was also specified in the

[**] https://ssd.jpl.nasa.gov/horizons/

[††] *https://docs.scipy.org/doc/scipy/reference/generated/scipy.integrate.solve_ivp.html*

implementation to ensure accurate capture of the satellite's motion around Triton. The time step in the integrator was set to be the orbital period of the satellite determined from the initial conditions in seconds divided by one hundred ($dt_{selected} = T_{sat}/100\ sec$). The derivatives function input into the solver contains the Equations of Motion for the natural bodies and the satellite in the Neptune centered Equatorial Frame. In the following derivatives, all the **v** terms are taken from the initial conditions state vector. The **p** terms of the perturbing forces are given after the Equations of Motion. The equations of motion of the satellite are

$$\dot{\mathbf{r}}_{sat} = \mathbf{v}_{sat} \tag{52}$$

$$\ddot{\mathbf{r}}_{sat} = -\mu_{Neptune}\left(\frac{\mathbf{r}}{r^3}\right) + \mathbf{p}_{Triton} + \mathbf{p}_{Sol} + \mathbf{p}_{J2_{Triton}} + \mathbf{p}_{J2_{Neptune}} \tag{53}$$

Triton's motion is governed by the following equations

$$\dot{\mathbf{r}}_{tri} = \mathbf{v}_{tri} \tag{54}$$

$$\ddot{\mathbf{r}}_{sat} = -\mu_{system}\left(\frac{\mathbf{r}}{r^3}\right) + \mathbf{p}_{Sol} + \mathbf{p}_{J2_{Neptune}} \tag{55}$$

The equations of motion governing the motion of the sun relative to Neptune are given as

$$\dot{\mathbf{r}}_{sun=}\,\mathbf{v}_{sun} \tag{56}$$

$$\ddot{\mathbf{r}}_{sat} = -\mu_{sun}\left(\frac{\mathbf{r}}{r^3}\right) \tag{57}$$

For the natural body perturbations, the general form of the $\boldsymbol{p}_{body}$ force term in (39) and (41) is given as

$$\boldsymbol{p}_{body} = \mu_{body/sat}\left(\frac{\boldsymbol{r}_{body/satellite}}{\boldsymbol{r}^3_{body/stellite}} - \frac{\boldsymbol{r}_{body/primary}}{\boldsymbol{r}^3_{body/primary}}\right) \tag{58}$$

The *body* is the perturbing body in the system and the *primary* is the body in the center of the Neptune Equatorial coordinate system. Figure 4 shows the vector relationships of (44). The J_2 expression from (28) is re framed more specifically as

$$\boldsymbol{p}_{J_{2-body}} = \frac{3J_2\mu_{body}R^2}{2r^4}\left[\frac{x}{r}\left(5\frac{z^2}{r^2} - 1\right)\hat{\mathbf{i}} + \frac{y}{r}\left(5\frac{z^2}{r^2} - 1\right)\hat{\mathbf{j}} + \frac{z}{r}\left(5\frac{z^2}{r^2} - 3\right)\hat{\mathbf{k}}\right] \tag{59}$$

with **i, j, k** the unit vectors in the body centered equatorial frame and r the radius from the body's center of mass. The R term is the equatorial radius of the body and x, y, z are the appropriate distances making up the radius vector of the satellite's orbit. When called, 'solve_ivp' outputs a "state" vector and a "time" vector. Where the state vector corresponds to the Initial State with radius and velocity information at each time interval and the time vector is a single large vector of the time in seconds stepped through by the $dt_{selected}$ value. The program then uses the iteration data to plot the orbit and other relevant information, elements, and values. The program reverses reference frame shifts and rotations and converts cartesian vector information back to perifocal elements when appropriate and necessary. Finally, the program plots the information of interest for further analysis.

Iterator program-

To test a large number of initial conditions in one computing run, an iterating program was built to vary the semi-major axis and eccentricity of the satellite's initial orbit around Triton. A nested loop was utilized to iterate through the initial configurations. The previously setup process of orbit propagation over time was used and the outcome of each initial configuration was plotted on a color map.

Initial conditions-

The positions of the natural bodies in the study were taken from JPL Horizons Ephemeris database for the date of 1 January 2000. All initial integrations forward or backward in time start at this same configuration. The satellite's initial conditions vary depending on the initial conditions (IC) matrix. The IC matrix was two-dimensional, the x-axis varied the semi-major axis (SMA) from 2476.4 km to 19,811.2 km. The y-axis varied the eccentricity (ECC) of the satellite's initial orbit from 0.005 to 0.9. The values used were settled on after initial calculations showed those ranges encompassed all the orbits that were of interest to the study.

Duration and Resolutions of Integrations-

Integrations of the satellite's motion from the IC matrix were conducted on the time scale of 30 days, 1 year, 5 years, and 10 years both forward and backward in time. Computation times for the different integration periods range from a few seconds for a 30 day integration to 30+ hours for the 10 year plots. The computation time was the same for forward and backward computations. To minimize computation time the resolutions of the plots are adjusted. A 200 x 200 or 175 x 175 initial conditions matrix is used for the 30 day and 1year integrations as this provided enough detail to identify "Focus Areas" of likely chaotic motion. The "Focus Areas" were then integrated with resolutions up to 450 x 450. The 5-year and 10-year integrations were lengthy even with a reduced resolution of 100 x 100. The longer integrations were split into several smaller bands of Initial Conditions and then stitched together for the final 100 x 100 plot.

Forward Time Integration of Backward Time Escape Trajectories-

There are three integrations that are performed in this analysis. When performed and analyzed in sequence they yield a potential trajectory for a chaotic capture of the satellite around Triton. The first integration is a forward time integration from the Initial Conditions matrix described previously. This integration is used to find the potentially stable orbits around Triton while the satellite is affected by the other perturbing forces. The second integration is a backward time integration from the same Initial Conditions matrix as the first forward time integration. The goal of the second integration is to identify escape events that occur from the initial conditions. The third integration is performed with the end state of the reverse time integrations used as the initial conditions for a forward time integration. The integration is performed in forward time for slightly longer than the backward time integration and is filtered to not perform the integration for any reverse time initial conditions that start inside Triton, i.e. ended in collision. From this integration the results of interest are the initial states that originated from a reverse time escape that end in a capture or escape. The forward integration was performed in two different ways. The initial plot is a large map of the results on the same scale as the initial conditions. The second way the forward time plots are shown is with individual trajectories plotted forward from the reverse trajectory initial conditions. The sequence of integrations and plots is a technique that was used to identify a set of initial conditions that result in a natural capture event into a potentially stable orbit around Triton. The initial conditions are the end state conditions from the reverse time escape that when run back forward time resulted in a capture that leads to similar initial conditions for the first forward time integration. Figure. 9 presents the process visually, demonstrating the connections between the different integrations.

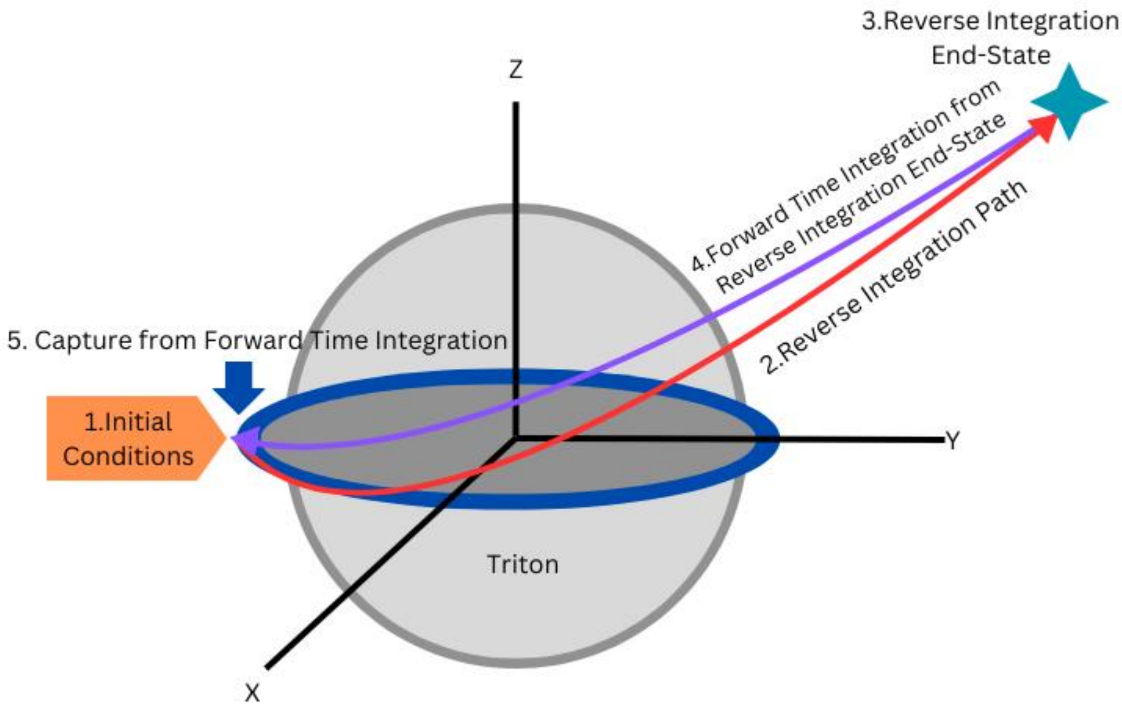

Figure 10- Method of Finding Chaotic Captures

Finding the Specific Trajectories of Captures to Potential Stable Orbits-

The plots following in the results section were used as aids to find and focus on the areas most likely to have the characteristics necessary for the kind of natural chaotic capture described above. Specific initial conditions were integrated with the non-iterating orbital simulator to generate a plot of the trajectory of the satellite and the two-body orbital elements with respect to Triton. The results of the plots were used to determine the utility of the trajectory to specific mission planning.

Chapter 4. Results

The integrations were carried out with the assistance of the OU Supercomputer Center for Education and Research (OSCER)[‡‡] and two commercial commercially available laptops. The Python code for the simulation was run multiple times on the various processors and the outputs collated and analyzed. This chapter explains the output plots and describes the results obtained.

‡‡ https://www.ou.edu/oscer

Analysis Techniques

Four main analysis techniques were used to identify areas of potential chaotic motion; time in orbit, stability analysis, the two perturbation indices, and the value of r-bar. Each technique provides a piece of information on the nature of the orbits calculated from the initial conditions matrix. These pieces of information are combined with the forward time integrations from the end state plots to find the most likely places for chaotic, natural capture of a satellite. Once the desired combination of end-states are identified, the actual trajectories of the specific initial conditions are simulated and can be further analyzed using traditional orbital mechanics. Resolutions varied from 100 x 100 to 500 x 500 points along each axis in the initial conditions matrix. Utilizing higher resolutions of the initial conditions matrix revealed additional details and potential areas of interest. Lower resolution was used on the longer integration times as the plots did not change significantly after more than 1-year. The highest resolution plots were performed on focus areas with the best indications of chaotic potential. Integrations were calculated for 30-day, 1-year, 5-year, and 10-year integration times. The integrations were run in both forward and backward time.

Orbital Duration

The first measure of the orbit found from a particular set of initial conditions is the length of time a satellite stays in orbit around Triton. The plots of orbital duration are shown on a spectral colormap over the grid of initial conditions. In the forward time plots, the colors range from red for short stability time to blue for long stability time. Fully saturated red indicates orbital stability of zero or near zero length of time, while fully saturated blue indicates that the integration ran for the total time of integration. In each plot there are revealed areas that have a long orbital duration around Triton, areas of low orbital duration, and areas of duration in between. The shape of the areas and proximity to each other can indicate areas of potential chaotic motion. Sections of the plot with long duration times bordering closely areas with shot duration times were the primary areas of interest of the study.

Stability, End State definitions

The ‘end state’ of the satellite is one of three options in the scope of the study; stable, collision, and escape. The satellite is considered to have ‘escaped from Triton’s orbit when the eccentricity of the satellite’s orbit exceeds 0.99. The satellite will be considered to have collided with the surface of Triton if the orbital radius of the satellite’s orbit falls below the average radius of Triton of 1352 km. For the purposes of this study any orbit that has not escaped or collided with the primary body over the integration time is considered 'stable.' The stability plots consist of three colors mapped on the initial conditions grid: grey for escape, blue for collision, and green for 'stable' orbits. The areas of interest for the study are the places where escape and stable meet or are interleaved. Other areas of note are the structures of collision surrounded by escape, these 'filaments' of collision end states are indicative of a close pass of the satellite to Triton that results in a hyperbolic orbit or a collision if the pass is too close to Triton.

<u>R-bar</u>

The r-bar values are plotted using a 'terrain' style color map overlaid on the initial conditions matrix. Deep blue hues are values of zero or near zero. The palette moves from blue to green then yellow and brown. Areas of white have the highest values of r-bar, usually over four. Similarly to the previous plots areas of interest are those areas where values change rapidly over a short interval of either initial condition axis. The most interesting points are the areas where there is a large value surrounded by smaller values of r-bar.

<u>Perturbation Indices</u>

The perturbation maps are color maps plotted over the initial conditions matrix. Both P_{ii} and P_{iv} are plotted separately as averages over the integration time. The P_{ii} map is centered on zero and spans positive and negative 0.1 m/s per day. The values may be higher or lower than the range of the scale, but for the purposes of the current study the effects of higher values are not pertinent as the outcomes measured would be the same. Visually, the deeper the brown hue on the plot, the more energy is depleted from the satellite's orbit per day. Conceptually, "brown is down" is a way to think about the plot as a loss of energy will decrease the satellite's semi-major axis and lead to a collision with Triton if no other forces intervene. The green/blue hue follows the mnemonic that "green is good," as green is indicative of positive energy change on the satellite's orbit. The positive energy over time will result in an escape from Triton's orbit. An orbit that is near zero average P_{ii} will tend to keep the same semi-major axis as the average energy change of the satellite is very small. For the study, areas in the initial conditions matrix that have a rapid change in P_{ii} over a small difference in initial conditions. P_{iv} plots mapped over the initial conditions matrix uses a brown to purple color map. P_{iv} is a measure of total perturbation averaged over the integration time. Fully saturated brown on the plot is a zero or near zero value of the perturbation index. Fully saturated purple is a relatively large value, for the satellite, Triton, Neptune, Sun system. Similarly to the P_{ii} plot, the areas of interest on the P_{iv} plot are areas with moderate perturbations near areas of little to no perturbation. An area with little to no perturbation at all would be more likely to be stable and not a candidate for chaotic capture or escape.

Two-body Energy Relative to Triton

The final plot is the two-body energy relative to Triton. The plot is made over the initial conditions matrix like the other plots. The plot shows the energy state at the end of the integration. The plot is in a green scale in units of km^2/s^2. Bright yellow-green is positive energy state while a dark bluish color is an negative energy state. The saturation value of the negative depends on the plot and was selected to highlight variations and structures in the energy state plot for each integration. Energy greater than zero is an escape trajectory, after the energy becomes positive the actual value is of lesser importance as the fact that the energy is positive. The energy plot was compared to the stability plot for each integration time. It is desired to find areas on the perturbed stability plot that are escape trajectories, but that still have negative energy on the two-body energy with respect to Triton. Trajectories that escape with negative energy are the goal of the study to identify and quantify.

Forward Time Plots

The forward integrations were run for 30-days, 1-year, 5-years, and 10-years. Each integration was plotted on a grid of initial conditions of semi-major axis and eccentricity. The plots included the previously described, orbit duration, stability plot, r-bar, and Perturbation Indices. The forward plots were used to identify potential areas of chaotic behavior and areas where orbits were 'stable' to narrow down the areas of interest in the reverse time plots.

Orbital Duration

The orbital duration plots for the satellite in forward time show that long term stability, by the definitions of this study, occurs in a region with a semi-major axis of 4000 km to 9000 km and eccentricity of zero to 0.3. The 30-day plot demonstrates the most variation in orbital duration. The 200 x 200 resolution plot shows the main area of 'stability.' There is also a definite central line of relatively longer orbits of fifteen days, with branching bands sometimes reaching the full thirty days of the integration in orbit. Each of the bands and their borders with the shorter stability orbits are good candidates for the types of orbit the study is looking to find. However, as integration time increases to one year at a resolution of 175 x 175, the main stability area starts to become more defined and the bands of potential stability start to fade. The bands near eccentricities of 0.34 to 0.4 and a semi major axis between 9000 km and 11000 km show some stability longer than thirty days and a few areas up to nearly two hundred days. The 5-year and 10-year plots are both 100 x 100 resolution and continue the trend begun between the 30-day and 1-year plots. Both plots show a well defined ‘stability’ area matching the initial dimensions noted in the 30-day plot. The bands of longer stability have all but disappeared outside the well-defined area, but the area between 8000 km and 9500 km is somewhat chaotic as there is not a clear transition between the satellite reaching the end of the integration time without collision or escape and not surviving more than 250 to 500 days. In contrast the border between long term duration and quick escape or collision when the satellite starts at a semi-major axis between 4000 km and 7000 km is very sharp. The plots show that a chaotic capture area is most likely to be short lived or in the 8000 km to 9000 region of the semi-major axis. While the duration plots are very useful, they do not show how the orbit met its end.

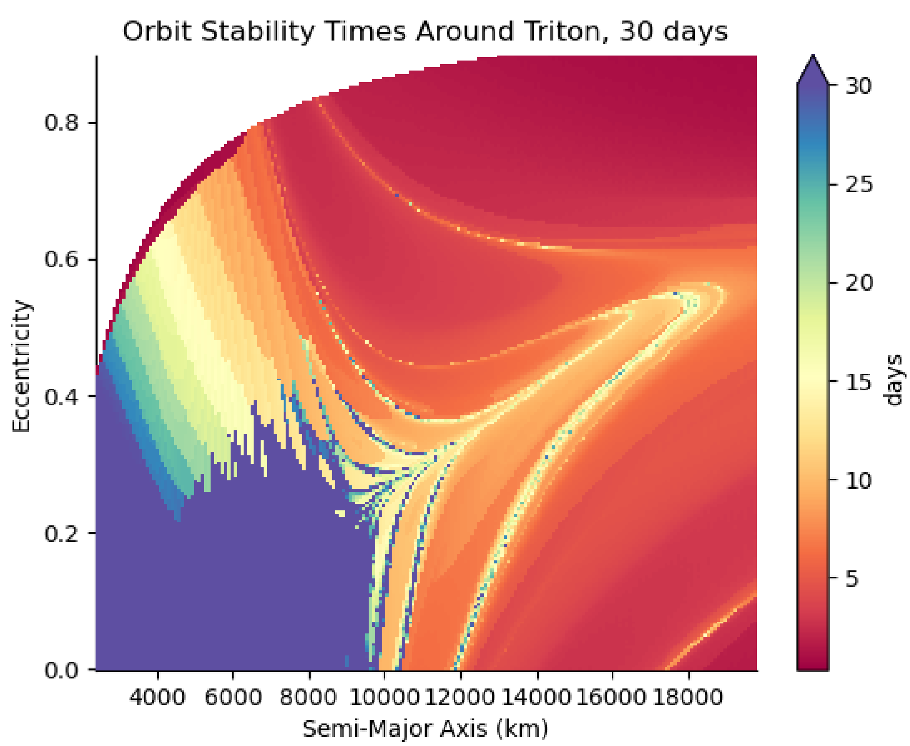

Figure 11- Orbital Duration, Forward Integration 30-days

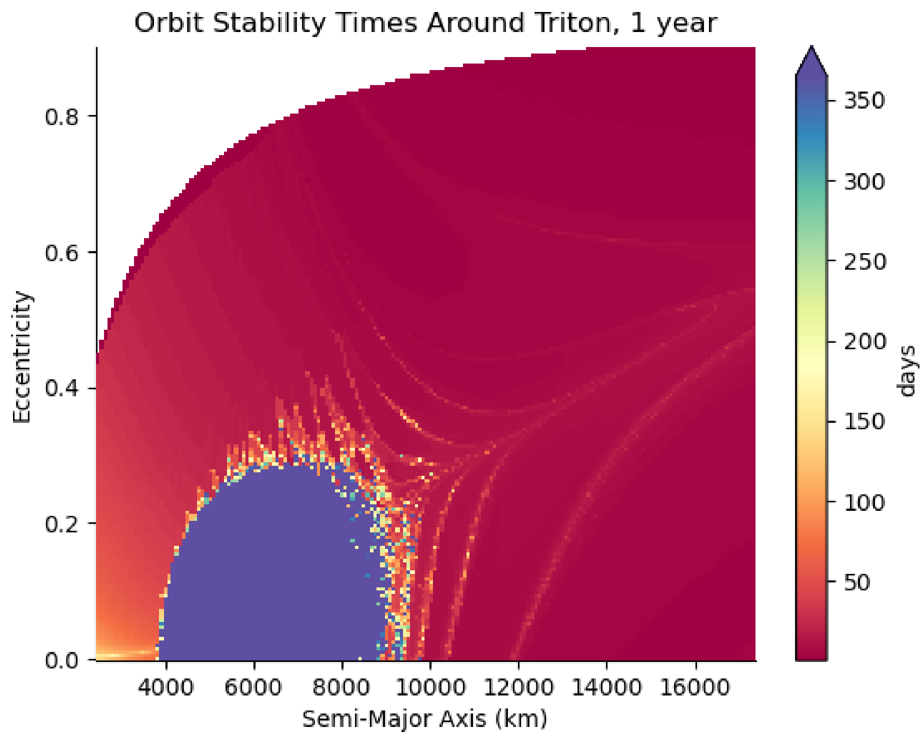

Figure 12- Orbital Duration, Forward Integration 1-year

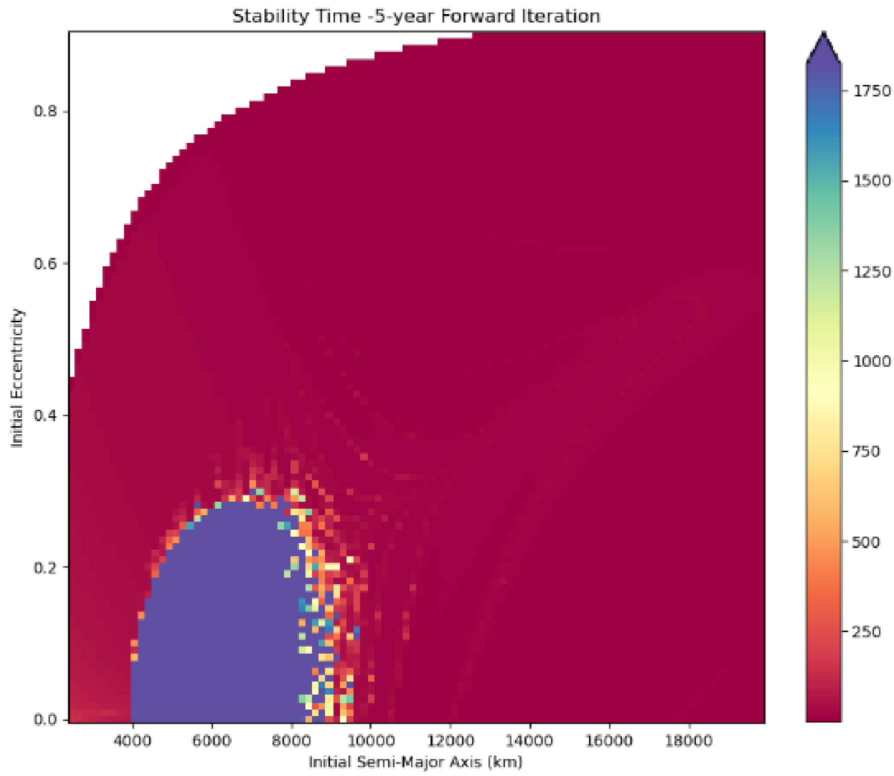

Figure 13- Orbital Duration, Forward Integration 5-years

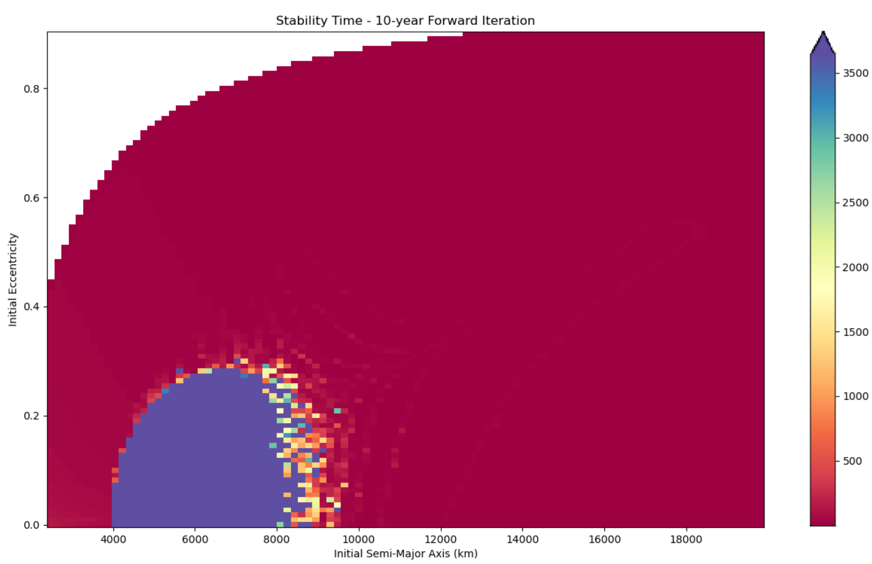

Figure 14- Orbital Duration, Forward Integration 10-years

Stability Plot

The stability plot shows the end-state of the satellite's orbit on the initial conditions matrix. All the stability plots reveal additional detail in the areas of low orbital endurance. In the orbital endurance plots, large areas are shown as having little to no orbital duration and in the stability plot what happens in those areas becomes clear. The structures of the collision/escape interactions reveal where close fly-by trajectories take place or initial conditions that will end up in a collision with Triton. The general trend from the stability area is a kind of funnel shape of collision trajectories surrounded by escape trajectories with the funnel narrowing as the semi-major axis and eccentricity increase together.

The end-states for the 30-day plot echo the plot of the 30-day orbital duration plot with the longest orbital duration times generally coinciding the green capture/stable areas on the stability plot. The bands of longer duration orbits also match up with the bands of capture/stable areas on the stability plot. The large long duration 'stability area' is mirrored on the 30-day plot as well. The one-year plot continues to mirror the orbital duration plot, however, it becomes clear that the large stability area between 4000 and 8000 km is bordered by collision trajectories more than escape trajectories. The 5-year and 10-year plots look very similar with only small differences between them. The stability area and the funneling of escape/collision end-states is still apparent and in generally the same areas of the initial conditions matrix. This suggests that after a year if the satellite is still in orbit, it is very likely that it will stay in orbit for a long period of time.

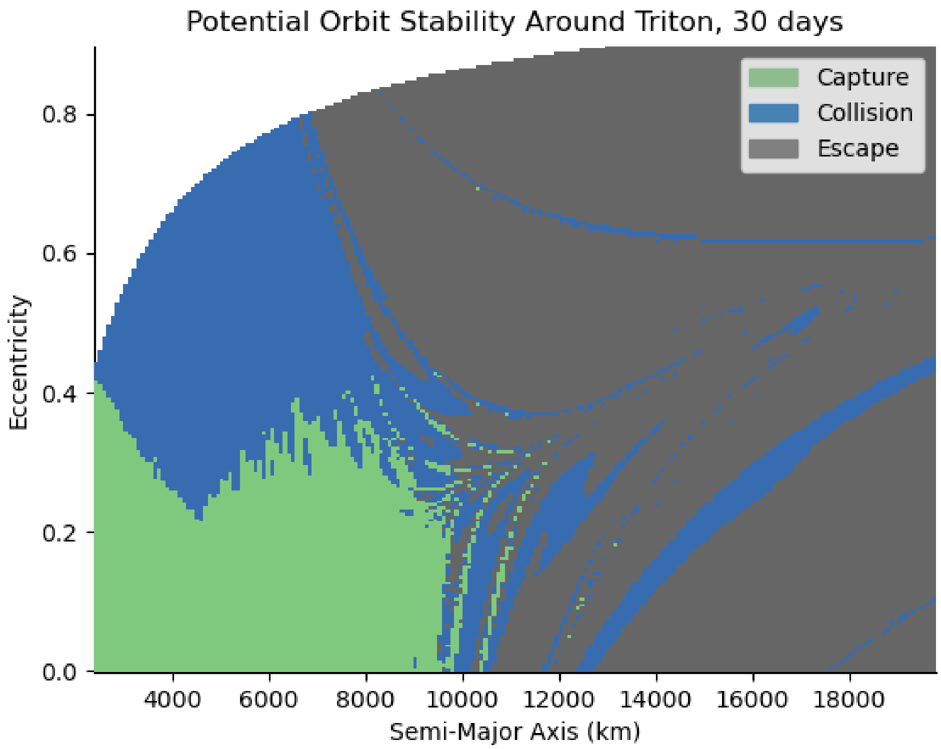

Figure 15- Stability Plot, Forward Integration 30-days

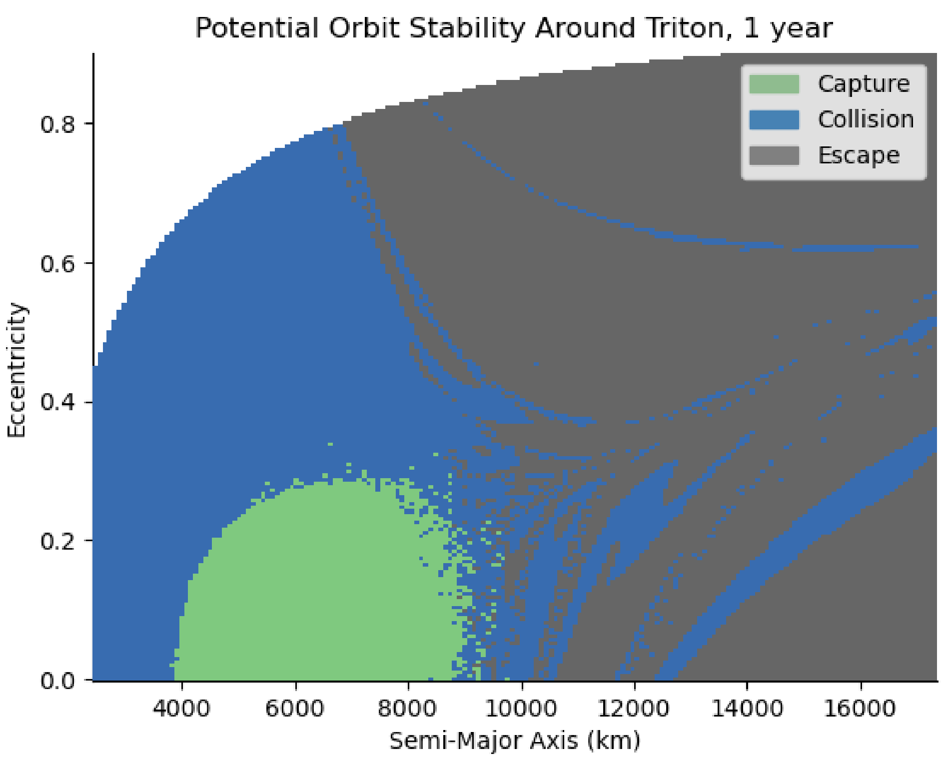

Figure 16- Stability Plot, Forward Integration 1-year

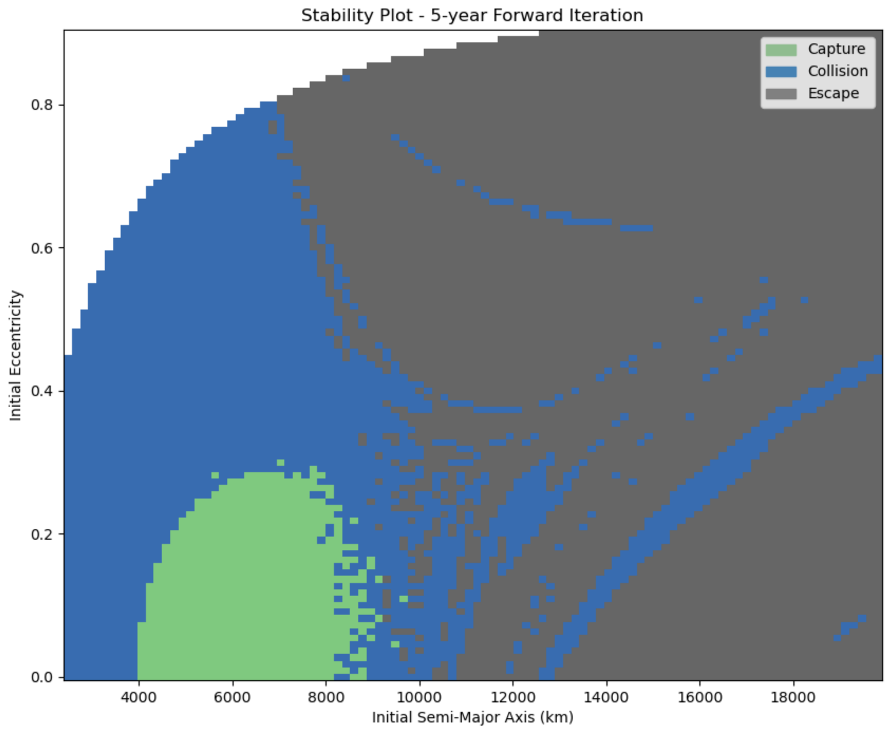

Figure 17- Stability Plot, Forward Integration 5-year

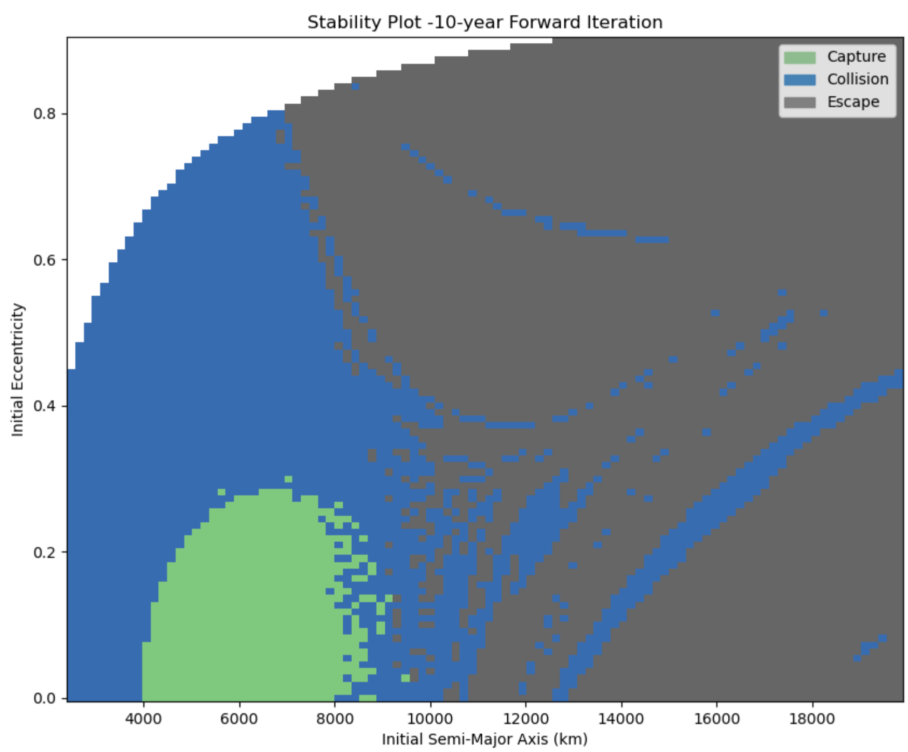

Figure 18- Stability Plot, Forward Integration 10-years

R-bar

The r-bar values, plotted on the initial conditions matrix using a 'terrain' style color map are uniquely suited to showing the variations in the orbits based on the initial conditions. The 30-day plot shows the most variation in orbit from the initial conditions as there are very few areas of less than one. In the 30-day plot there is an interesting 'filament' that is a line of zero-values of r-bar that form and move to the 'funnel' structure present in the plot. If a satellite was very accurately placed on a trajectory with those particular points as initial conditions it would stay in that orbit so long as the r-bar stayed zero. The line of values has a couple of echoes in the 1-year plot, as there are still a couple of short segments of near zero r-bar, but has disappeared for the most part. The rest of the 30-day plot shows the now familiar funnel shape of high r-bar values surrounded by lower values of r-bar. On the 30-day plot the brown areas edged with yellow are the areas of interest for finding chaotic motion. As the integration time increases to one year or more, the plots settle into a similar configuration. In the longer timeframe plots, there are a few areas around 16,000 – 19000 km with an eccentricity of zero to 0.2 that have low values. While they look as if they would be 'stable' areas, they are actually areas that are 'fly-by' trajectories that do not change over time.

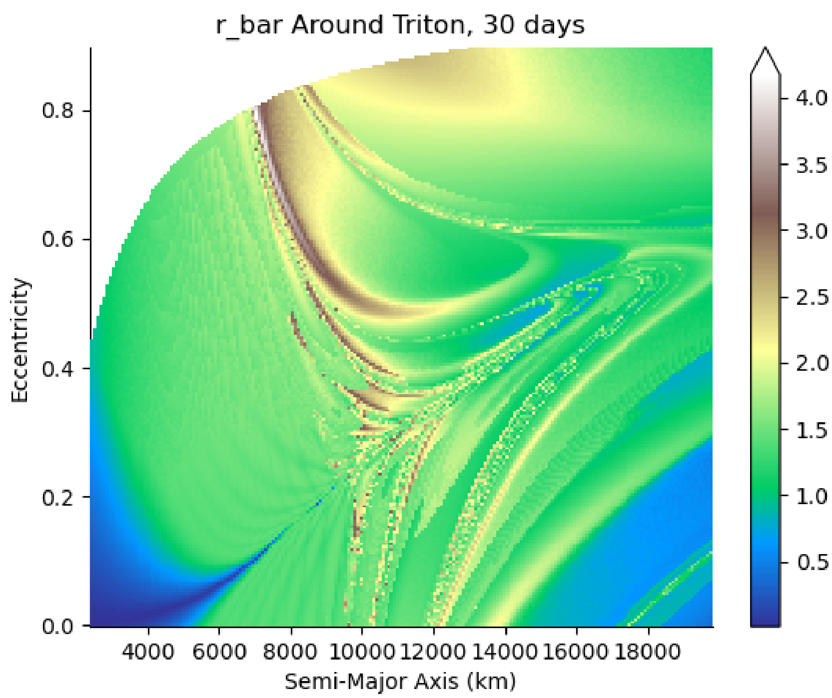

Figure 19- r-bar, Forward Integration 30-days

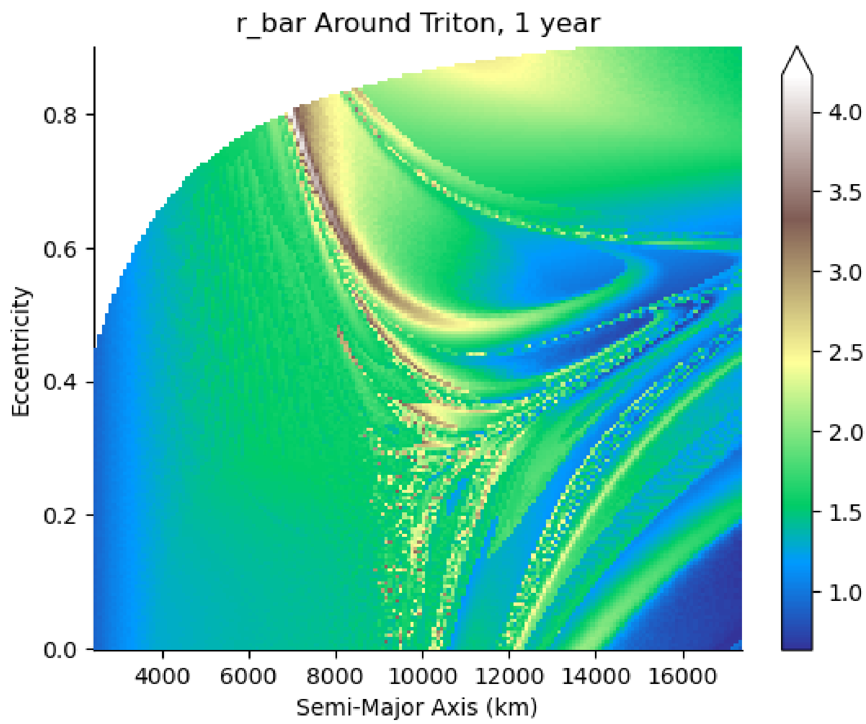

Figure 20- r-bar, Forward Integration, 1-year

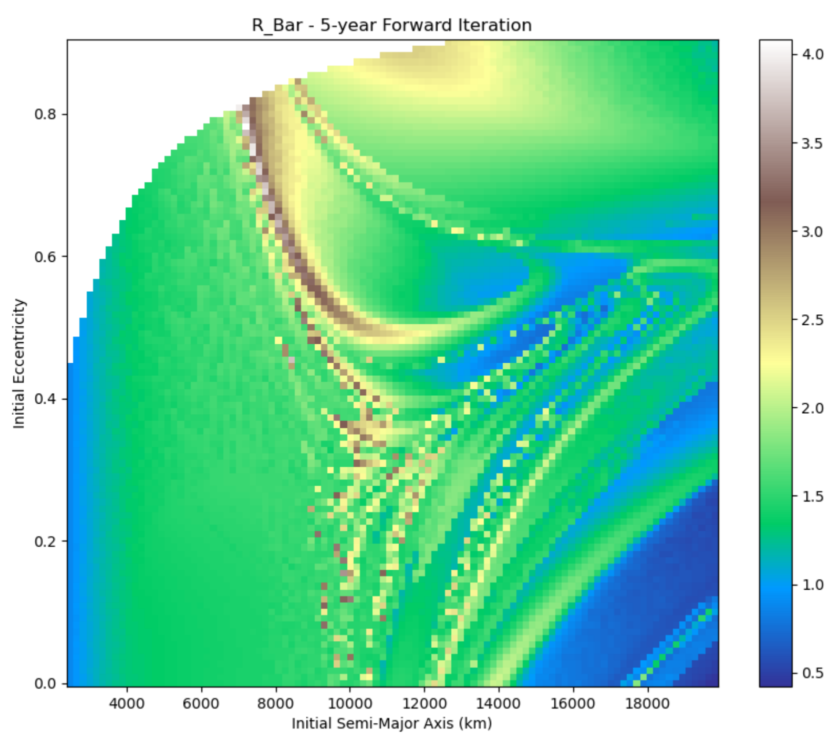

Figure 21- r-bar, Forward Integration, 5-years

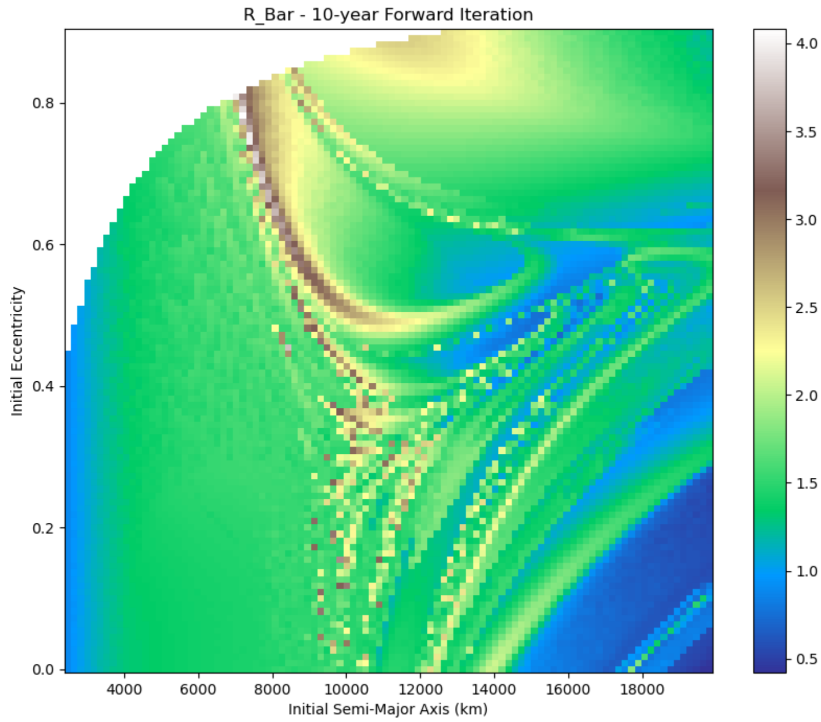

Figure 22- r-bar, Forward Integration, 10-years

<u>Perturbation Indices</u>

The two Perturbation Indices were plotted on the initial conditions matrix as well. Both indices are plotted in $m/_s$ per day with P_{ii} the average of the total perturbation along the velocity vector of the satellite for the integration time and P_{iv} being the total average perturbation force on the satellite. The 30-day and 1-year plots are very similar as they have same initial conditions, but there are some small changes as the average P_{ii} and P_{iv} changes over time. Interestingly, some close fly-by trajectories of the satellite that escape show a negative P_{ii} as the initial inbound perturbation is very strong. The rest of the plots do show areas of little to no perturbation in the more stable regions already identified. After analyzing the r-bar, orbital duration, and P_{ii} plots, the P_{iv} plot does not present any unexpected new results but does help show how quickly a particular trajectory will change over time based on the average acceleration per day.

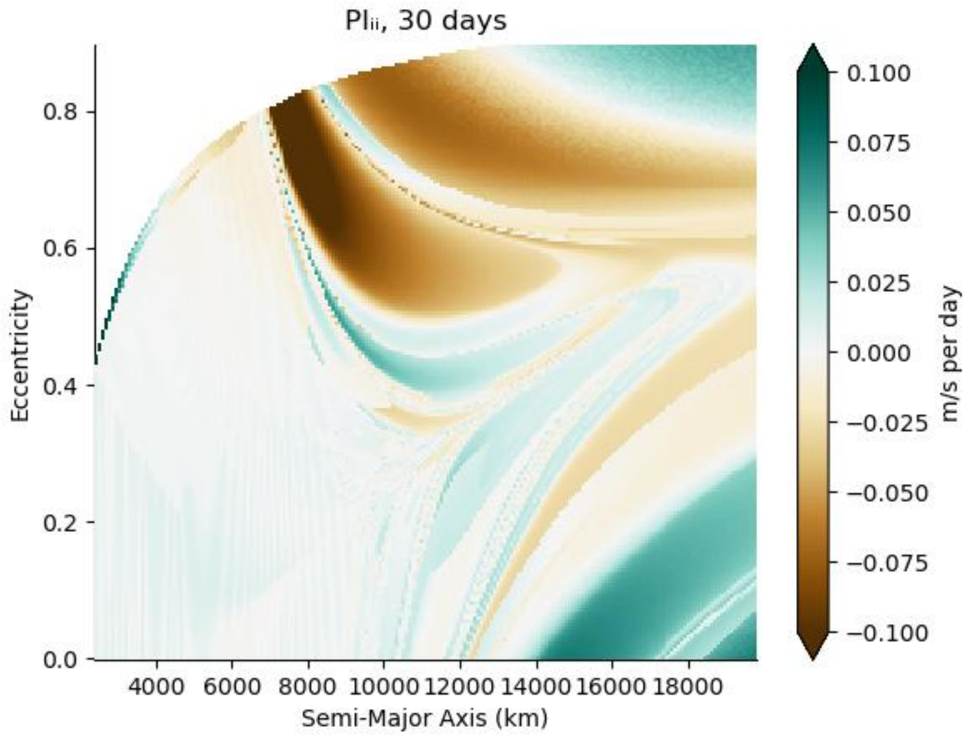

Figure 23- P_{ii}, Forward Integration, 30-day

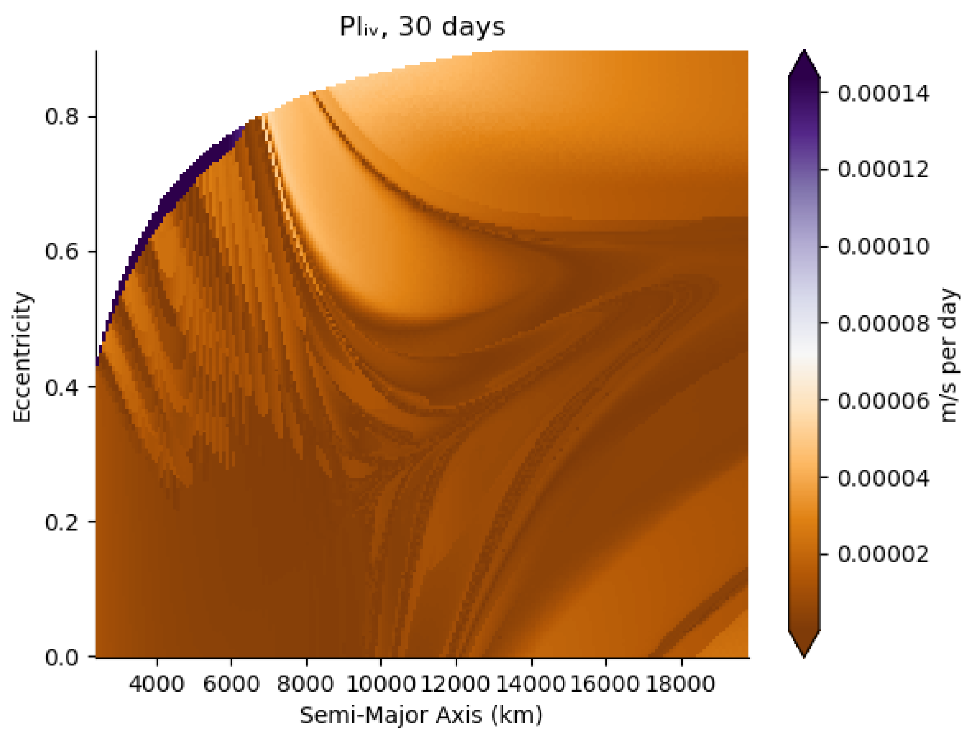

Figure 24- P_{iv}, Forward Integration, 30-day

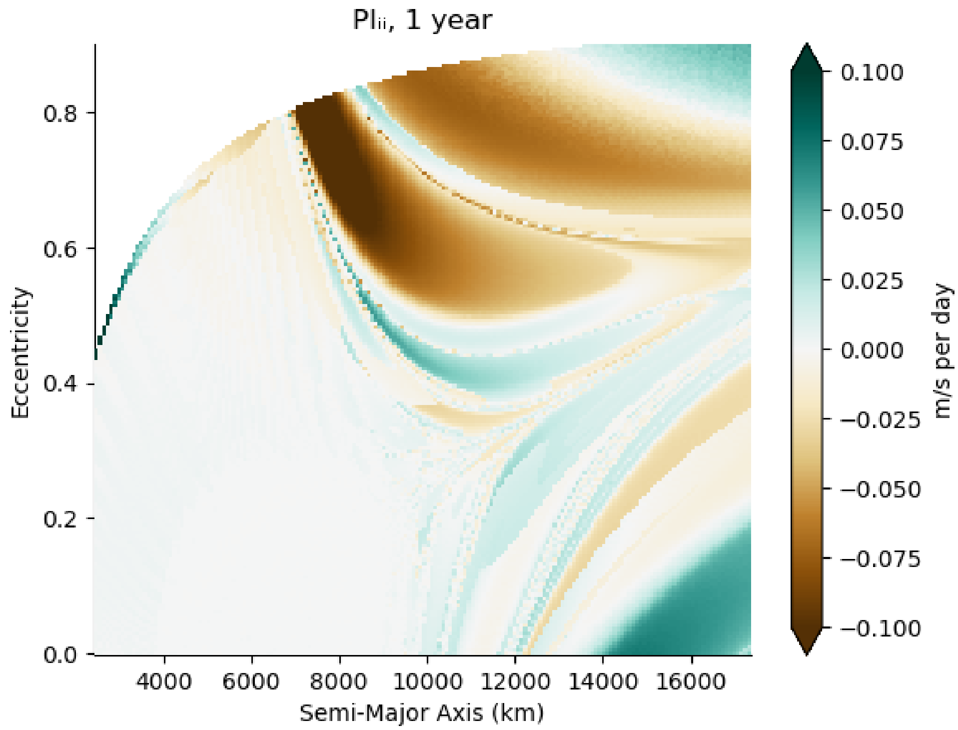

Figure 25- P_{ii}, Forward Integration, 1-year

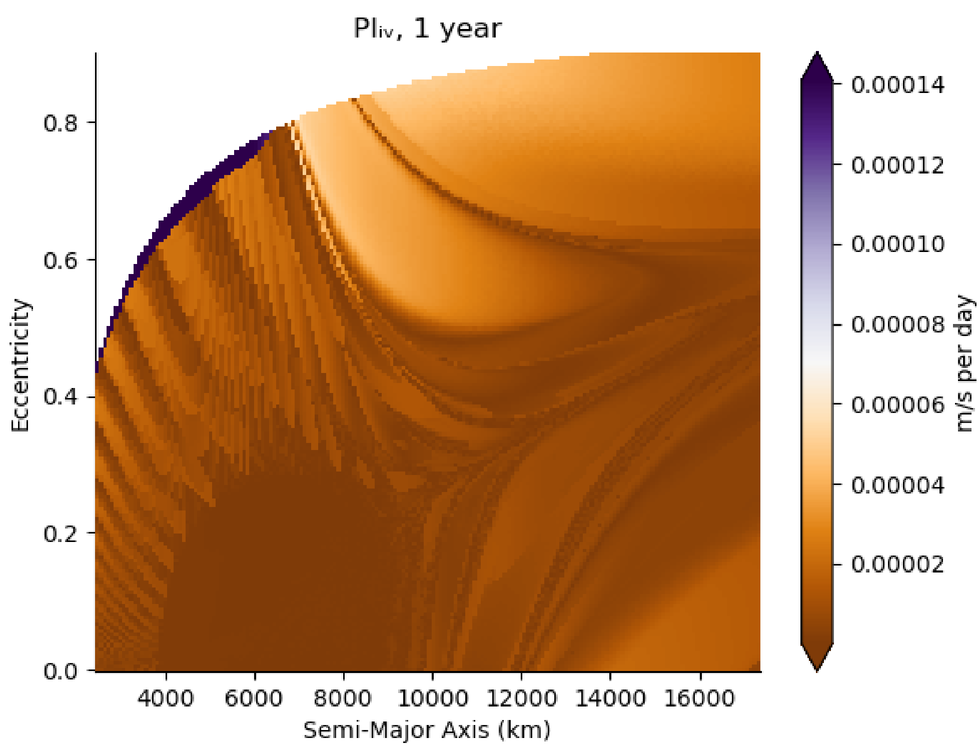

Figure 26- P_{iv}, Forward Integration, 1-year

Triton 2-body Energy

The 2-body energy plots for the initial conditions matrix are very similar across all the integration times. As many of the escape events happen at the same time during the integration, this is an expected result. When looking for areas that could enable a satellite to be captured with negative energy in relation to Triton, the areas will be near a positive energy region and bordering it in slightly negative in energy. Another good potential area to find the orbits of interest are the areas that have positive and negative energy interleaved between each other. An example would be the band of 'static-y' negative energy that starts at 12000 km and 0.0 eccentricity and arcs toward higher eccentricity and semi-major axis. An additional example is the region of semi-major axis between 9000 km and 11000 km and eccentricity of zero to 0.35.

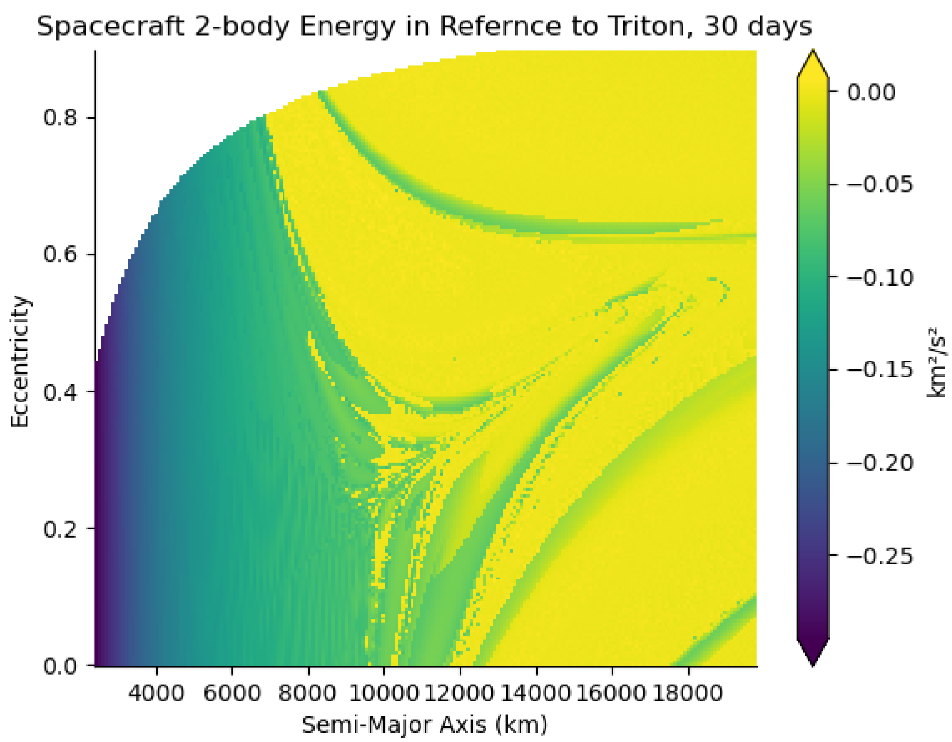

Figure 27- Two-body Energy with respect to Triton, Forward Integration, 30-days

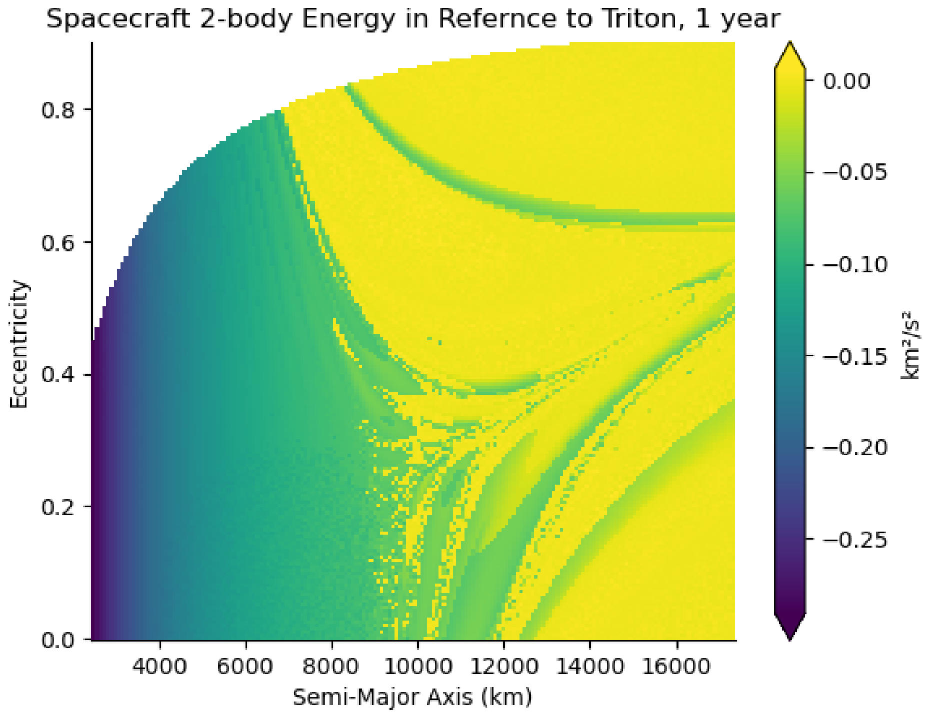

Figure 28- Two-body Energy with respect to Triton, Forward Integration, 1-year

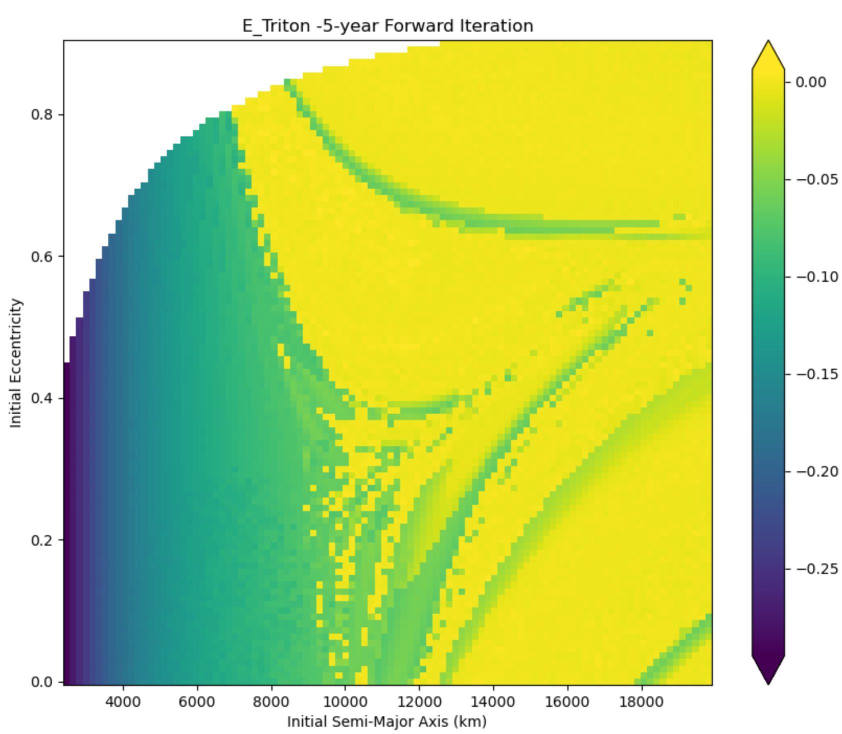

Figure 29- Two-body Energy with respect to Triton, Forward Integration, 5-years

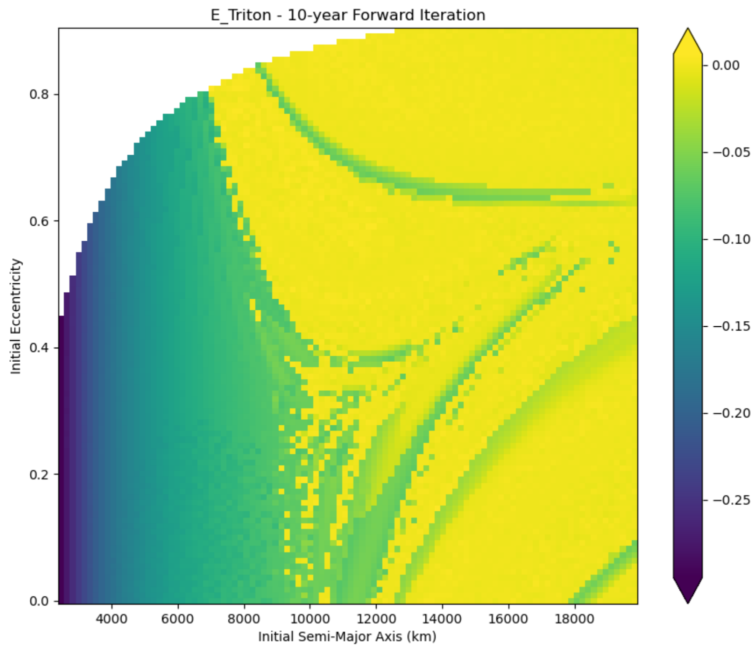

Figure 30- Two-body Energy with respect to Triton, Forward Integration, 10-years

Reverse Time Plots

The reverse integrations were run for 30-days, 1-year, 5-years, and 10-years. Each integration was plotted on a grid of initial conditions of semi-major axis and eccentricity. The plots included the previously described, orbit duration, stability plot, r-bar, and Perturbation Indices. Reverse time integrations were accomplished to identify areas of potential chaotic behavior and more specifically determine which initial conditions yield an escape in reverse time that correspond to a 'stable' orbit in forward time. The orbits that escape in reverse time and are 'stable' in forward time are the 'chaotic capture' orbits that this study is designed to locate.

Orbital Duration

The reverse time orbital duration plots have a distinctly different shape to them and have much more clearly defined bands and structures. Like the forward plots there is an area of initial conditions that leads to an extended period of orbital duration form 4000 km – 9000 km along the semi-major axis and between zero and 0.3 eccentricity. While slightly smaller, the area roughly coincides with the long duration areas in the forward time plot. The 30-day plot shows a distinct 'funnel' or sideways 'crown' shape from a semi-major axis of 9000 km – 12000 km with eccentricities of zero to 0.23. This shape has several bands or layers or long duration orbits adjacent to orbits of lower duration and has a fuzzy or ‘static-y’ boundary that indicates potential chaotic motion. Another area of longer duration orbits on the 30-day plot extends in an arc from 8000 km semi-major axis and eccentricity of 0.4 to a semi-major axis of 12000 km and eccentricity of 0.2. This arc also exhibits the fuzzy or ‘static-y’ boundaries that indicate potential chaotic motion. Both the ‘crown’ and the arc fade as the integration time extends to a year or longer, but the ‘stable’ area remains prominent.

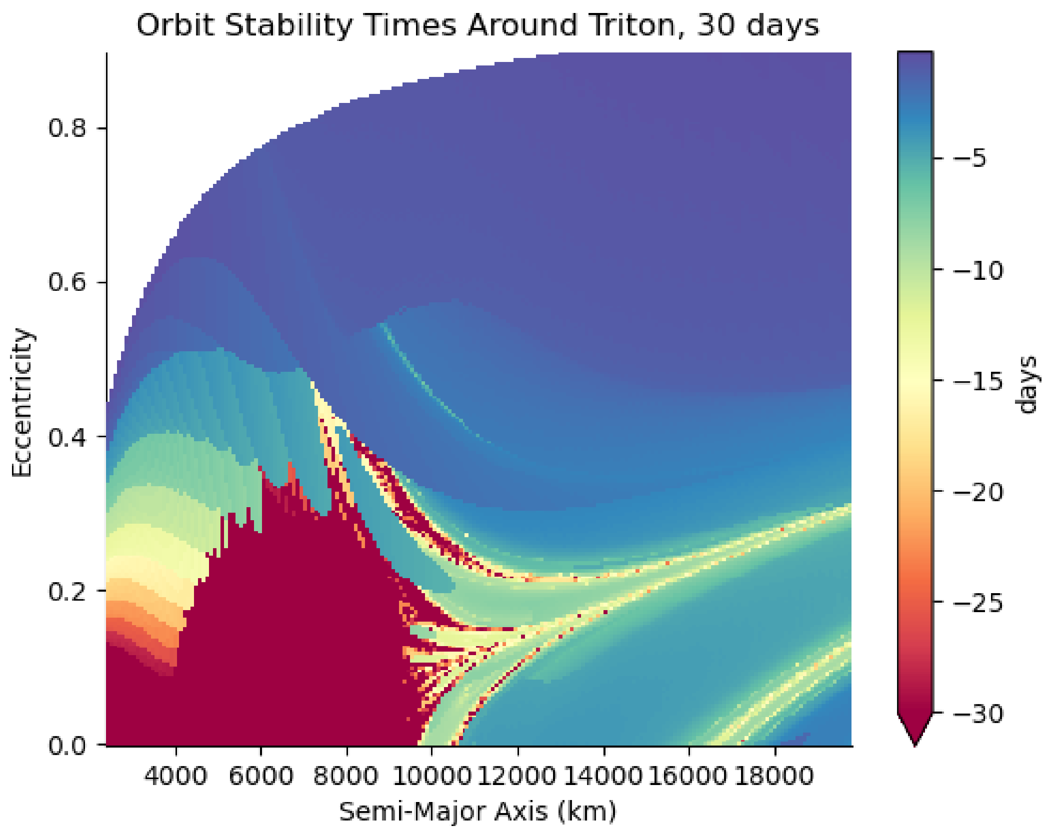

Figure 31- Orbital Duration, Reverse Integration, 30-days

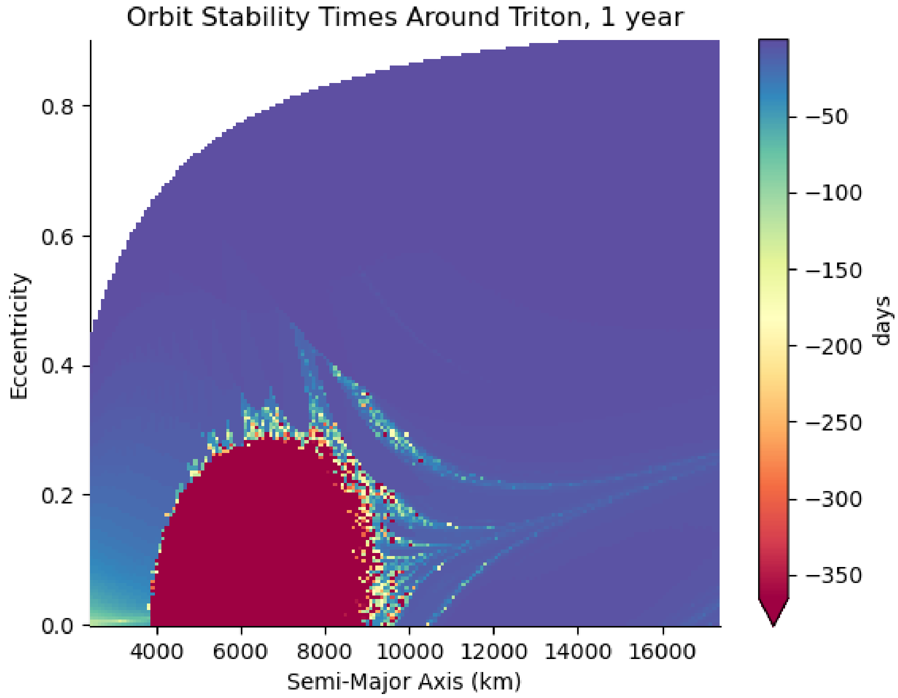

Figure 32- - Orbital Duration, Reverse Integration, 1-year

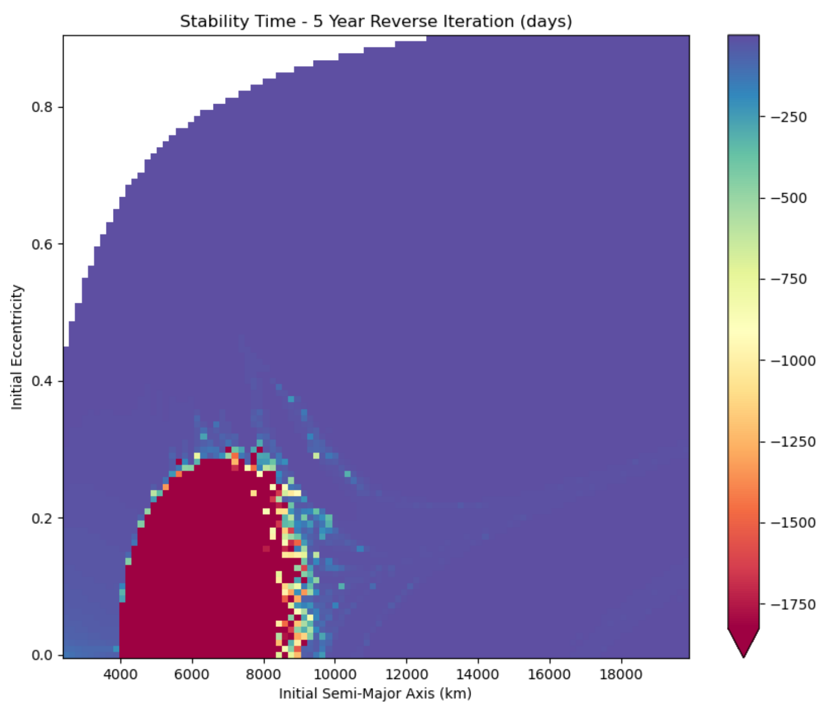

Figure 33- - Orbital Duration, Reverse Integration, 5-years

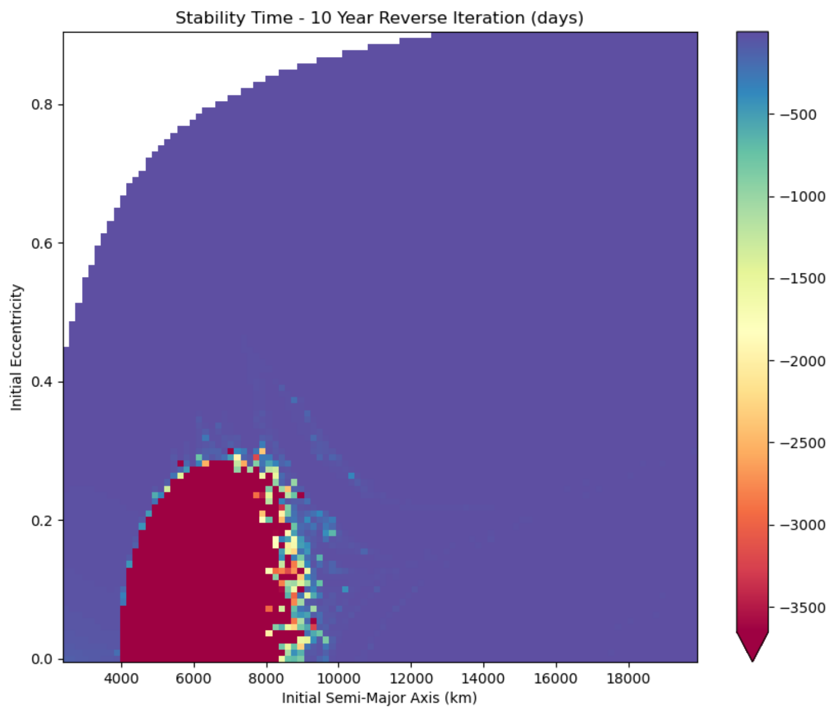

Figure 34- - Orbital Duration, Reverse Integration, 10-years

<u>Stability Plot</u>

The plot for the 30-day reverse integration shows the 'arc' and sideways 'crown' structures of the orbital duration plot. The arc having an area of orbits that last 30 days or more shown in green and the crown section layered with 'stable' areas, collisions and escapes. The arc is also bordered by collisions and escapes with escapes prevalent on the side of higher eccentricity and collisions with lower eccentricity and semi-major axis. There are areas in both structures that have all three end-states mixed together and both areas are still good candidates for chaotic motion. The 1-year, 5-year, and 10-year plots echo the orbital duration plots as the detailed structures in the 30-day plot disappear for longer integration times. The 'stable' bubble does persist even in reverse time through 10-years. As in the forward plots, narrow bands of 'too close' of a flyby appear as streaks of blue collision end-states in the large areas of escape trajectories in the parts of the plot with semi-major axes larger than 10000 km.

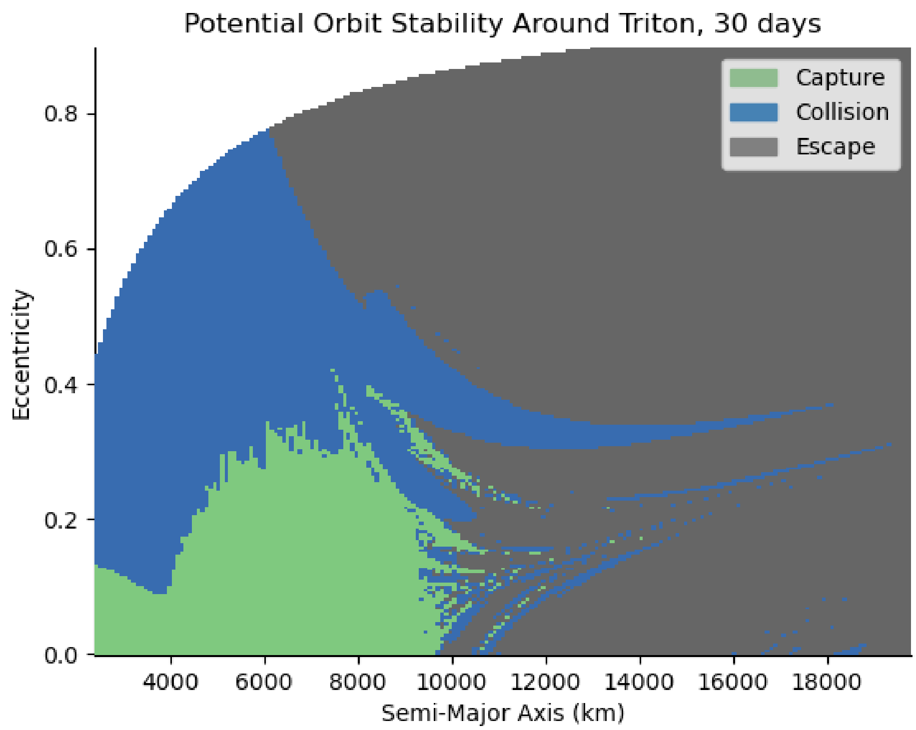

Figure 35- Stability Plot, Reverse Integration, 30-days

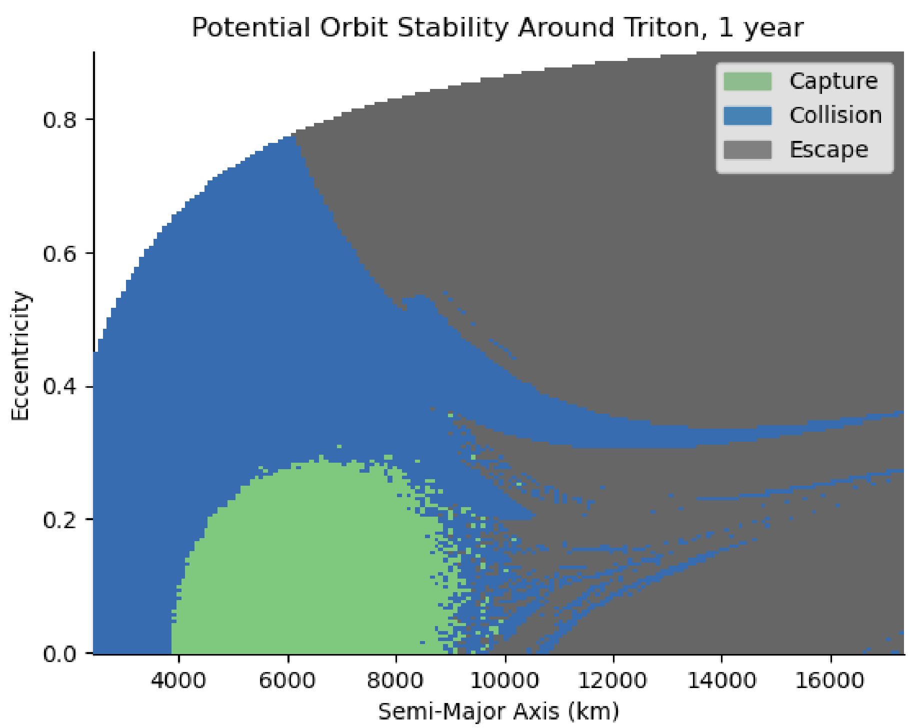

Figure 36- Stability Plot, Reverse Integration, 1-year

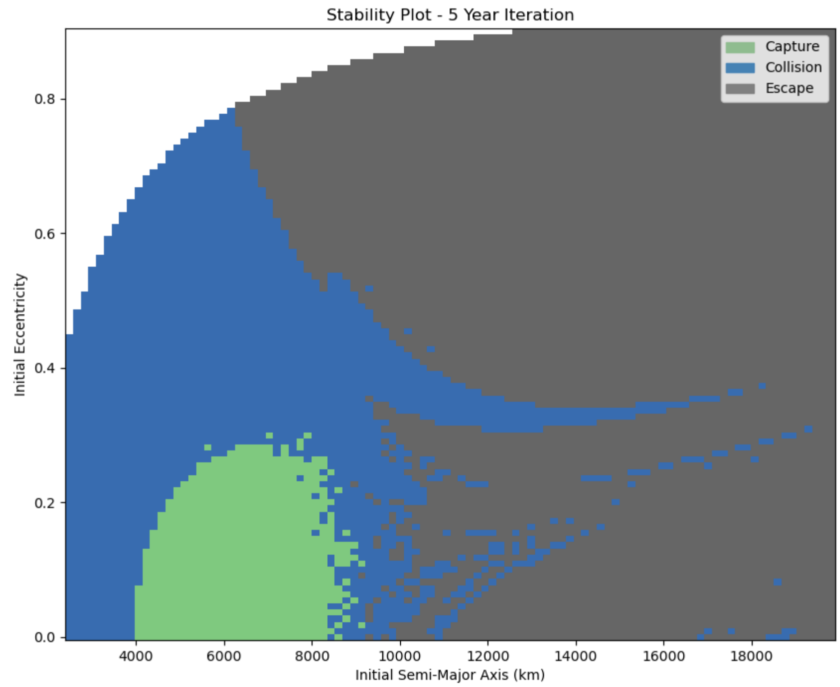

Figure 37- Stability Plot, Reverse Integration, 5-years

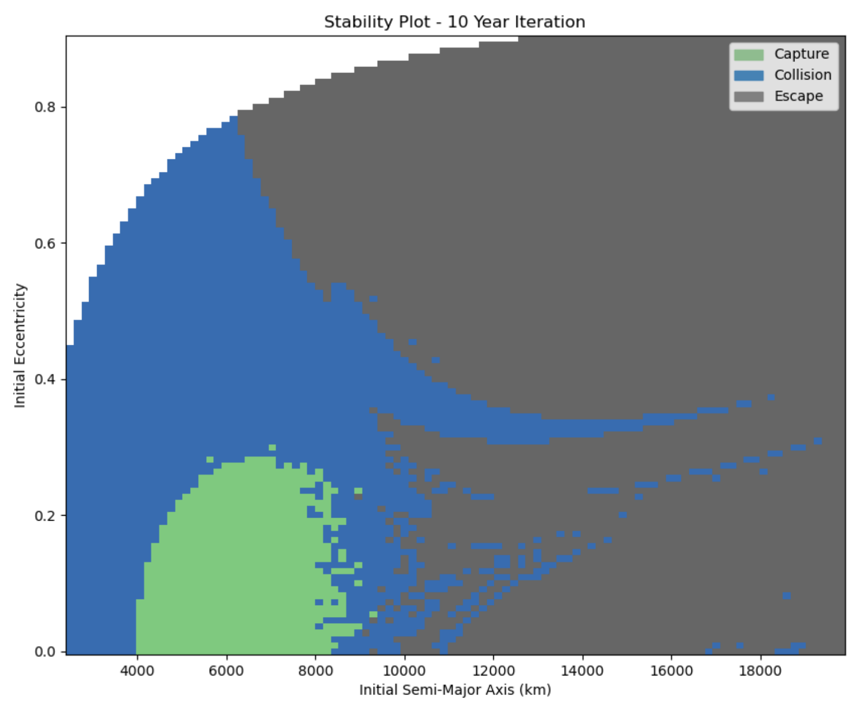

Figure 38- Stability Plot, Reverse Integration, 10-years

R-bar

The r-bar plots for 30-day reverse integration are a good indication of the areas sought for chaotic motion and capture. The previously identified arc and crown structures are surrounded and occasionally run through by ‘static-y’ r-bar values. The likelihood of chaotic motion is much greater in these areas rather than in areas with smoothly transitioning r-bar values. The 30-day plot also exhibits a ‘filament’ of zero to near zero r-bar values running towards the center of the crown/funnel structure similar to the one on the forward time plot. The longer integration time plots also show the same characteristics with small changes based on orbital duration and resolution of the plots.

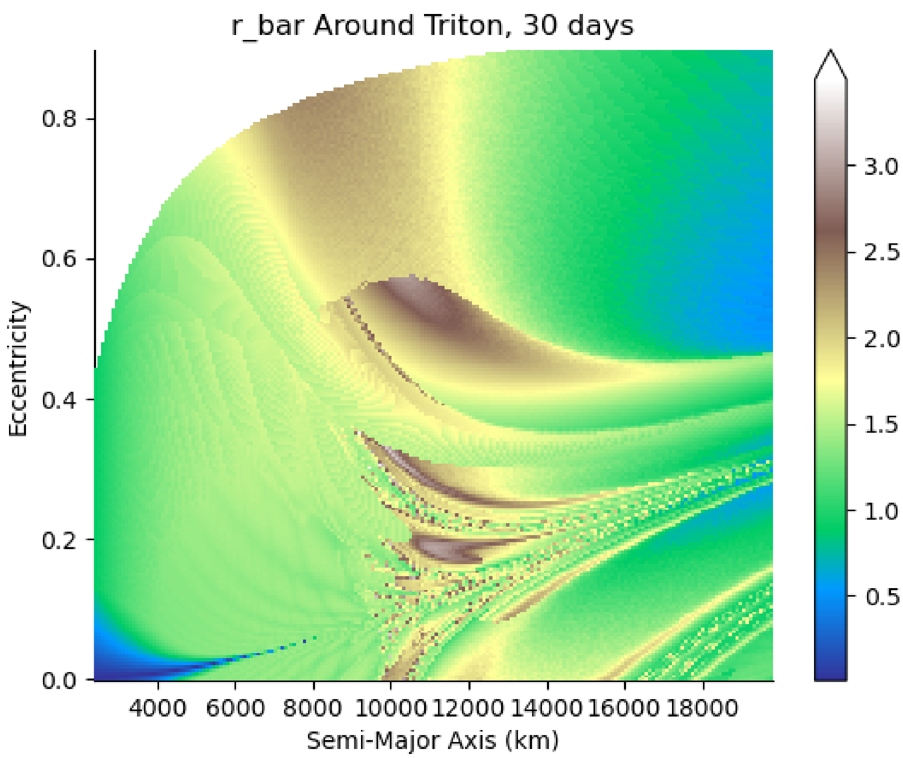

Figure 39- r-bar, Reverse Integration, 30-days

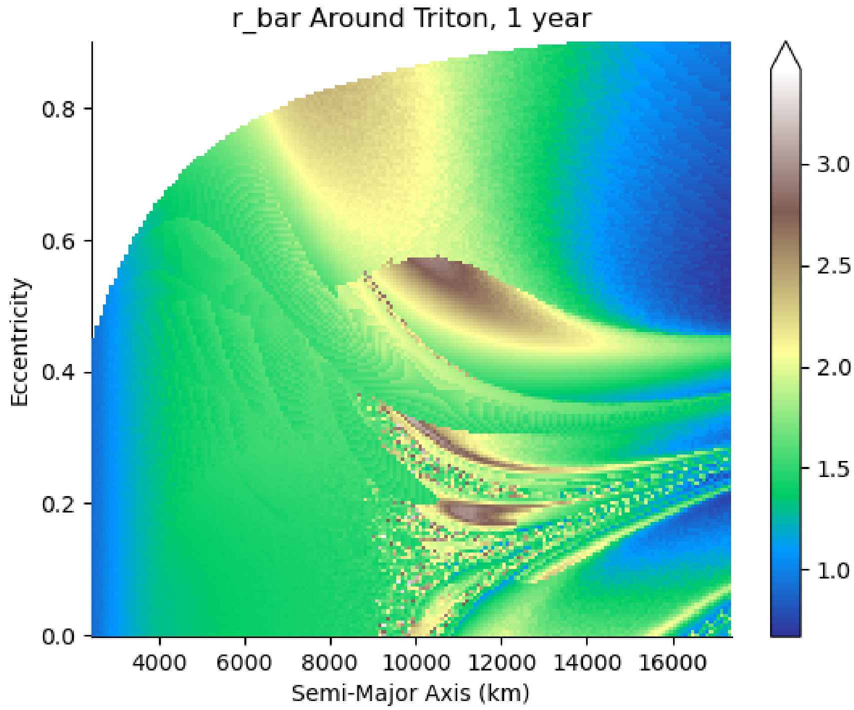

Figure 40- r-bar, Reverse Integration, 1-year

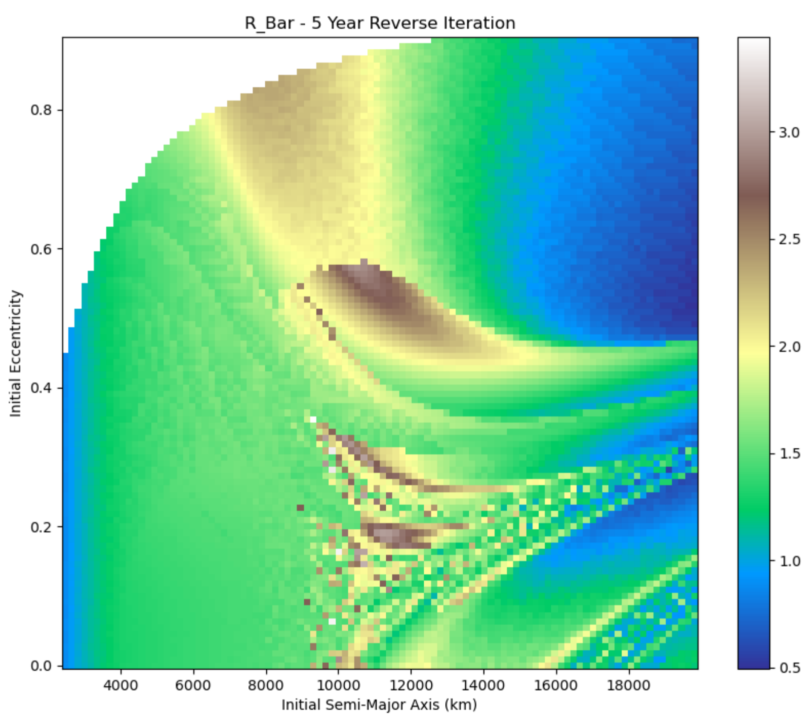

Figure 41- r-bar, Reverse Integration, 5-years

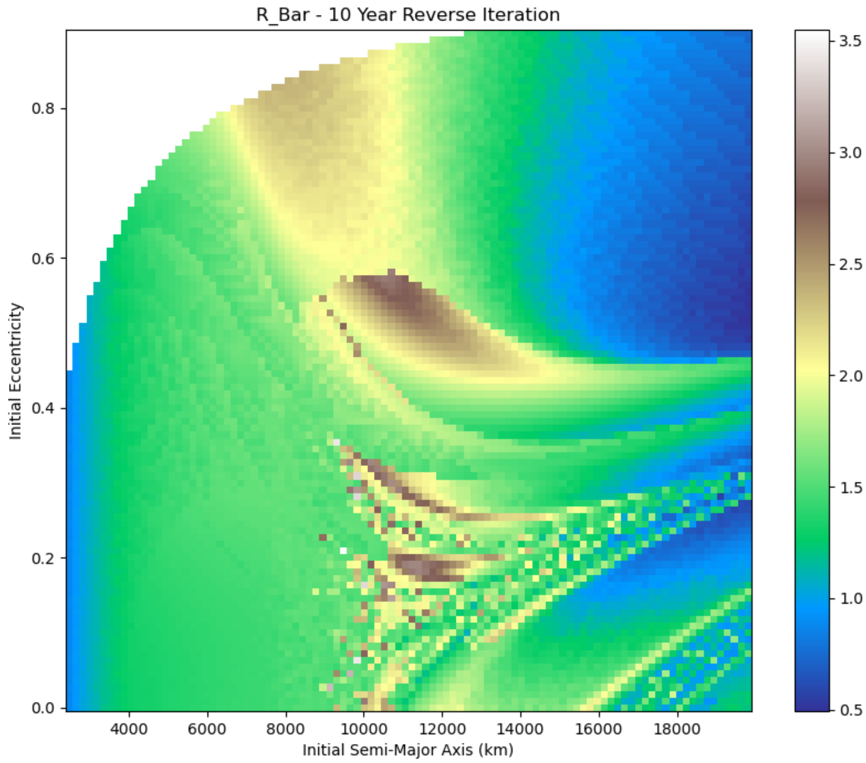

Figure 42- r-bar, Reverse Integration, 10-years

Perturbation Indices

P_{ii} on the 30-day and 1-year plots shows similar results to the r-bar plots. The arc and crown areas show both positive and negative values of P_{ii} mixed together or in very close proximity with some regions of little to no perturbation. These are excellent indicators of potential chaotic motion and can lead to escape trajectories. The indications of escape in the stability plot are reinforced with the areas of positive P_{ii} being on the side of the arc with higher values of eccentricity and semi-major axis. The large stability areas also has low P_{ii} values. The P_{iv} plots also follow the trend of low total values in areas with longer orbital duration and low values of r-bar.

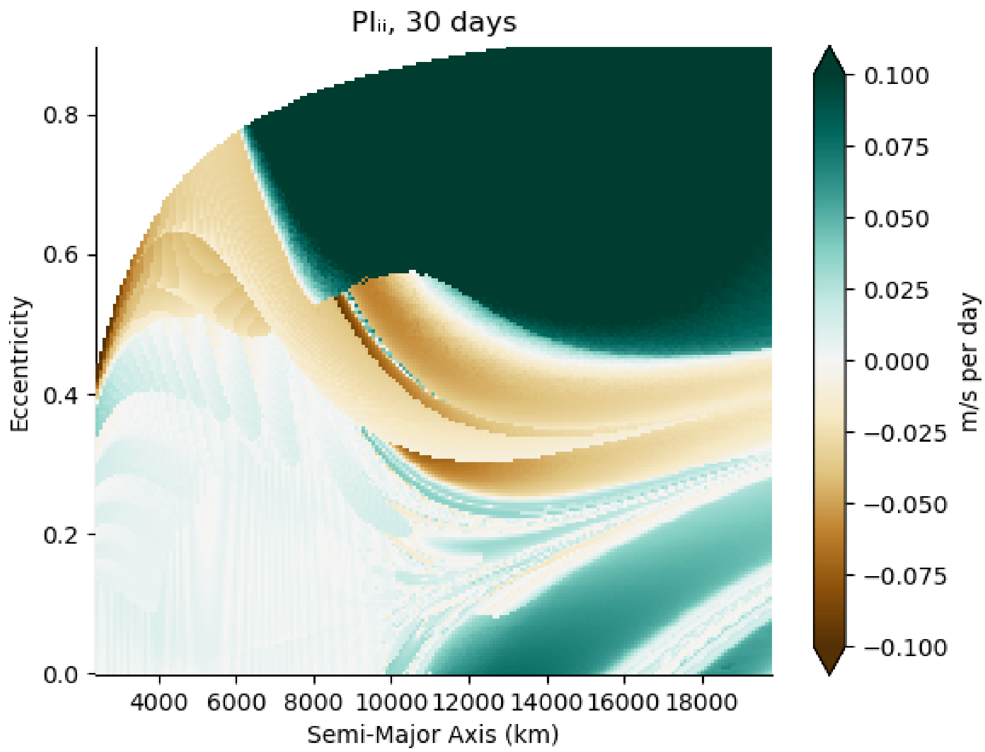

Figure 43- P_{ii}, Reverse Integration, 30-days

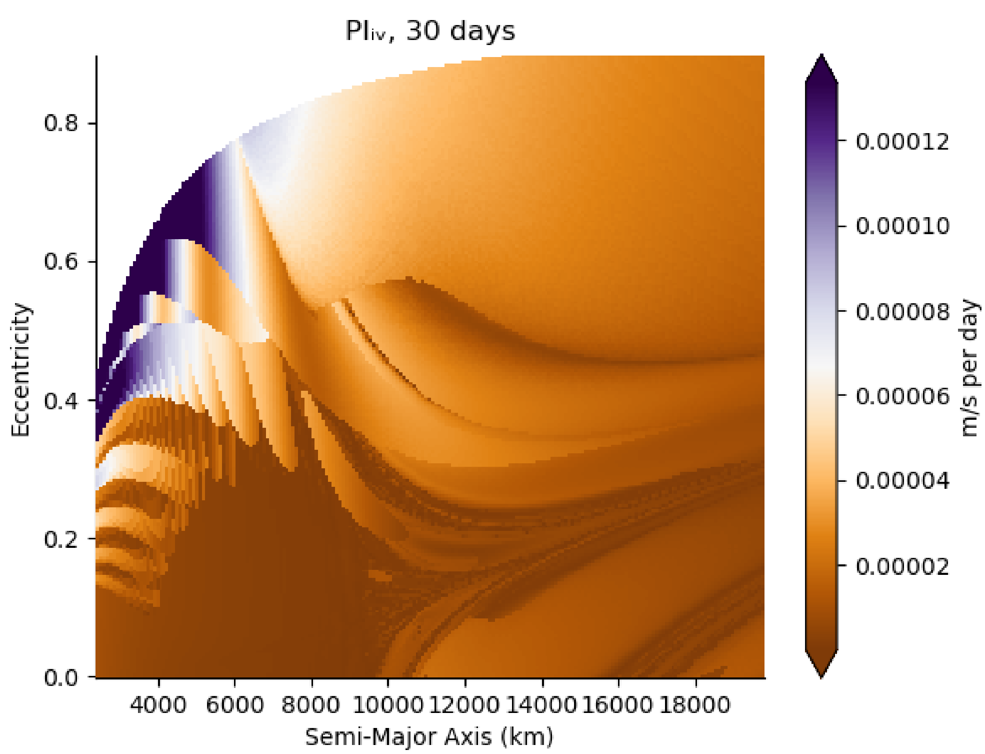

Figure 44- P_{iv}, Reverse Integration, 30-days

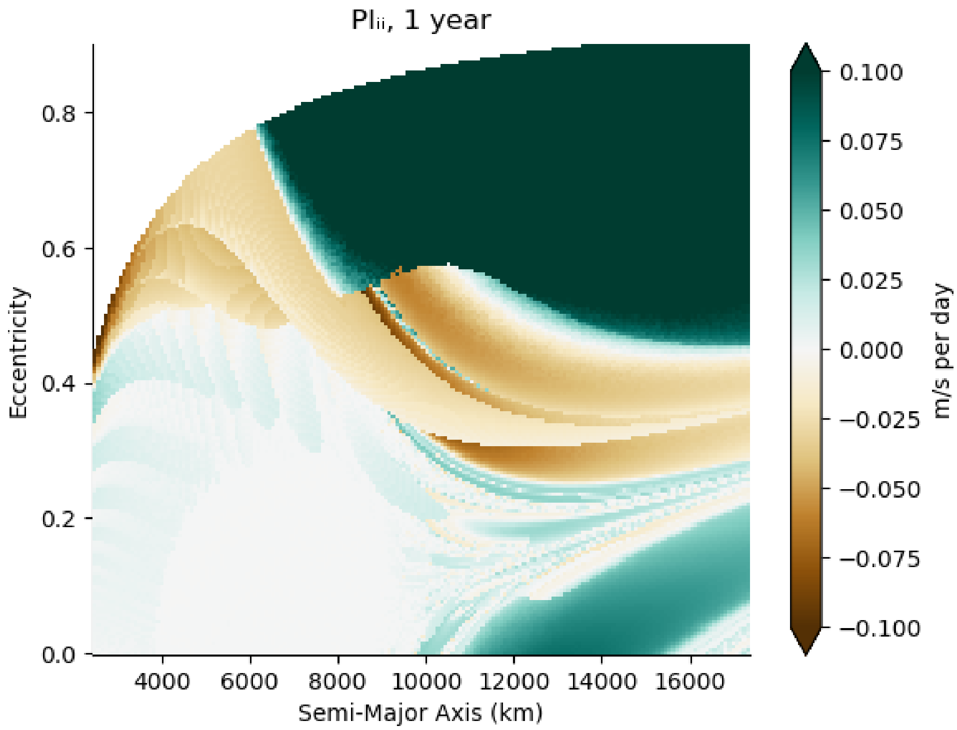

Figure 45- P_{ii}, Reverse Integration, 1-year

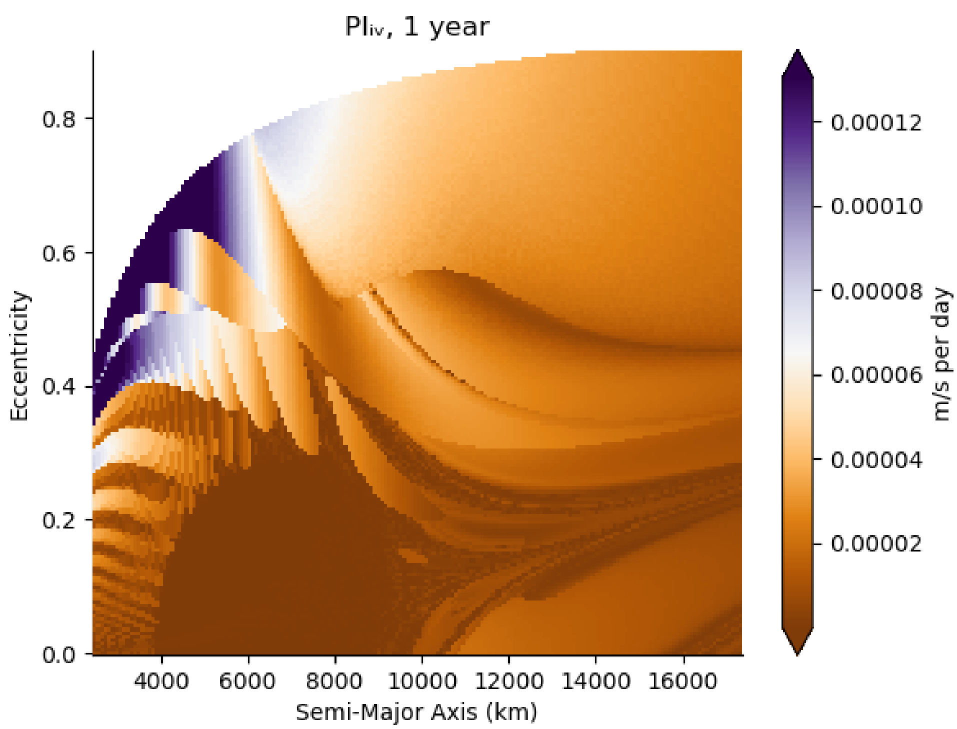

Figure 46- P_{iv}, Reverse Integration, 1-year

Triton 2-body Energy

The reverse plots of the satellite's two-body energy are all similar to each other as they show the energy state of the satellite at the end of the integration time or at the moment of escape or capture. As most of the captures or escapes occur within the first 30 days, this an expected result. The arc and crown structures continue to show good indications of chaotic motion with values ranging from zero to roughly -0.06 intermingled throughout their respective regions. The 1-year, 5-year, and 10-year plots all follow the same pattern similar to the forward time plots.

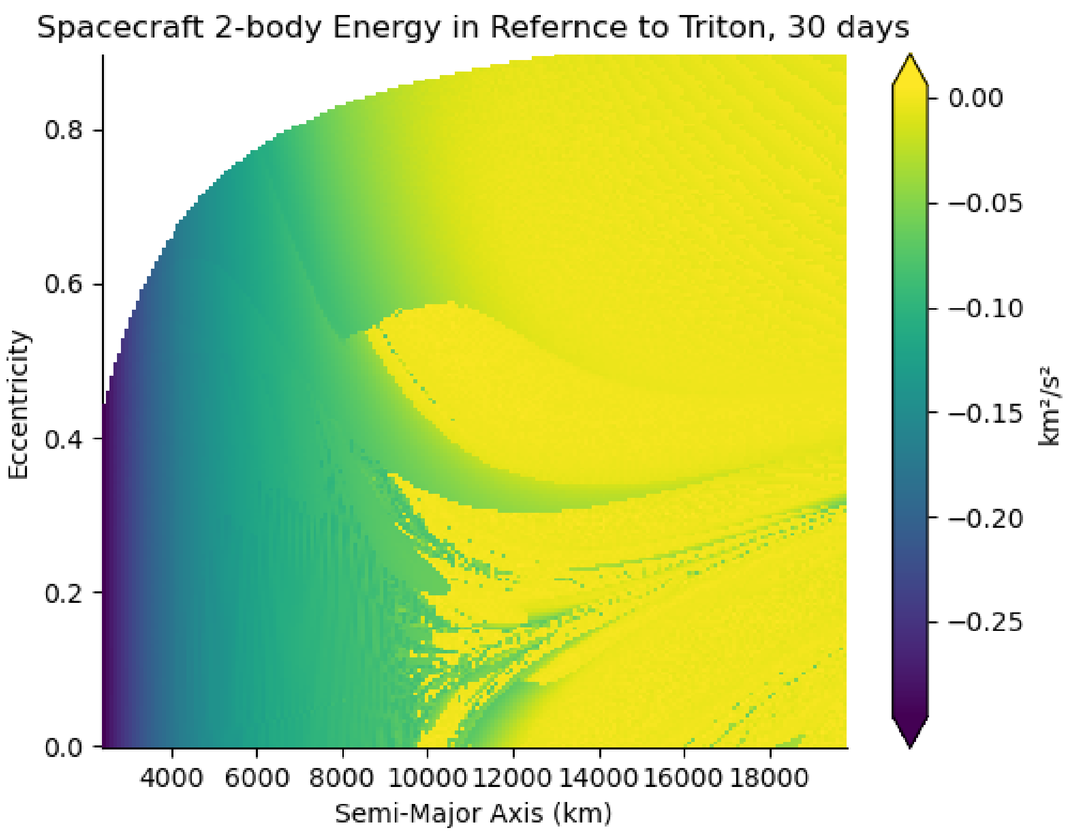

Figure 47- Two-body Energy with respect to Triton, Reverse Integration, 30-days

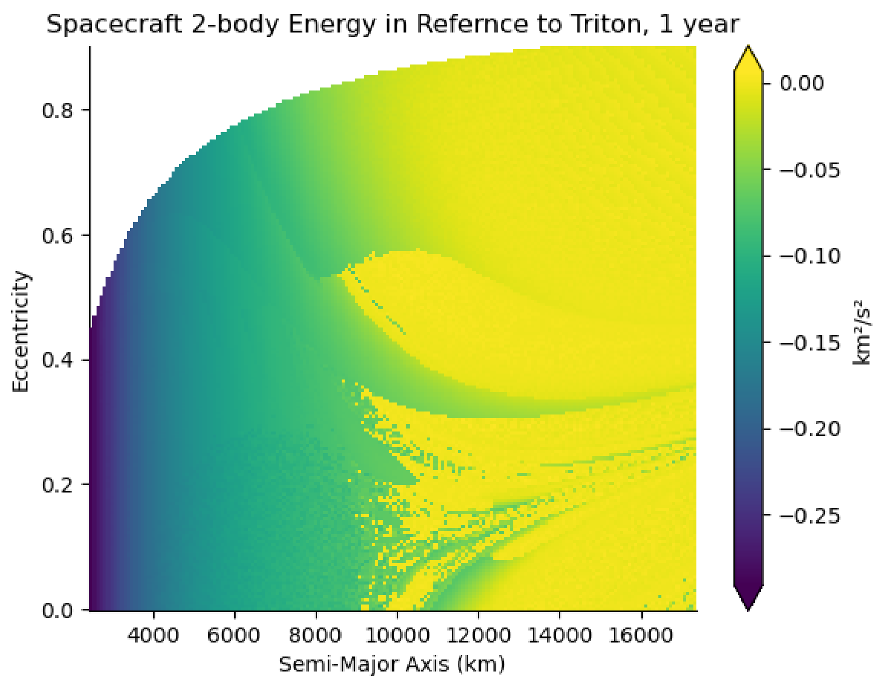

Figure 48- Two-body Energy with respect to Triton, Reverse Integration, 1-year

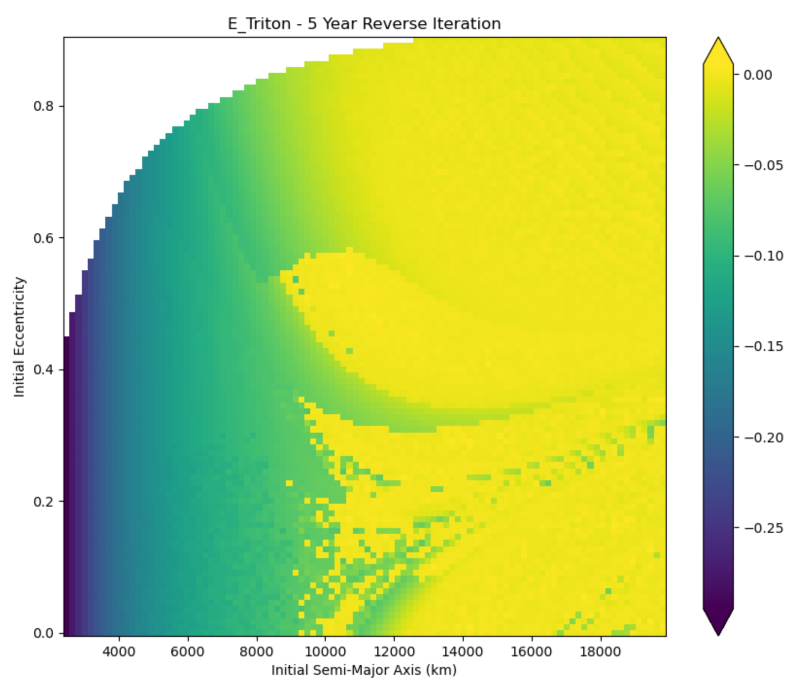

Figure 49- Two-body Energy with respect to Triton, Reverse Integration, 5-years

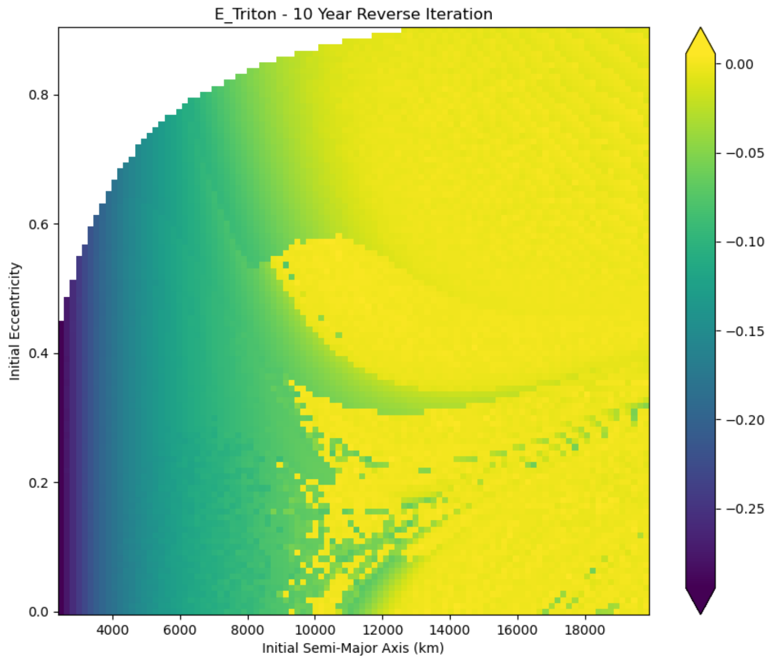

Figure 50- Two-body Energy with respect to Triton, Reverse Integration, 10-years

Identification of Focus Areas

The forward and reverse plots revealed areas of semi-major axis and eccentricity combinations that were more likely to show chaotic motion and be favorable to chaotic escape and capture. The reverse time areas were more critical to identifying the specific initial conditions desired. In the reverse integration plots the two areas described as the 'arc' and the 'sideways crown' were plotted in greater detail to further narrow the number of initial conditions to check for chaotic capture and escape. The 'arc' was called Focus Area A and the 'sideways crown' was called Focus Area B. Using the OSCER capabilities Focus Area A was plotted for a semi-major axis of 7000 km to 12500 km and eccentricities of 0.2 to 0.4 on a 500 x 500 resolution initial conditions grid. Focus Area B was plotted for a semi-major axis of 8000 km to 14000 km and eccentricities of zero to 0.22 on a 450 x 450 resolution initial conditions grid. The same family of plots were made for the focus areas as the full initial conditions grid. The greater detail in the focus area plots allow the identification of narrow bands of quickly alternating lengths of orbital duration, stability, r-bar, and energy. The r-bar plots in particular show the rapidly changing effects of the perturbations on the satellite trajectory with very small differences in initial conditions. The detailed focus views give the best confirmation of the areas of potential chaotic motion. Along the edges of the stable bands in Focus Area B there are areas where capture, escape, and stable orbits are alternating with a very tiny amount of change in the semi-major axis and eccentricity. The stability plots of both focus areas confirm the end-state changes desired when looking for chaotic motion captures and the rest of the plots also show the same variation of end-state with small changes in initial conditions.

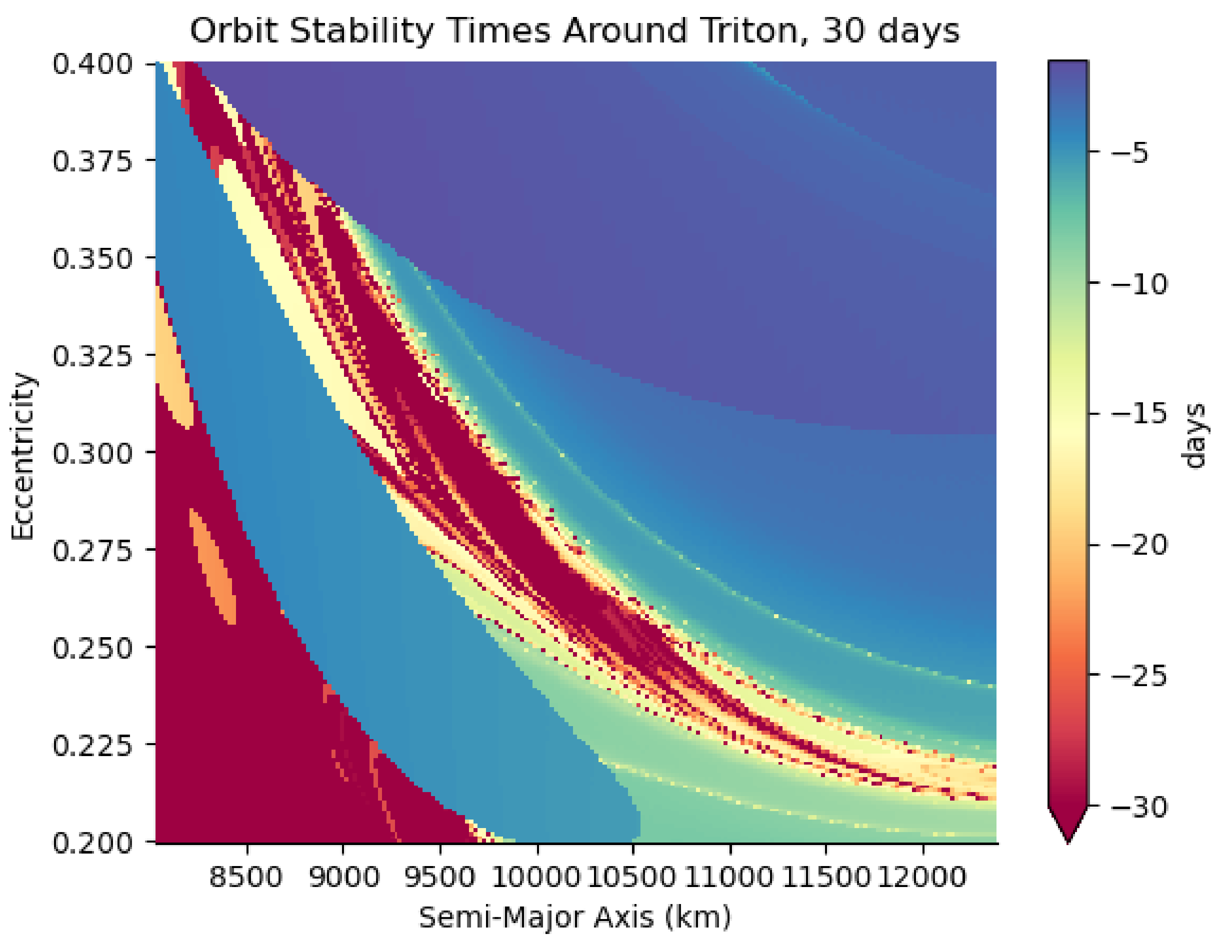

Figure 51- Focus Area A, Orbit Duration, Reverse Integration, 30-days

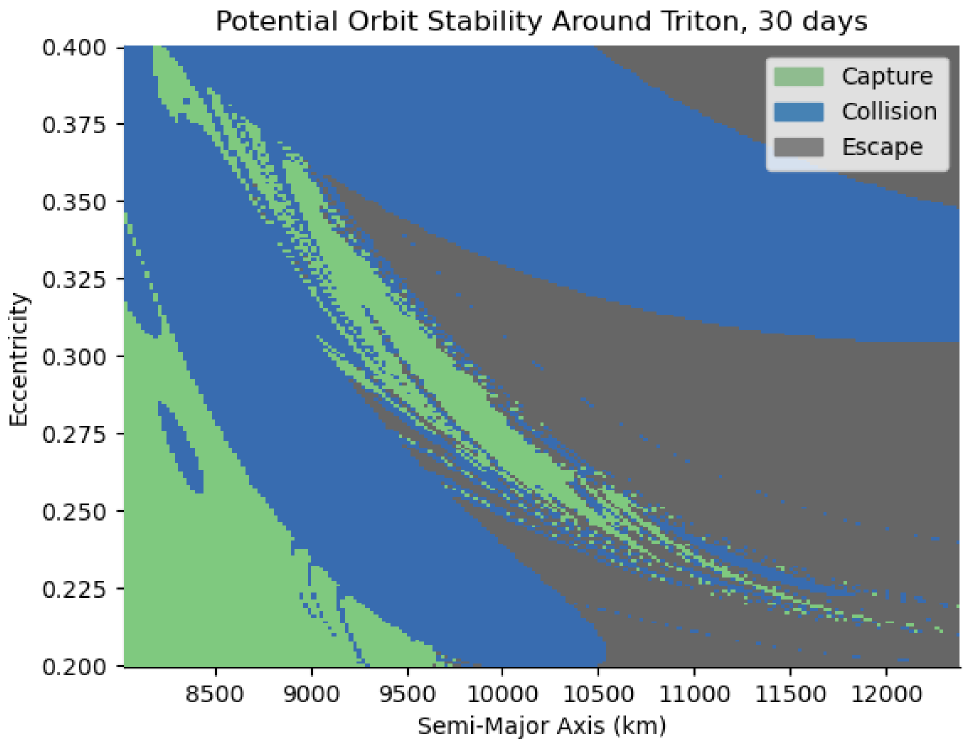

Figure 52- Focus Area A, Orbit Stability, Reverse Integration, 30-days

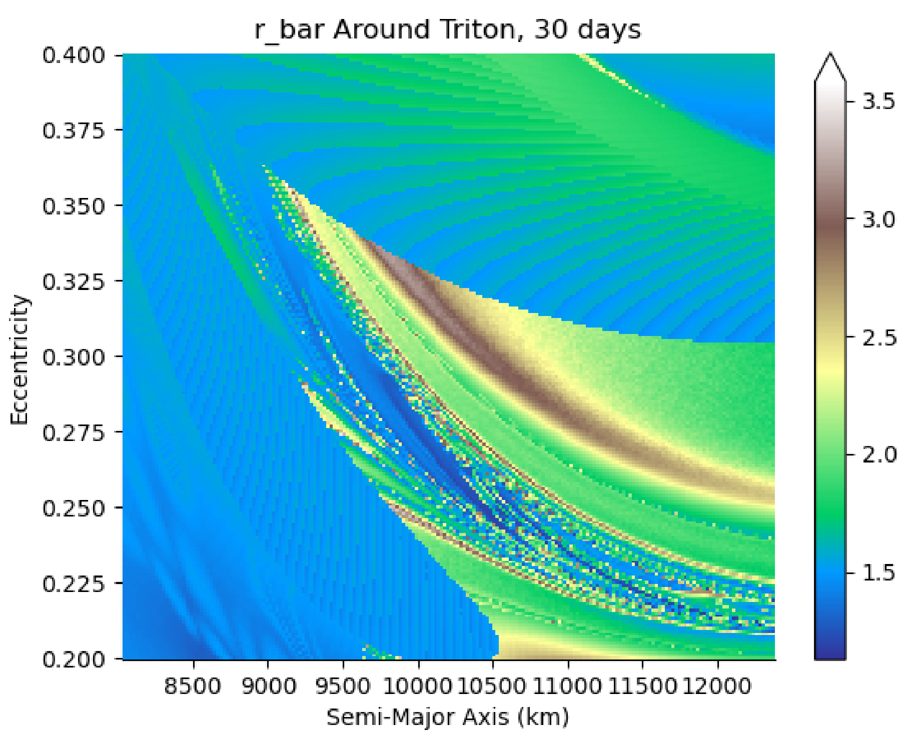

Figure 53- Focus Area A, r-bar, Reverse Integration, 30-days

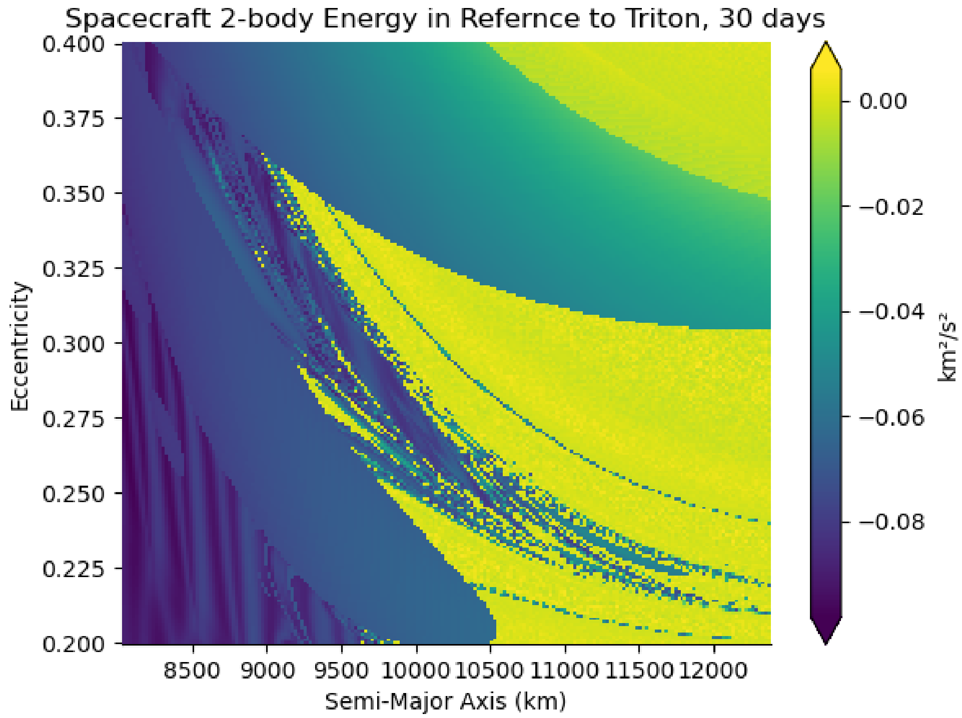

Figure 54- Focus Area A,Two-body Energy with respect to Trition, Reverse Integration, 30-days

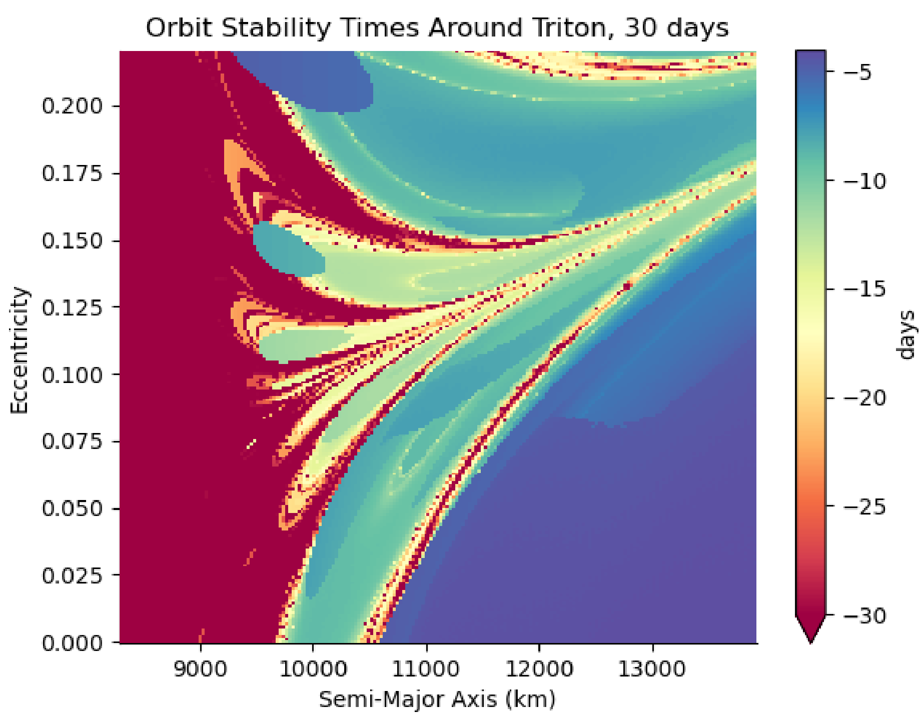

Figure 55- Focus Area B, Orbit Duration, Reverse Integration, 30-days

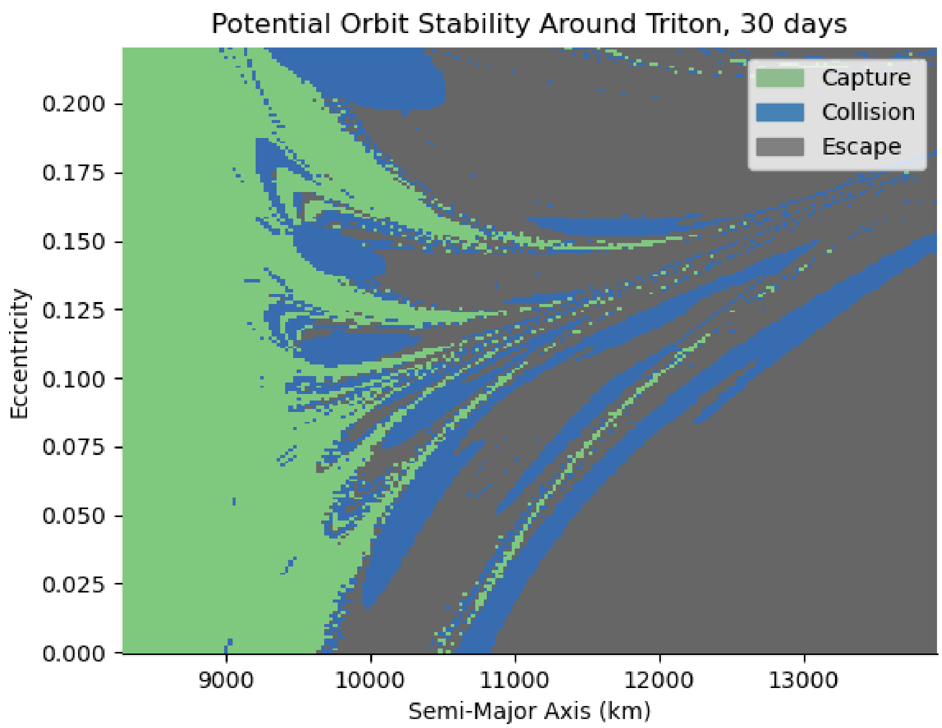

Figure 56- Focus Area B, Orbit Stability, Reverse Integration, 30-days

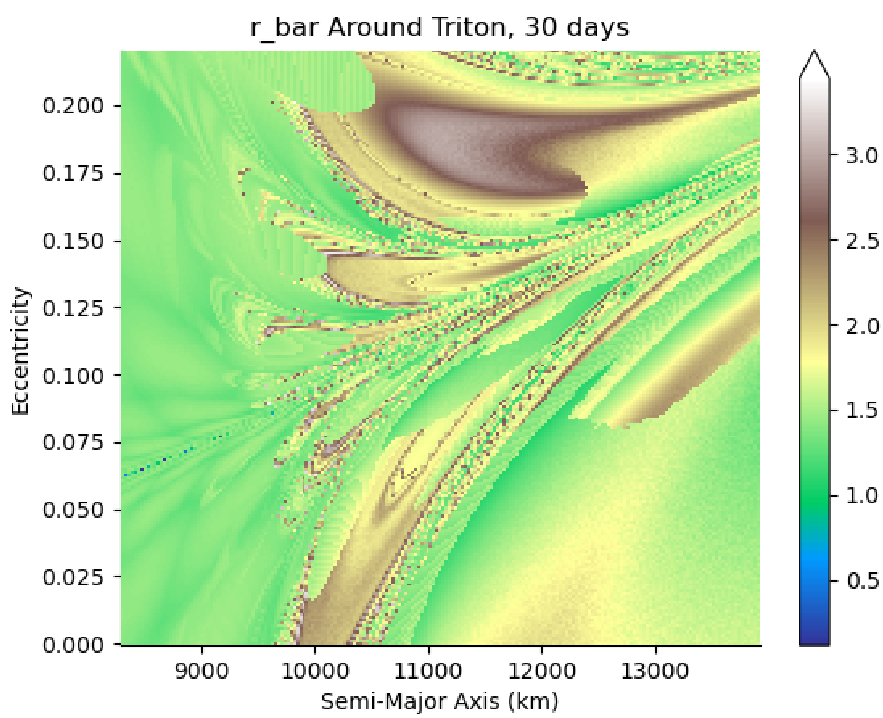

Figure 57- Focus Area B, r-bar, Reverse Integration, 30-days

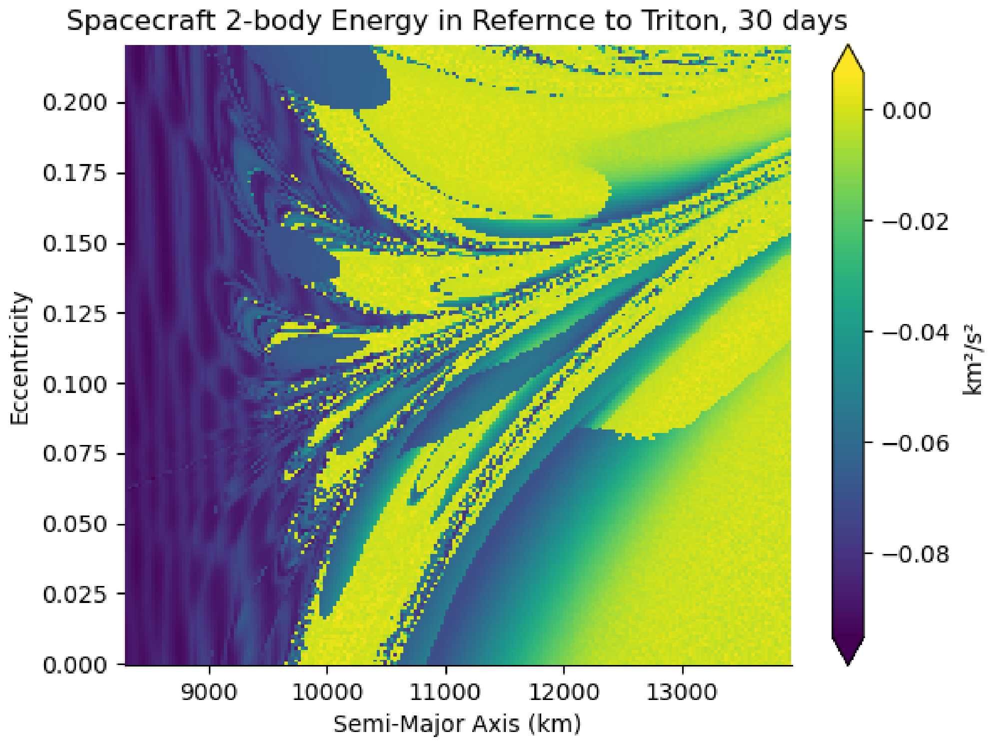

Figure 58- - Focus Area B, Two-body Energy with respect to Triton, Reverse Integration, 30-days

Reverse Time Initial Condition - Forward Integration

With the greater detail of the Focus areas plots, the last type of analysis was performed. The final state vector of the 4-body system reverse time integration was used as the initial conditions for a forward time integration for 70 days. The reverse time initial conditions were checked for collision end-states and only the initial conditions that resulted in a satellite orbiting were plotted. In the Focus Area plots of the reverse time initial conditions, blank areas are areas where collisions were the end state of the reverse time integration. The plots for the forward time integration are mapped to the initial conditions of the reverse time integration and previous forward time integration. This allows comparison and selection of target orbits from the full initial conditions matrix. The plots reveal a new structure of capture, escape and stable end-states as well as different orbital durations on the forward plot. R-bar is very scattered with orbits with near zero or low r-bar values adjacent to orbits with moderate r-bar values. The 2-body energy with respect to Triton is also scattered with low and high energy orbits interleaved. The most interesting areas of the reverse time initial conditions integrated forward in time are the areas on the stability plot that are 'stable' or border a stable region. In Focus Area A, regions in the vicinity of 10000 km to 10750 km and eccentricity of 0.225 to 0.265 and the area on the arc between 9500 km to 10250 km and eccentricity between 0.2540 and 0.320 are of interest. In Focus Area B, regions between 10250 km and 10500 km and eccentricities from zero to 0.040 and the larger region between 10250 km and 11000 km and eccentricities from 0.075 to 0.175 are the areas of interest.

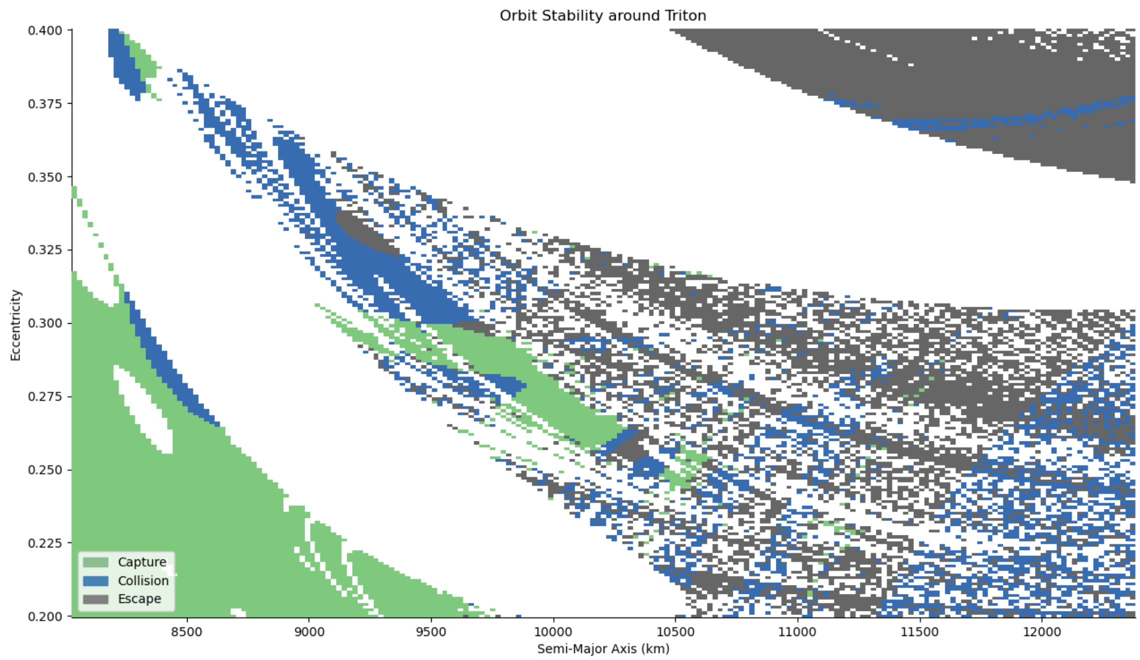

Figure 59- Forward Integration from Reverse Integration End-State, Focus Area A, Orbit Stability

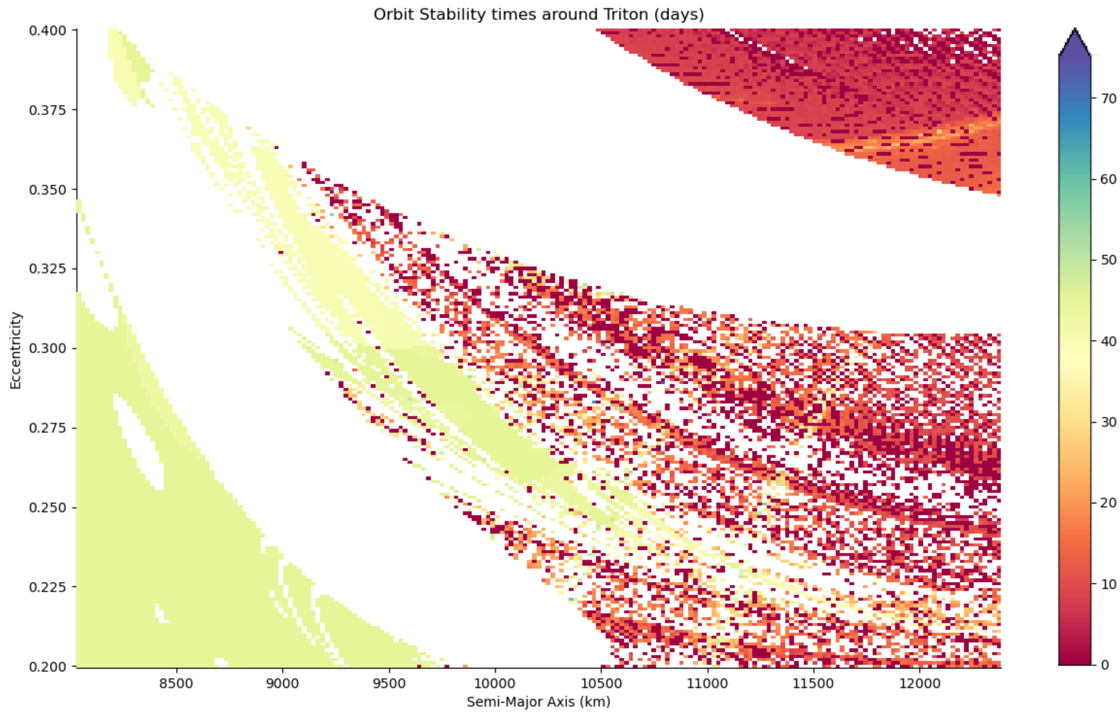

Figure 60- Forward Integration from Reverse Integration End-State, Focus Area A, Orbit Duration

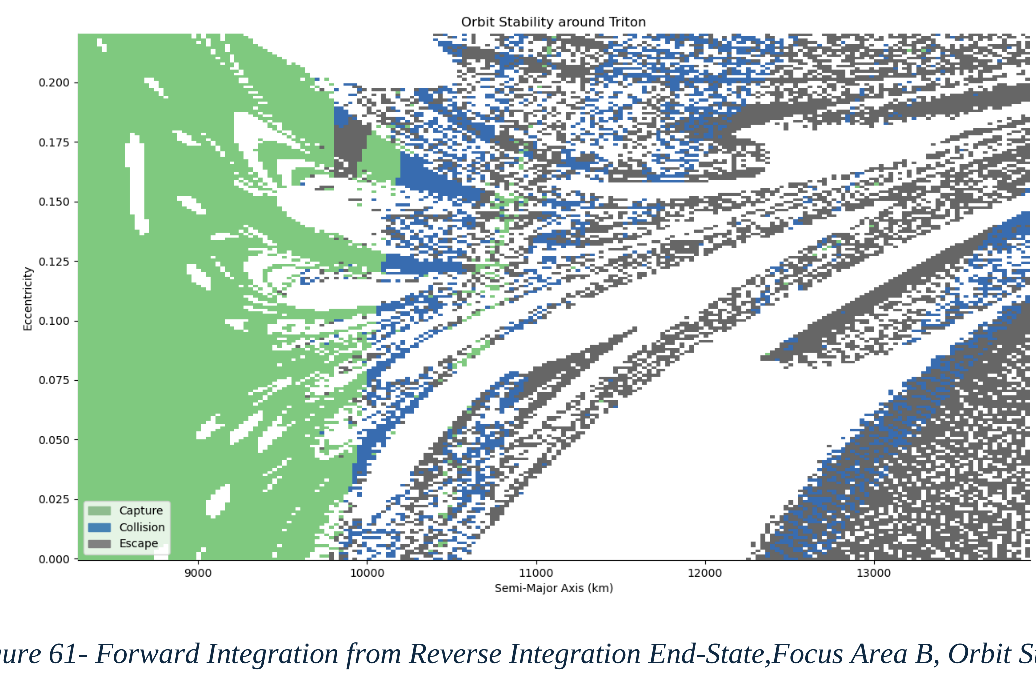

Figure 61- Forward Integration from Reverse Integration End-State,Focus Area B, Orbit Stability

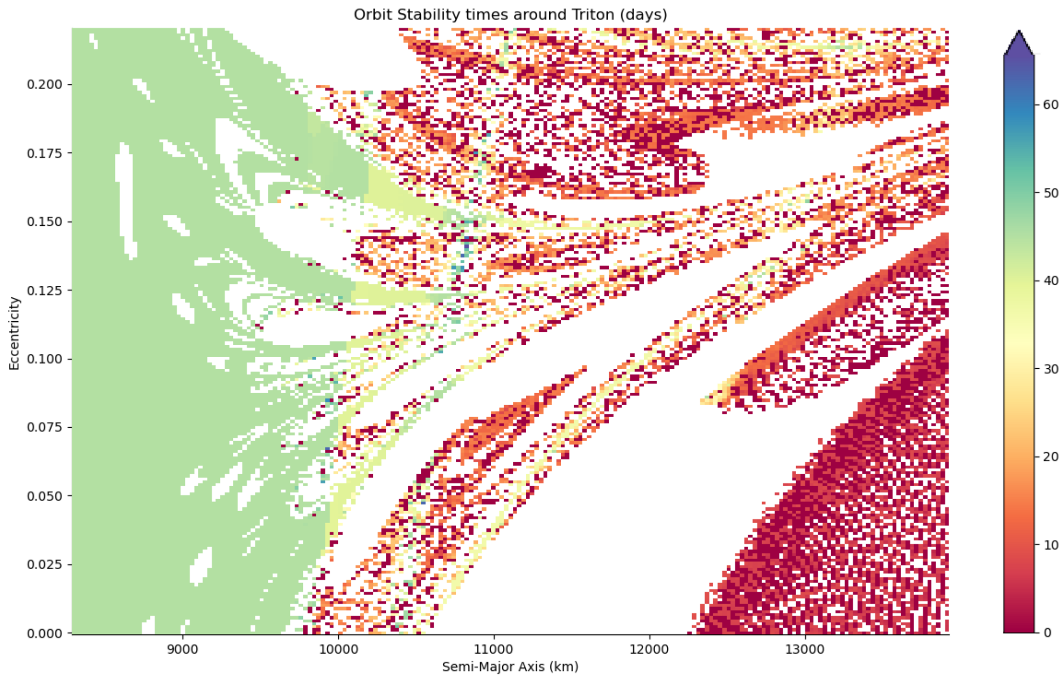

Figure 62- Forward Integration from Reverse Integration End-State,Focus Area B, Orbit Duration

<u>Location of desired orbits</u>

Using the Reverse Time Initial Condition to Forward Integration plots to narrow the search area, the Reverse Time plots of 2-body energy and end-state of the satellite were compared with a simple algorithm to find initial conditions which lead to a reverse time escape with negative 2-body energy with respect to Triton. Through successive iterations of the search utilizing different values of negative energy as a threshold of reporting, a value of -0.07 was selected as a the 'sweet spot' of enough orbits to plot individually, but not so many that computation and analysis time would be prohibitive. From the smaller set of orbits, the ones corresponding to the interest areas in the Reverse Time Initial Conditions to Forward Integration plots were simulated trajectory by trajectory to find the orbits that escape in reverse time, then using the escape conditions as the initial conditions the trajectory was run in forward time to determine if the satellite would be captured by Triton. This style of natural capture was termed a 'chaotic capture' for the purpose of this study. Several orbits were found to orbit Triton for a span of time and then either escape to a Neptune centered orbit or collide with Triton. These types of capture events are termed 'sticky orbits'[19] and are also useful even if there is not a complete capture for a long period of time.

Specific Orbits Identified

Four orbits were discovered that were escapes during reverse integration and captures when run forwards from the reverse integration end-state. Two were captured and maintained orbit up to the end of the 30-day integration time and two were ‘sticky captures’ that ended at 29 days after the initial capture. Of the two ‘full captures’ one orbit was very, very slightly positive energy but demonstrated the techniques used to identify the orbit well. One sticky capture resulted in another escape, and one resulted in a collision with Triton.

<u>Orbit 1</u>

A specific orbit was found at a: 10,076 km and e: 0.245. The orbit was run backward in time for 30 days and the spacecraft escaped with a 2-body energy of: 0.0000785 km2/s2. The end-state of the reverse integration was used in a forward integration. While the negative energy is very slight, it is a good example of the possibilities of the type of captures shown in this paper. It also demonstrates the interesting geometry that is evident when a spacecraft that is unbound by Triton in a quasi-satellite orbit is captured by Triton.

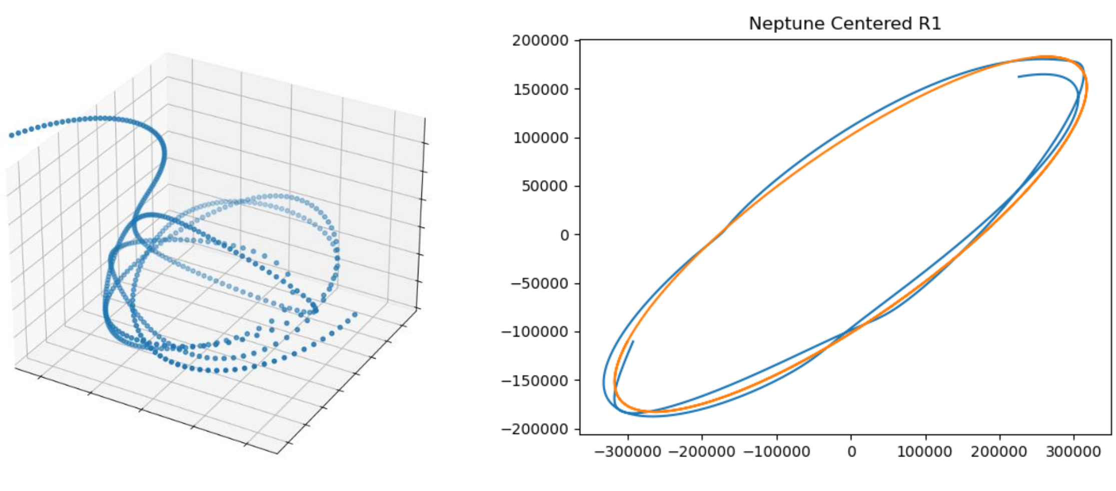

Figure 63- 10 day Reverse Integration Isometric and Neptune Centered View

(Triton plotted in Orange, Satellite in blue)

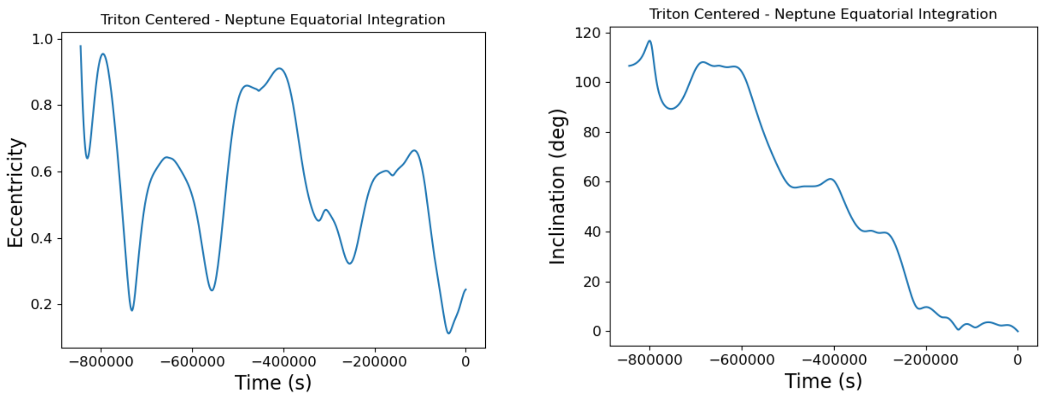

Figure 64- 10 day Reverse Integration of Orbit 1: Eccentricity and Inclination

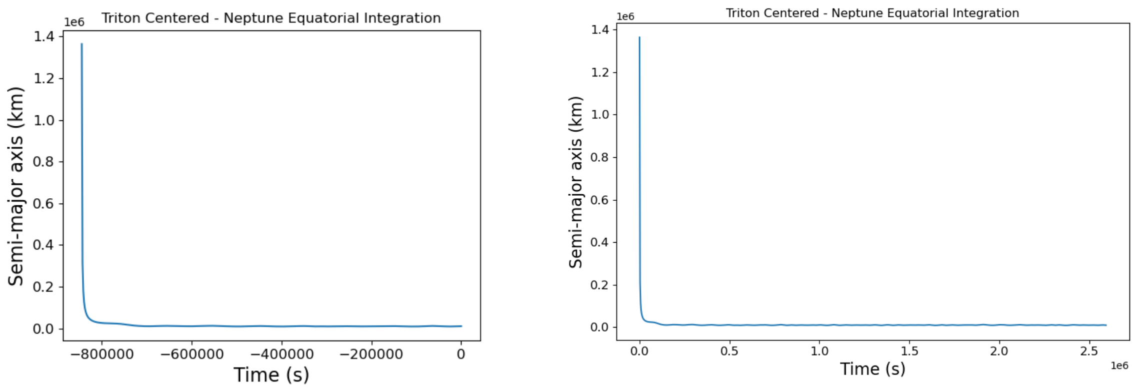

Figure 65- Semi-Major Axis: left, 10-day reverse integration. right, 30-day Forward Integration

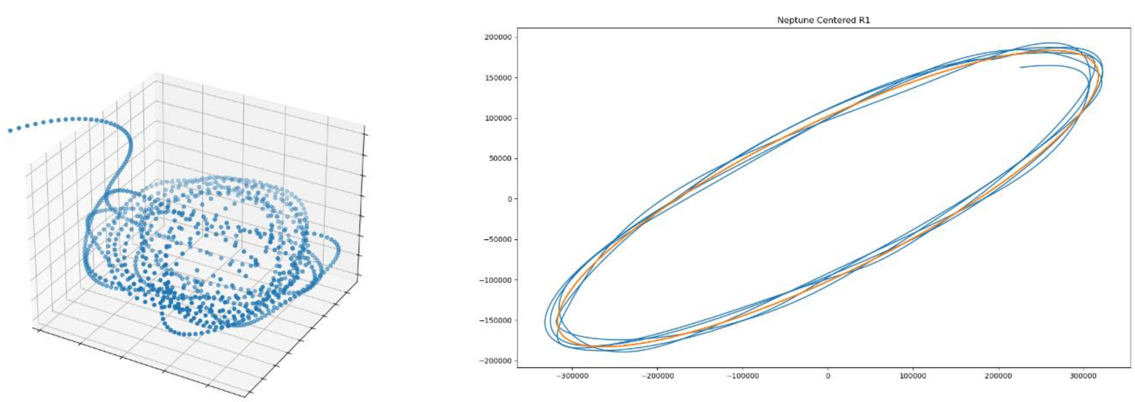

Figure 66- Isometric View, Neptune Centered View 30 day Forward Integration.

(Triton is plotted in orange, Satellite in blue)

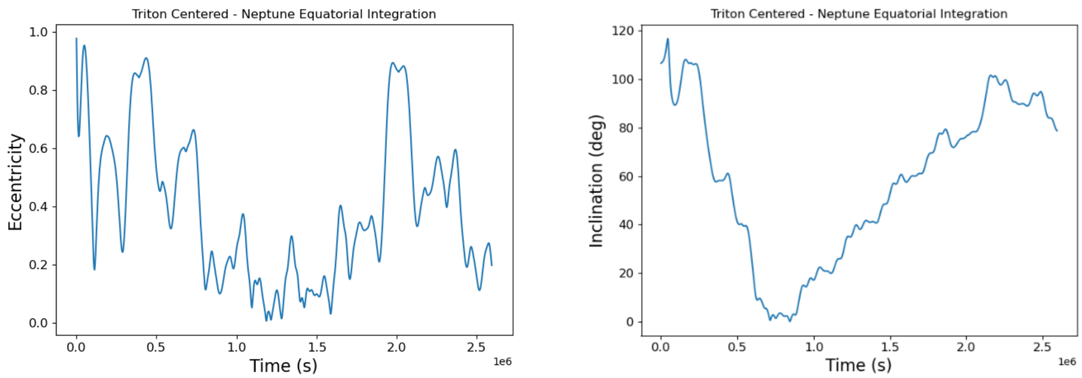

Figure 67- Eccentricity and Inclination, 30-day Forward Integration

In Figure 65, the standing ‘hook’ is the inbound trajectory of the satellite, showing the satellite being pulled into Triton’s influence. The plots, while not identical, show that the forward time capture integration time ends in a similar orbit with respect to eccentricity and semi-major axis to the initial conditions of the reverse integration time.

<u>Orbit 2</u>

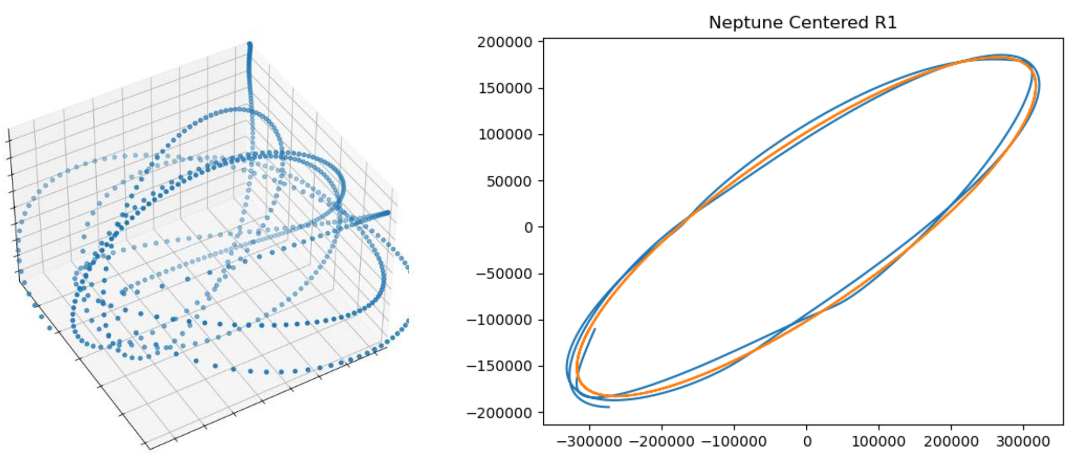

Figure 68- Isometric and Neptune Centered View, 12-day Reverse Integration

(Triton plotted in orange, Satellite in Blue)

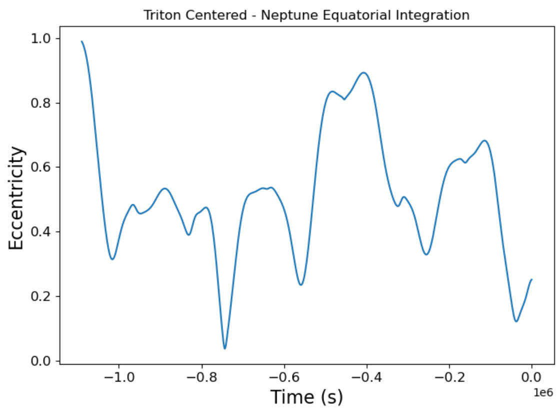

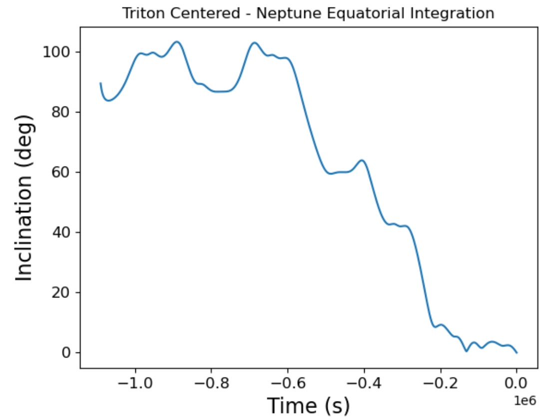

Figure 69- Eccentricity and Inclination, 12-day Reverse Integration.

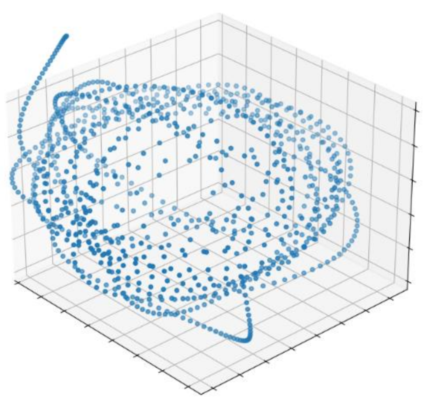
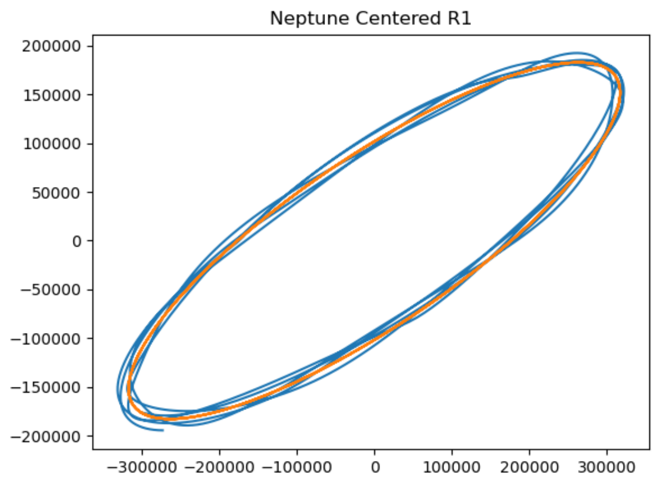

Figure 70- Sticky Capture/Collision Isometric and Neptune Centered View, 30-day Forward Integration.

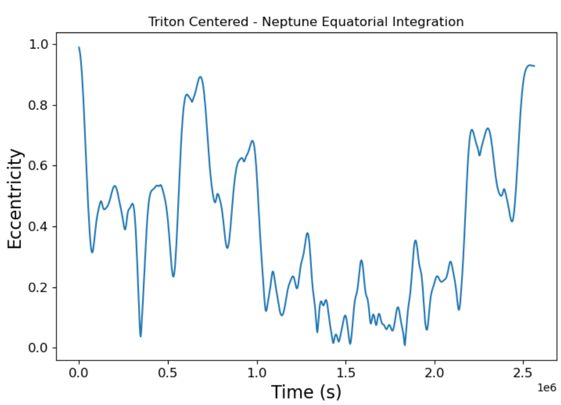

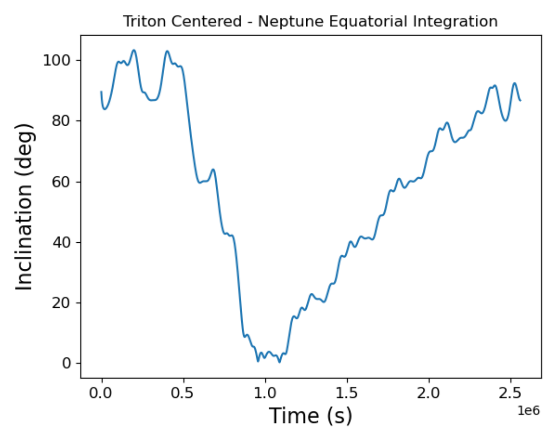

Figure 71- Eccentricity and Inclination of Sticky Capture/Collision, 30-day forward integration

A sticky orbit was found at a: 10,076 km and e:0.251. A change of eccentricity of only 0.006

resulted in a different outcome at the end of the integration period. This is a strong indicator that this is indeed a chaotic region. These initial conditions lead to a collision with Triton after capture, but the satellite is in a ‘sticky’ stable orbit until the last half period. During this ‘sticky’ period the orbit varies in inclination and eccentricity and would be useful for final orbital selection using only natural forces.

<u>Orbit 3</u>

An additional sticky orbit was identified at a: 10,488 km and e: 0.262. Another small change to semi-major axis and eccentricity leads to a sticky capture/escape trajectory. This particular interaction is useful for potential missions visiting several bodies in the Neptune system. The escape trajectory is particularly interesting as the spacecraft is released into a quasi-satellite orbit still in the vicinity of Triton.

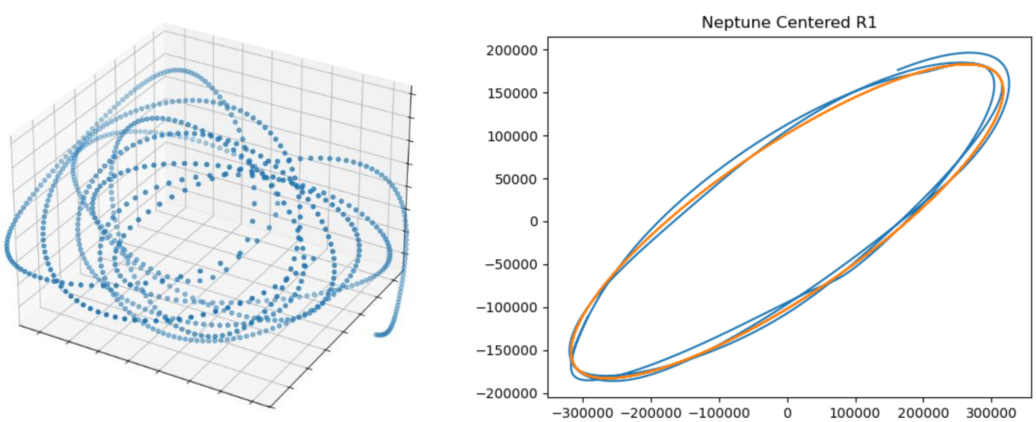

Figure 72- Isometric and Neptune centered view, 16-day Reverse Integration

(Triton plotted in orange, Satellite in blue)

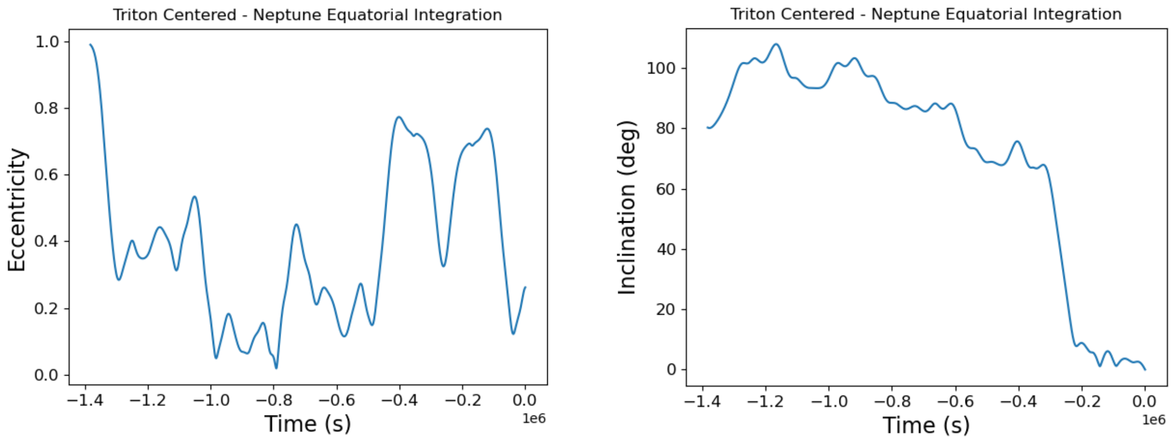

Figure 73- Eccentricity and Inclination, 16-day Reverse Integration

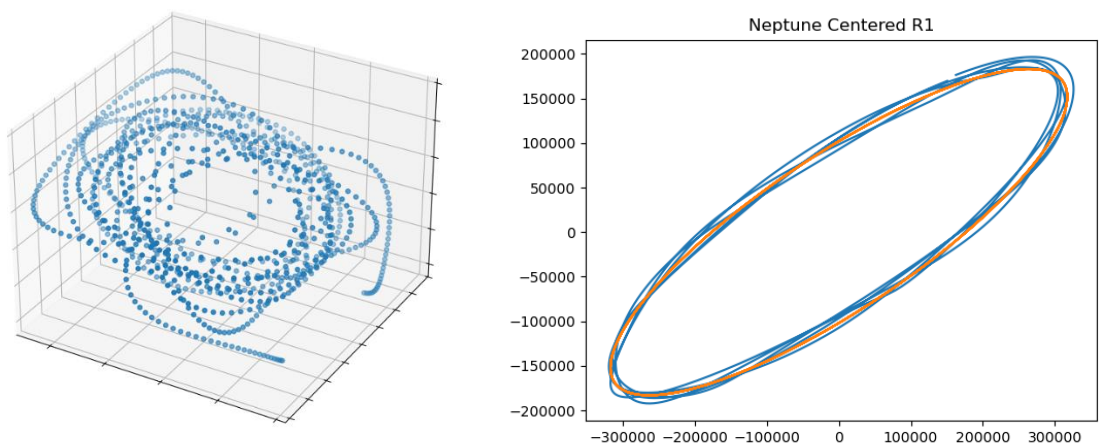

Figure 74- Isometric and Neptune centered view of Sticky Capture/Escape, 29-day Forward Integration

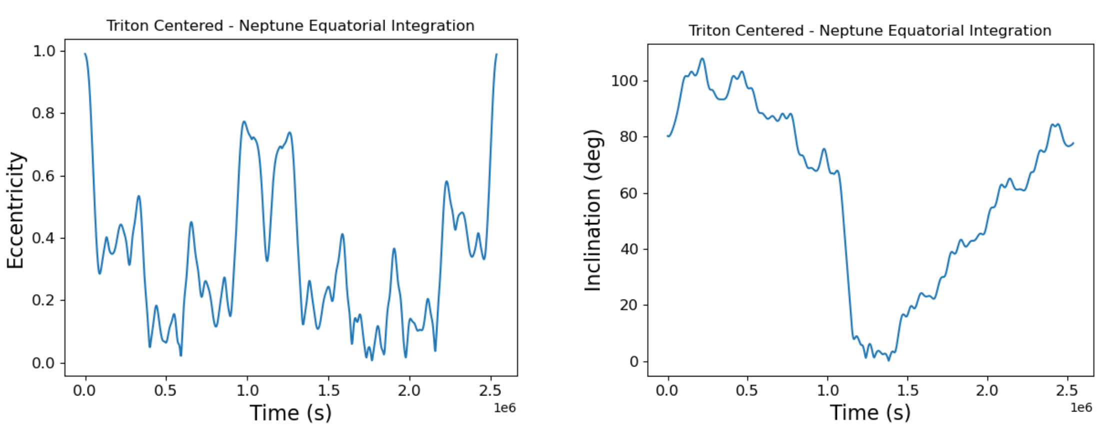

Figure 75- Eccentricity and Inclination, Sticky Capture/Escape, 29-day Forward Integration

Orbit 4

The last example orbit initial conditions are a: 10,686 and e: 0.1001. In the reverse integration, escape was made with an energy of -0.071 km2/s2, significantly less than the initial example orbit and a better example of the orbits sought in this study. After capture, the satellite stays in orbit until the end of the forward integration time. For this particular orbital trajectory, PI_{ii} was graphed over the integration time in Figure 80. The value oscillates around 0.0 indicating that the orbit is potentially stable over a long period of time, even if highly perturbed.

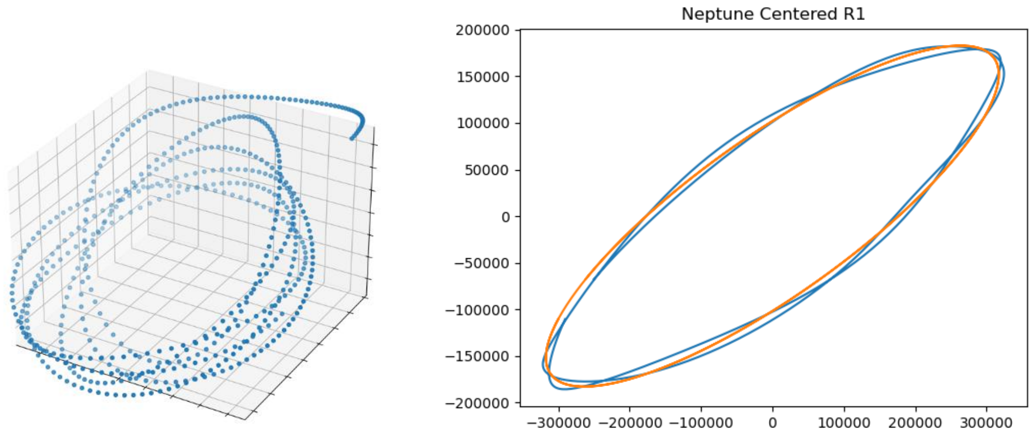

Figure 76- Isometric and Neptune Centric View, 12-day Reverse Integration to Escape

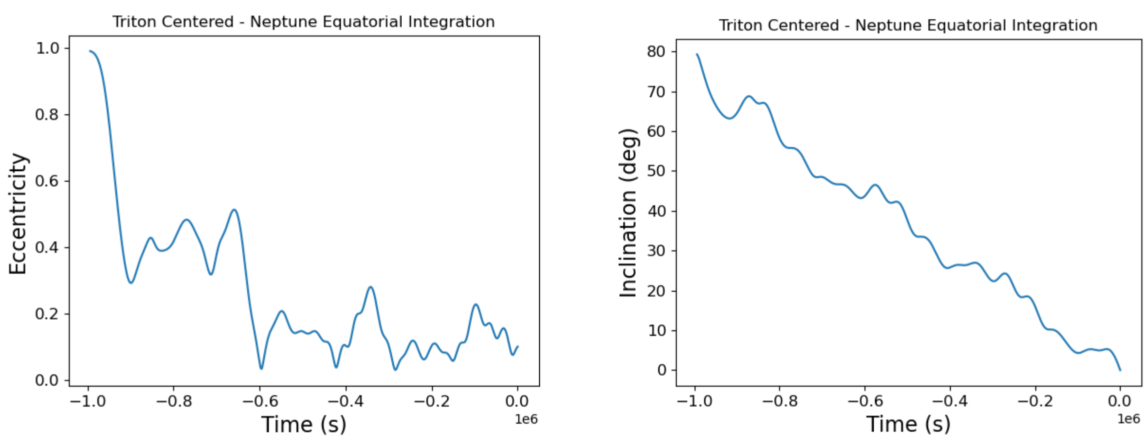

Figure 77- Eccentricity and Inclination, 12-day Reverse Integration to Escape

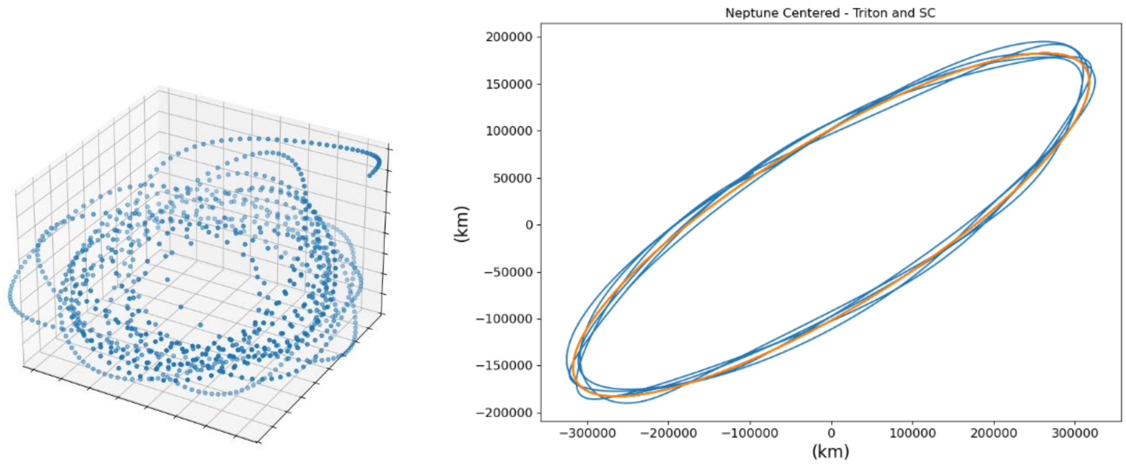

Figure 78- Isometric and Neptune Centric View, 30-day Forward Integration to Capture

(Triton plotted in orange, Satellite in blue)

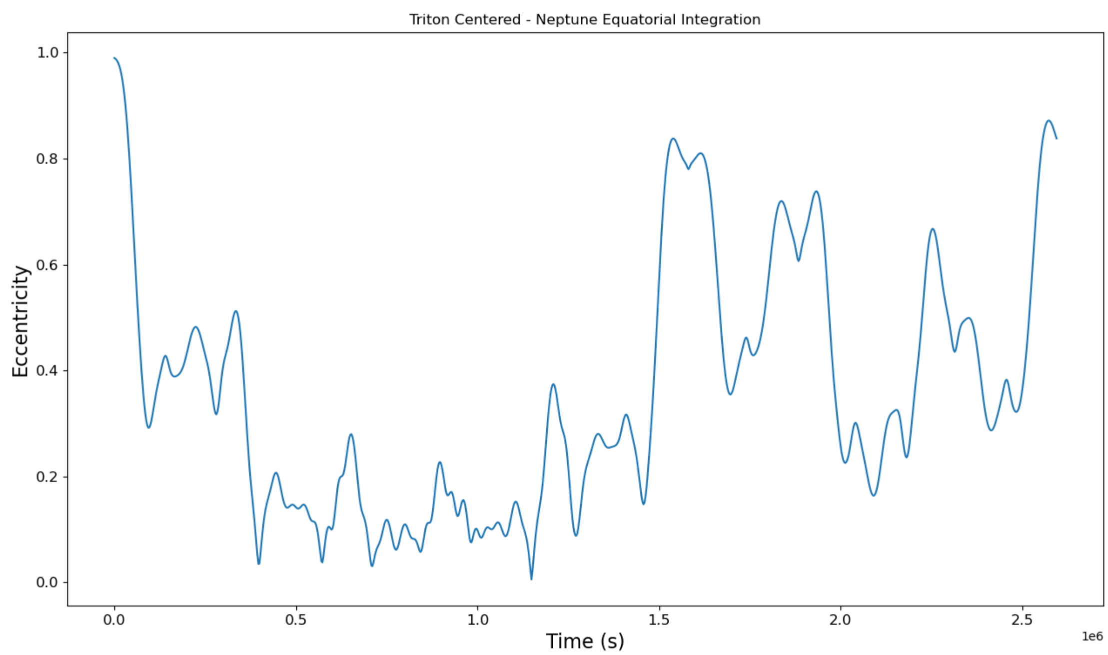

Figure 79- Eccentricity of Satellite, 30-day Forward Integration to Capture

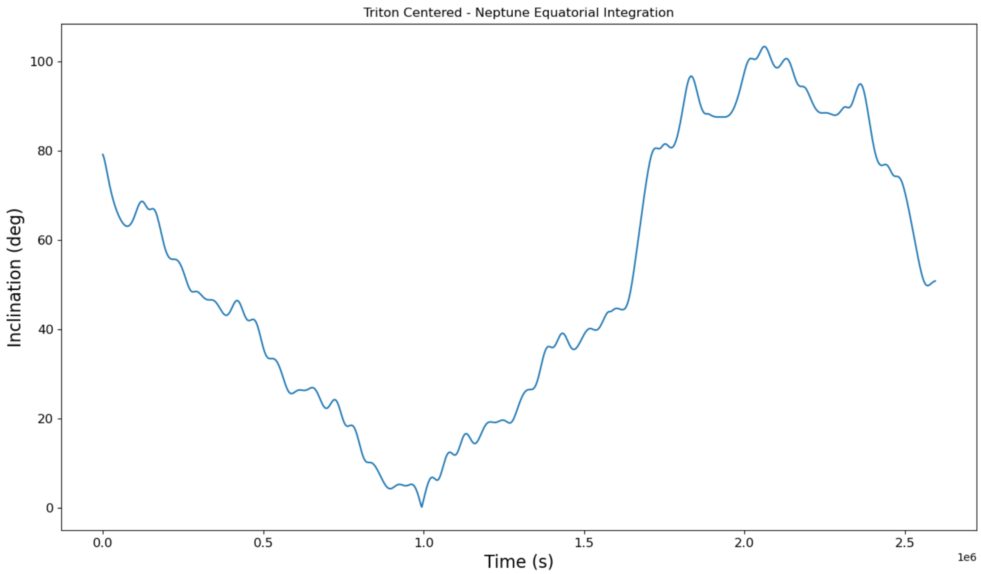

Figure 80- Inclination of Satellite, 30-day Forward Integration to Capture

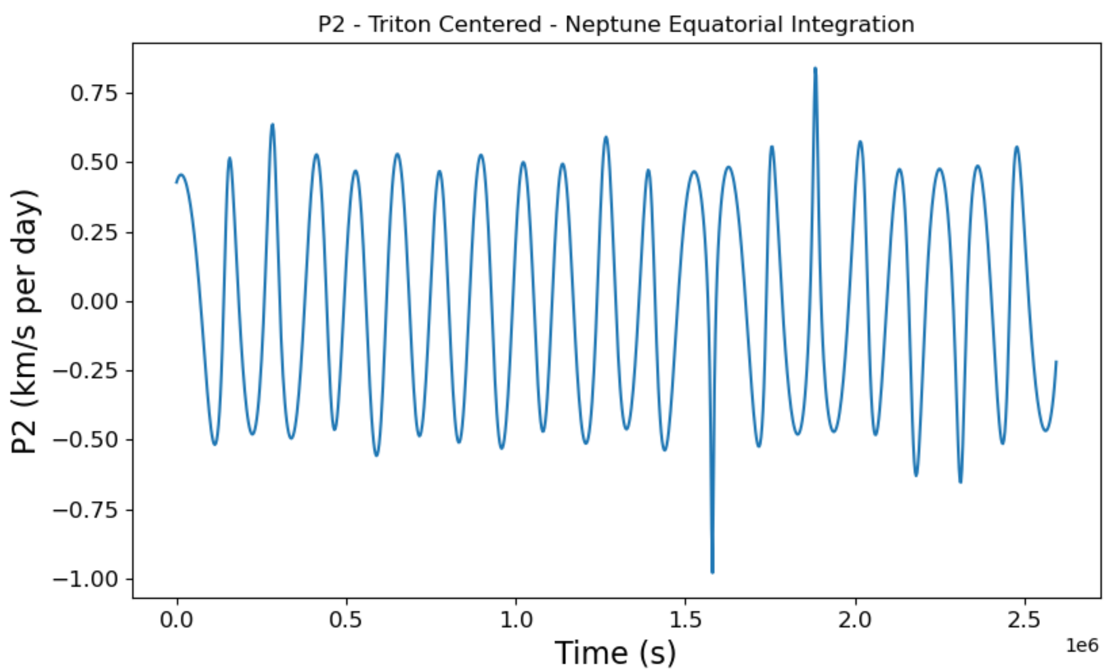

Figure 81- P_{ii} values or Statellite in 30-day Forward Integration to Capture.

The orbits presented above all show similar peaks and valleys in the eccentricity and inclination plots. Many also hint at mirroring or repeating some portions of the elements variations over time. While the 30-day integration time for the purposes of this study is not long enough to specifically determine what resonances are at work, further research could reveal interesting and useful resonances in the Neptune-Triton-Satellite interaction. All four orbits are potentially useful for a variety of future missions as they all demonstrate changes in eccentricity and inclination over the course of the integration period. Using the natural changes in the orbital elements, a beneficial orbit can be achieved without further use of propellant. Waiting until the orbit matches the desired configuration and making a calculated impulse to regularize the orbit and stay 'on station.' The 'sticky' orbits are potentially useful as well. In the case of the capture/escape orbit a 'tour' of the moons of Neptune could be made using only natural changes in the spacecraft velocity. In the case of the capture/collision sticky orbit, a lander or impactor could be set down without further propellant needed.

Delta V Analysis

The three negative energy escapes were further analyzed to determine an estimate of the Δv saved by utilizing capture via natural perturbations. Two of the example orbits were revealed to be on a very fine energy threshold between escape and collision with no 'stable' orbit for use as a reference of Δv. The third orbit did move into a 'stable' orbit with a reduction in initial energy and the Δv savings could be estimated. In each case the energy was reduced by a percentage and the trajectory integrated in reverse time. The initial reductions were made in percentages, and the resulting new initial velocity and energy were integrated in reverse time. For the two orbits that are on the energy threshold of a collision, the initial energy was reduced until collision, the resulting Δv calculated is the maximum change in velocity and energy that could be made to the initial conditions before loss of the satellite. Additionally, a value just before the collision threshold is the energy state needed that would change the nature of the satellite's subsequent escape from Triton's influence. The third orbits energy state moved from collision to brief escape and then back to stable orbit with less than 1% change of initial energy. The quickly changing nature of the trajectory/energy interactions further show chaotic motion at work and highlight the many trajectories possible to move through and between utilizing the unique 4-body dynamics of the system. In Table 6 the values of Δv corresponding to the percentage change in initial energy are shown. The Orbit Numbers correspond to the numbered orbits in the previous section. Orbit 1 is not shown as it had a slightly positive energy at escape.

Table 6. Δv changes resulting from chaotic motion

Orbit Number (Initial Conditions)	% change in initial energy	Δv (km/s)	End-State
2 (a=10076km, e=0.251)	-1.05%	1.2	Collision
3 (a=10488km, e=0.262)	-0.4%	0.287	'Stable'
4 (a=10686km, e=.1001)	-0.37%	0.835	Collision

Chapter 5. Future Work

The work presented shows that the process of mapping orbits and finding the chaotic capture trajectories is possible and yield usable orbits for a variety of potential missions. The next step in the research path is to determine and catalog a variety of orbits using the technique outlined in this thesis. Finding many orbits will allow the characterization of the possible orbits with respect to a particular set of initial conditions. This will allow the further development of specific transfer trajectories from a Neptune centered orbit and lead to potential mission-oriented trajectory planning in the future. To this end the initial conditions can be adjusted for an epoch in the future rather than the year 2000 epoch used in this work. The work presented mapped the initial conditions of the satellite around Triton along semi-major axis and *eccentricity* changes. The relationship between chaotic capture using initial conditions that vary semi-major axis and *inclination* may yield different unique capture and escape trajectories. The codebase is fully developed and could be adapted with a small amount of effort. A thorough investigation of the many different trajectories and interactions that are present in the identified potentially chaotic orbital regions in the Neptune-Triton system and a more detailed look at the Δv changes and savings in particular would greatly benefit future mission planning and further investigations of the Neptune-Triton system. The current technique is effective but is highly manual and time intensive. A more specifically targeted and automated code would be beneficial and the groundwork for developing that code is available in this work. Also, in a few of the individual trajectories there was an interchange between inclination and eccentricity due to natural perturbations. It is possible that the satellite undergoes Kozai Resonance in certain configurations of initial conditions and the possibility and impact of this resonance would be of interest for future orbital and mission design studies. Additional resonances may be present in the 4-body system modeled in this study and could be studied and utilized for mission/orbital design as well.

Potential Practical Applications

The most direct application of the prior work is in using the information and simulations for trajectory planning on an actual mission to the Neptune/Triton system. Utilizing additional orbits found from further simulations, capture trajectories at Neptune and Triton can be planned to take advantage of the natural perturbations of the system. Arrival trajectories to the Neptune system can be planned to place the spacecraft in a naturally perturbed capture around Triton or the trajectories could be planned for a powered insertion to a sticky orbit and natural perturbations used to continue the exploration of the system.

Development of the 'chaotic mapping' technique used in this study for other four-to-n body systems like Jupiter, Saturn and the Earth/Moon system would enable planning for naturally perturbed captures and orbital transitions in a variety of locations around the solar system. In particular, the Saturn system with Titan being a large moon orbiting a much larger primary body like Triton's relationship with Neptune is ideally suited to expand the technique's utilization. Similarly, the Earth Moon system is also an ideal area to utilize the technique. Further uses in the Earth/Moon/Sun system could be to save propellant on sample return missions by placing the returning spacecraft on a trajectory that takes advantage of a natural perturbation capture around Earth. Additional uses in the Earth/Moon system include using a small amount of propellent to move a spacecraft to a chaotic region, utilize the perturbations to adjust the orbit of the spacecraft and then use a small amount of propellant to 'stabilize' the new orbit rather than directly burn to the new orbit. A continuation of that technique would be to use minimum propellant to move a retiring spacecraft to a naturally perturbed orbit that results in de-orbit/collision in a specific time frame.

Conclusion

Using an original n-body simulation of the Neptune/Triton system and an initial conditions grid of varying eccentricity and semi-major axis a map of the orbit endurance times and end-states after integration times was built. Further analysis of Perturbation Indices and Perturbation Maps narrowed and defined chaotic orbital areas. Using these areas as a guide, reverse integrations were undertaken on likely initial conditions to yield an escape trajectory in reverse time with negative two-body energy with relation to Triton. These trajectories were used to create initial conditions for a forward integration to accomplish spacecraft capture. These negative energy captures and subsequent stability analysis allow capture at lower, naturally imparted velocity changes. The results of the study show that chaotic capture of spacecraft can be accomplished. A variety of useful orbits can be achieved with this technique either directly or with carefully planned maneuvers.

References

[1] Curtis, H. D., *Orbital Mechanics for Engineering Students*, Kidlington, Oxford, United Kingdom: Butterworth-Heinemann, An imprint of Elsevier, 2021.

[2] Miner, Ellis D, and Wessen, Randii R. *Neptune : The Planet, Rings and Satellites / Ellis D. Miner and Randii R. Wessen.* London ; New York: Springer in association with Praxis Pub., Chichester, UK, 2002. Print.

[3] Chen, E. M. A, F Nimmo, and G. A Glatzmaier. "Tidal Heating in Icy Satellite Oceans." *Icarus (New York, N.Y. 1962)* 229 (2014): 11–30. Web.

[4] Greeley, R., and Batson, R. M., *The NASA atlas of the solar system*, "Neptune," Cambridge England: Cambridge University Press, 1997.

[5] "Neptune," *NASA* Available:https://science.nasa.gov/neptune/. Accesses 31 March 2025

[6] Esper, Jaime. "The Neptune/Triton Explorer Mission: A Concept Feasibility Study." *Acta astronautica* 59.8 (2006): 627–637. Web.

[7] Girija, Athul Pradeepkumar et al. "Feasibility and Performance Analysis of Neptune Aerocapture Using Heritage Blunt-Body Aeroshells." *Journal of spacecraft and rockets* 57.6, 1186–1203. Web, 2020

[8] Christophe, B et al. "OSS (Outer Solar System): A Fundamental and Planetary Physics Mission to Neptune, Triton and the Kuiper Belt." *Experimental astronomy* 34.2 (2012): 203–242. Web.

[9] "Proposed NASA mission would visit Neptune's curious moon triton," *NASA* Available: https://www.nasa.gov/centers-and-facilities/jpl/proposed-nasa-mission-would-visit-neptunes-curious-moon-triton/.

[10] Rymer, Abigail M et al. "Neptune Odyssey: A Flagship Concept for the Exploration of the Neptune–Triton System." *The planetary science journal* 2.5 (2021): 184. Web.

[11] Solórzano, C.R.H, A.A Sukhanov, and A.F.B.A Prado. "A Study of Trajectories to the Neptune System Using Gravity Assists." *Advances in space research* 40.1 (2007): 125–133. Web.

[12] Smith, TR; Bosanac, Natasha "Motion Primitive Approach to Spacecraft Trajectory Design in a Multi-body System," *Journal of the Astronautical Sciences*, Vol 70, Issue 5, 2023

[13] Miceli, Giuliana Elena; Bosanac, Natasha; Stuart, Jeffrey R; Alibay, Farah "Motion Primitive Approach to Spacecraft Trajectory Design in the Neptune-Triton System," AIAA SCITECH 2024 Forum, 2024

[14] Belbruno, Edward, *Capture dynamics and chaotic motions in celestial mechanics : with applications to the construction of low energy transfers,* Chapter 3, Princeton University Press, 2018

[15] Diogo M. Sanchez, Antonio F. Bertachini de Almeida Prado and Tadashi Yokoyama. "Gravitational Capture and Maintenance of a Spacecraft Around Pluto," AIAA 2014-4280. *AIAA/AAS Astrodynamics Specialist Conference*. August 2014.

[16] Wang, B., Yan, J., Gao, W., Yuan, Y., Sun, S., Ye, M., and Barriot, J.-P., “The Neptunian gravity estimated from the motion of Triton based on astrometric observations,” *Astronomy & Astrophysics*, vol. 671, Mar. 2023.

[17] Stiles, B. W., Kirk, R. L., Lorenz, R. D., Hensley, S., Lee, E., Ostro, S. J., Allison, M. D., Callahan, P. S., Gim, Y., Iess, L., del Marmo, P. P., Hamilton, G., Johnson, W. T., West, R. D., and Cassini RADAR Team, T., “Determining titan’s spin state from *Cassini* radar images,” *The Astronomical Journal*, vol. 135, Mar. 2008, pp. 1669–1680.

[18] Merguizo Sanchez, Diogo, “On the Exploration of the Asteroid 2011 UW158”, *2024 AAS Conference Paper,* (Final) AS 24-235

[19] *Chaos Detection and Predictability (Lecture Notes in Physics)*, Vol 915, Springer, 2016

APPENDIX A – Block Diagrams

Orbit Simulator Code Block Diagram

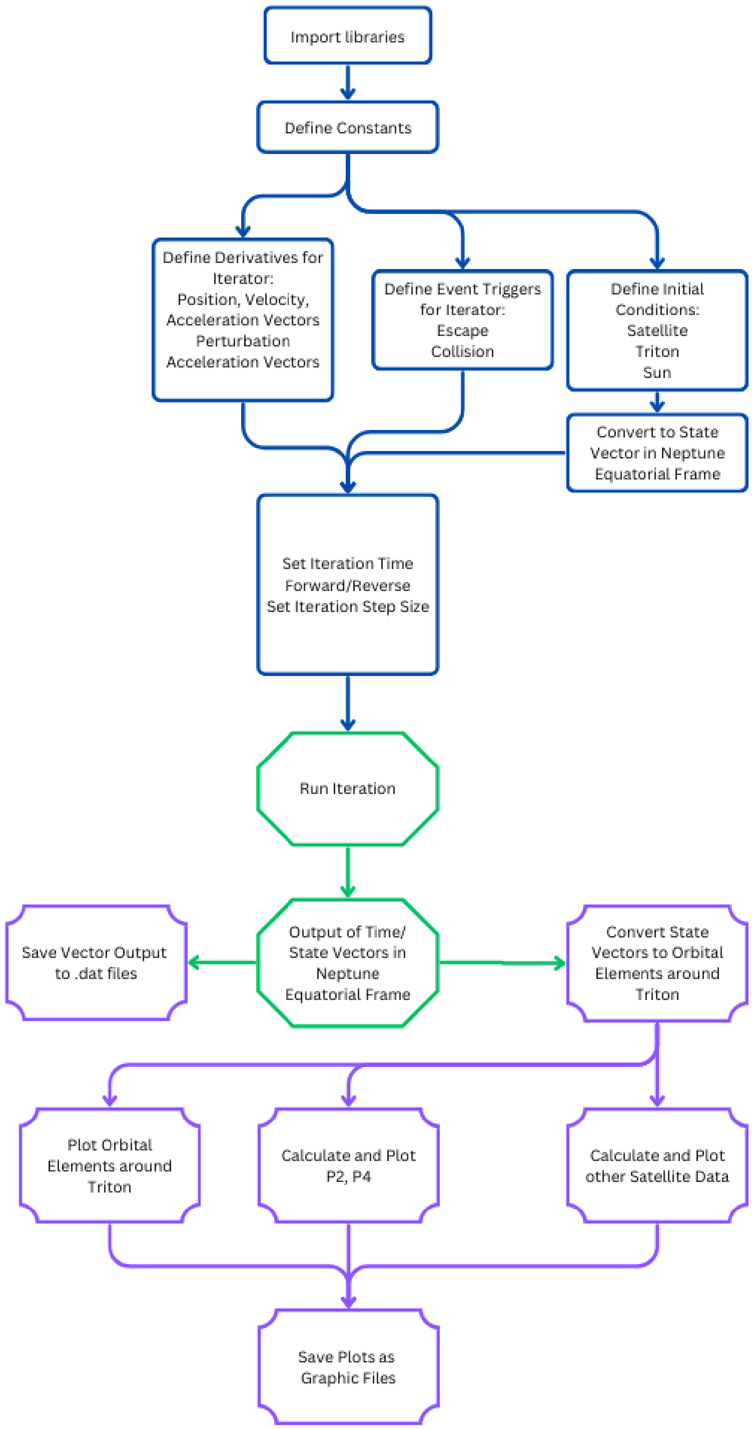

Initial Conditions Iterator Code Block Diagram

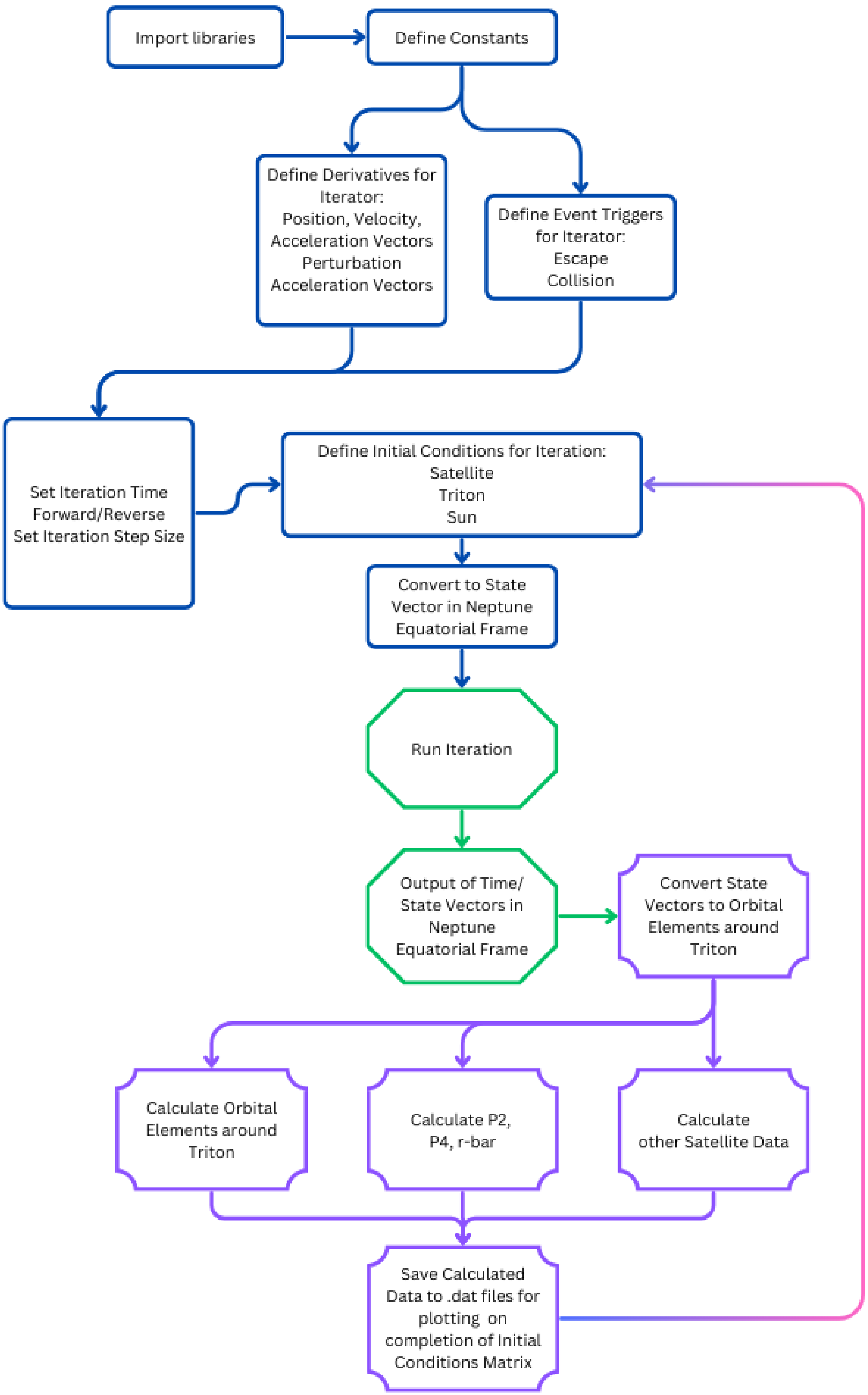

APPENDIX B. GitHub link

Matthew Dobbs' personal GitHub
https://github.com/ErroCal